Technische Universität München

Fakultät für Medizin

Magnetic Resonance Imaging and Spectroscopy based Quantification of Proton Density Fat Fraction and Fatty Acid Composition

Jan Syväri

Vollständiger Abdruck der von der Fakultät für Medizin der Technischen Universität München zur Erlangung eines

Doktors der Medizinischen Wissenschaft (Dr. med. sci.)

genehmigten Dissertation.

Vorsitz:	Prof. Dr. Wolfgang A. Weber
Prüfer*innen der Dissertation:	1. Prof. Dimitrios Karampinos, Ph. D.
	2. Prof. Dr. Franz Schilling

Die Dissertation wurde am 09.01.2023 bei der Technischen Universität München eingereicht und durch die Fakultät für Medizin am 19.04.2023 angenommen.

Abstract

Lipids are physiologically distributed in various adipose tissue depots across the body, such as visceral adipose tissue, subcutaneous adipose tissue or bone marrow adipose tissue. They can also be displaced in other compartments of the body as a pathological change in the form of ectopic lipids like liver fat. Changes in adipose tissue or ectopic lipids can be caused by physiological and pathological reasons, which already play an important role in clinical routines or are part of current research in studying disease pathophysiology. Alternations in adipose tissue volume, except bone marrow adipose tissue, is mostly related to the nutritional status and a well established biomarker. Other changes of adipose tissue like the heterogeneous distribution of fat in the liver are not yet sufficiently understood. Technical progress in research offers new technologies to investigate adipose tissue even further and help to understand the composition of adipose tissue better. These technologies will, once established, help to screen patients for risk factors or enable earlier diagnosis of diseases such as the metabolic syndrome and help with more individual therapies. Magnetic resonance (MR) can measure specific fat properties, such as proton density fat fraction or triglyceride unsaturation, to understand the mechanism of fat distribution or the influence of adipose tissue composition on tissue properties. MR has the advantage of non-invasively measuring these quantities and can therefore be applied in healthy subjects to compare normative parameters with those of diseased patients.

Magnetic resonance imaging (MRI) and magnetic resonance spectroscopy (MRS) are both powerful tools to non-invasively assess the structure of soft tissue without ionising radiation. Both methods can differentiate between hydrogen protons bound in water molecules or triglycerides. MRI is focused on high spatial resolution and differentiating between water and fat. Single-voxel MRS has a much lower spatial resolution but offers the opportunity to investigate more distinct the composition of triglycerides by resolving their spectral properties as function of chemical shift.

This cumulative thesis is about two journal publications in the field of human fat imaging with quantitative MR. It offers a) a deeper investigation of the heterogeneous fat distribution in the liver and b) a new metric to help investigators in the reliable measurement of unsaturation rate in bone marrow adipose tissue.

The first journal publication describes the investigation of liver fat changes during a lifestyle intervention study. The purpose of the study was to show differences of liver fat changes between the two liver lobes by in- and decreasing total liver fat. It was shown that liver fat is not equally distributed between the right and the left liver lobe. In addition, liver fat changes independent of increase or decrease of liver fat, are stronger in the right lobe. Changes in liver fat were also found in each Couinaud segment of the liver.

Abstract

The second journal publication describes the development of a metric which will help investigators to decide whether the measurement of unsaturation rate of bone marrow adipose tissue is feasible or not. Due to broad linewidths and high amount of water within bone marrow the olefinic peak representing the unsaturation of triglycerides in MRS can be overlapped strongly by the water peak. In the publication a metric was developed and established to show whether the measured unsaturation is feasible.

The developed methods and findings in the two publications are being used in clinical studies and ongoing research in the field of adipose tissue imaging and metabolic studies.

List of Included Journal Publications

The present dissertation is based on the following two journal publications:

[JP-I] **Jan Syväri**, Daniela Junker, Lisa Patzelt, Katharina Kappo, Loubna Al Sadat, Sonia Erfanian, Marcus R Makowski, Hans Hauner, and Dimitrios C Karampinos. "Longitudinal changes on liver proton density fat fraction differ between liver segments". In: *Quantitative Imaging in Medicine and Surgery* 11.5 (2021), p. 1701.

[JP-II] **Jan Syväri**, Stefan Ruschke, Michael Dieckmeyer, Hans H Hauner, Daniela Junker, Marcus R Makowski, Thomas Baum, and Dimitrios C Karampinos. "Estimating vertebral bone marrow fat unsaturation based on short-TE STEAM MRS". In: *Magnetic Resonance in Medicine* 85.2 (2021), pp. 615–626.

The above two journal publications are referred to as JP-I and JP-II, respectively.
Please refer to section 6 for publication abstracts.

List of Related Publications

I also contributed to the following subject-related journal publications (ordered by year of appearance):

[J1] Thomas Baum, Alexander Rohrmeier, **Jan Syväri**, Maximilian N Diefenbach, Daniela Franz, Michael Dieckmeyer, Andreas Scharr, Hans Hauner, Stefan Ruschke, Jan S Kirschke, et al. "Anatomical variation of age-related changes in vertebral bone marrow composition using chemical shift encoding-based water–fat magnetic resonance imaging". In: *Frontiers in endocrinology* 9 (2018), p. 141.

[J2] Egon Burian, **Jan Syväri**, Christina Holzapfel, Theresa Drabsch, Jan S Kirschke, Ernst J Rummeny, Claus Zimmer, Hans Hauner, Dimitrios C Karampinos, Thomas Baum, et al. "Gender-and age-related changes in trunk muscle composition using chemical shift encoding-based water–fat MRI". In: *Nutrients* 10.12 (2018), p. 1972.

[J3] Daniela Franz, **Jan Syväri**, Dominik Weidlich, Thomas Baum, Ernst J Rummeny, and Dimitrios C Karampinos. "Magnetic resonance imaging of adipose tissue in metabolic dysfunction". In: *RöFo-Fortschritte auf dem Gebiet der Röntgenstrahlen und der bildgebenden Verfahren*. Vol. 190. 12. © Georg Thieme Verlag KG. 2018, pp. 1121–1130.

[J4] Daniela Franz, Maximilian N Diefenbach, Franziska Treibel, Dominik Weidlich, **Jan Syväri**, Stefan Ruschke, Mingming Wu, Christina Holzapfel, Theresa Drabsch, Thomas Baum, et al. "Differentiating supraclavicular from gluteal adipose tissue based on simultaneous PDFF and T2* mapping using a 20-echo gradient-echo acquisition". In: *Journal of Magnetic Resonance Imaging* 50.2 (2019), pp. 424–434.

[J5] Michael Dieckmeyer, Stefan Ruschke, Alexander Rohrmeier, **Jan Syväri**, Ingo Einspieler, Vanadin Seifert-Klauss, Monika Schmidmayr, Stephan Metz, Jan S Kirschke, Ernst J Rummeny, et al. "Vertebral bone marrow fat fraction changes in postmenopausal women with breast cancer receiving combined aromatase inhibitor and bisphosphonate". In: *BMC musculoskeletal disorders* 20.1 (2019), pp. 1–7.

[J6] Egon Burian, Alexander Rohrmeier, Sarah Schlaeger, Michael Dieckmeyer, Maximilian N Diefenbach, **Jan Syväri**, Elisabeth Klupp, Dominik Weidlich, Claus Zimmer, Ernst J Rummeny, et al. "Lumbar muscle and vertebral bodies segmentation of chemical shift encoding-based water-fat MRI: the reference database myosegmentum spine". In: *BMC musculoskeletal disorders* 20.1 (2019), pp. 1–7.

[J7] Egon Burian, **Jan Syväri**, Michael Dieckmeyer, Christina Holzapfel, Theresa Drabsch, Nico Sollmann, Jan S Kirschke, Ernst J Rummeny, Claus Zimmer, Hans Hauner, et al. "Age-and BMI-related variations of fat distribution in sacral and lumbar bone marrow and their association with local muscle fat content". In: *Scientific reports* 10.1 (2020), pp. 1–8.

[J8] Daniela Junker, **Jan Syväri**, Dominik Weidlich, Christina Holzapfel, Theresa Drabsch, Birgit Waschulzik, Ernst J Rummeny, Hans Hauner, and Dimitrios C Karampinos. "Investigation of the Relationship between MR-Based Supraclavicular Fat Fraction and Thyroid Hormones". In: *Obesity facts* 13.3 (2020), pp. 331–343.

[J9] Nico Sollmann, Agnes Zoffl, Daniela Franz, **Jan Syväri**, Michael Dieckmeyer, Egon Burian, Elisabeth Klupp, Dennis M Hedderich, Christina Holzapfel, Theresa Drabsch, et al. "Regional variation in paraspinal muscle composition using chemical shift encoding-based water-fat MRI". In: *Quantitative imaging in medicine and surgery* 10.2 (2020), p. 496.

[J10] Stefan Ruschke, **Jan Syväri**, Michael Dieckmeyer, Daniela Junker, Marcus R Makowski, Thomas Baum, and Dimitrios C Karampinos. "Physiological variation of the vertebral bone marrow water T2 relaxation time". In: *NMR in Biomedicine* 34.2 (2021), e4439.

[J11] Daniela Junker, **Jan Syväri**, Dominik Weidlich, Christina Holzapfel, Theresa Drabsch, Birgit Waschulzik, Ernst J Rummeny, Hans Hauner, and Dimitrios C Karampinos. "Investigation of the relationship between MR-based supraclavicular fat fraction and thyroid hormones". In: *Obesity facts* 13.3 (2020), pp. 331–343.

[J12] Lisa Patzelt, Daniela Junker, **Jan Syväri**, Egon Burian, Mingming Wu, Olga Prokopchuk, Ulrich Nitsche, Marcus R Makowski, Rickmer F Braren, Stephan Herzig, et al. "MRI-Determined Psoas Muscle Fat Infiltration Correlates with Severity of Weight Loss during Cancer Cachexia". In: *Cancers* 13.17 (2021), p. 4433.

[J13] Nico Sollmann, Michael Dieckmeyer, Sarah Schlaeger, Alexander Rohrmeier, Jan **Syväri**, Maximilian N Diefenbach, Dominik Weidlich, Stefan Ruschke, Elisabeth Klupp, Daniela Franz, et al. "Associations between lumbar vertebral bone marrow and paraspinal muscle fat compositions—an investigation by chemical shift encoding-based water-fat MRI". In: *Frontiers in Endocrinology* 9 (2018), p. 563.

I also contribute to the following subject-related conference papers (odered by year of appearance):

[C1] N. Sollmann, M. Dieckmeyer, S. Schlaeger, R. Rohrmeier, **Syväri, J.**, M.N. Diefenbach, D. Weidlich, S. Ruschke, E. Klupp, D. Franz, E.J. Rummeny, C. Zimmer, J.S. Kirschke, D.C. Karampinos, and T. Baum. "Associations between lumbar vertebral bone marrow and paraspinal muscle fat compositions—an investigation by chemical shift encoding-based water-fat MRI". In: *Proc. of 4th International Meeting on Bone Marrow Adiposity.* (oral presentation). Lille, France, 2018.

[C2] M.N. Diefenbach, F. Treibel, D. Franz, **Syväri, J.**, S. Ruschke, H. Eggers, and D.C. Karampinos. "Technical Challenges in Measuring Adipose Tissue T2". In: *Proceedings 26. Annual Meeting International Society for Magnetic Resonance in Medicine.* (electronic poster). Paris, France, 2018, p. 5612.

[C3] **Syväri, J.**, S. Ruschke, M. Dieckmeyer, D. Franz, H. Hauner, J. Kirschke, T. Baum, and D.C. Karampinos. "Sex dependence of age-related vertebral bone marrow PDFF and T2 relaxation time changes in a cohort of nearly 200 subjects using multi-TE single-voxel MR spectroscopy". In: *Proceedings 26. Annual Meeting International Society for Magnetic Resonance in Medicine.* (electronic poster). Paris, Franze, 2018, p. 5163.

[C4] **Syväri, J.**, S. Ruschke, M. Dieckmeyer, D. Franz, H. Hauner, J. Kirschke, T. Baum, and D.C. Karampinos. "Estimating vertebral bone marrow triglyceride unsaturation based on the extraction of the olefinic peak in short-TE STEAM MRS using a constrained fitting model". In: *Proceedings 26. Annual Meeting International Society for Magnetic Resonance in Medicine.* (electronic poster). Paris, Franze, 2018, p. 5162.

[C5] D. Franz, M. Diefenbach, **Syväri, J.**, D. Weidlich, E.J. Rummeny, H. Hauner, S. Ruschke, and D.C. Karampinos. "Differentiating supraclavicular from gluteal adipose tissue based on simultaneous PDFF and T2* mapping using a twenty-echo gradient echo acquisition". In: *Proceedings 26. Annual Meeting International Society for Magnetic Resonance in Medicine.* (traditional poster). Paris, Franze, 2018, p. 2498.

[C6] D. Franz, D. Weidlich, **Syväri, J.**, M. Diefenbach, C. Holzapfel, T. Drabsch, T. Baum, H. Eggers, E.J. Rummeny, H. Hauner, and D.C. Karampinos. "The presence of brown adipose tissue is associated with thyroid function in subjects with low and normal BMI". In: *Proceedings 26. Annual Meeting International Society for Magnetic Resonance in Medicine.* (oral). Paris, Franze, 2018, p. 1266.

[C7] T. Baum, A. Rohrmeier, **Syväri, J.**, M.N. Diefenbach, D. Franz, M. Dieckmeyer, A. Scharr, H. Hauner, S. Ruschke, J.S. Kirschke, and D.C. Karampinos. "Anatomical variation of age-related changes in vertebral bone marrow composition using chemical shift encoding-based water-fat MRI". In: *Proceedings 26. Annual Meeting International Society for Magnetic Resonance in Medicine.* oral, ISMRM Magna Cum Laude Merit Award). Paris, Franze, 2018, p. 1243.

[C8] A. Rohrmeier, **Syväri, J.**, M. Diefenbach, D. Franz, S. Ruschke, M. Dieckmeyer, J.S. Kirschke, D.C. Karampinos, and T. Baum. "Vertebral bone marrow composition: assessment of age and gender dependency using chemical shift encoding-based water-fat MRI". In: *European Congress of Radiology*. (oral). Vienna, Austria, 2018, B–0441.

[C9] D. Franz, **Syväri, J.**, C. Zoellner, M.N. Diefenbach, R. Brarn, U. Nitsche, O. Prokopchuk, E.J. Rummeny, and D.C. Karampinos. "Psoas volume and fat fraction in cancer patients: dynamics and association with severity of cachexia progression". In: *105th Annual Meeting of RSNA*. (oral). Chicaco, USA, 2019.

[C10] N. Sollmann, E. Burian, **Syväri, J.**, M. Dieckmeyer, C. Holzapfel, T. Drabsch, H. Hauner, D. Franz, D.C. Karampinos, and T. Baum. "Age-related variations of sacral and lumbar bone marrow composition and their associations with local muscle fat content". In: *5th Annual Meeting of the Bone Marrow Adiposity Society*. (oral). Odense, Denmark, 2019.

[C11] **Syväri, J.**, S. Ruschke, M. Dieckmeyer, H. Hauner, J.S. Kirschke, D. Franz, T. Baum, and D.C. Karampinos. "Estimating vertebral bone marrow fat unsaturation based on short-TE STEAM MRS". In: *5th Annual Meeting of the Bone Marrow Adiposity Society*. (power pitch presentation). Odense, Denmark, 2019.

[C12] D. Franz, L. Patzelt, **Syväri, J.**, C. Zoellner, M.N. Diefenbach, R. Braren, U. Nitsche, O. Prokopchuk, E.J. Rummeny, and D.C. Karampinos. "Psoas volume and PDFF in cancer patients: dynamics and association with severity of cachexia progression". In: *SMRM Workshop on MRI of Obesity and Metabolic Disorders*. (power pitch presentation). Singapore, 2019, p. 23.

[C13] D. Franz, D. Weidlich, **Syväri, J.**, S. Ruschke, M.M. Wu, C. Holzapfel, T. Drabsch, E. Rummeny, H. Hauner, and D.C. Karampinos. "MRS-based water T2 relaxation time in the supraclavicular fossa relates to anthropometric and imaging obesity markers". In: *Proceedings 27. Annual Meeting International Society for Magnetic Resonance in Medicine*. (digital poster). Montreal, Canada, 2019, p. 1942.

[C14] D. Franz, **Syväri, J.**, C. Zoellner, R. Braren, U. Nitsche, E. Rummeny, and D.C. Karampinos. "Proton density fat fraction mapping for tracking tissue changes under weight loss in cancer cachexia". In: *Proceedings 27. Annual Meeting International Society for Magnetic Resonance in Medicine*. (digital poster). Montreal, Canada, 2019, p. 1941.

[C15] M. Dieckmeyer, S. Ruschke, A. Rohrmeier, **Syväri, J.**, I. Einspieler, J. Kirschke, E. Rummeny, C. Zimmer, D.C. Karampinos, and T. Baum. "Vertebral bone marrow fat content changes in postmenopausal women receiving combined aromatase inhibitor and bisphosphonate therapy after one year". In: *Proceedings 27. Annual Meeting International Society for Magnetic Resonance in Medicine*. (digital poster). Montreal, Canada, 2019, p. 1304.

[C16] E. Burian, D. Franz, **Syväri, J.**, C. Holzapfel, T. Drabsch, J. Kirschke, E. Rummeny, C. Zimmer, H. Hauner, D.C. Karampinos, and T. Baum. "Gender- and age-related changes in trunk muscle composition using chemical shift encoding-based water-fat MRI". In: *Proceedings 27. Annual Meeting International Society for Magnetic Resonance in Medicine*. (digital poster). Montreal, Canada, 2019, p. 1278.

[C17] T. Drabsch, D. Junker, L. Stecher, **Syväri, J.**, H. Hauner, D.C. Karampinos, and C. Holzapfel. "Association between proton density fat fraction and resting metabolic rate in humans: no contribution by the FTO genotype". In: *European and International Congress on Obesity*. (digital poster). Virtual Conference, 2020, EP–550.

Contents

1 Introduction

Lipids can be found in various forms across the human body. They can be differentiated into adipose tissue and ectopic fat. Adipose tissue is a large accumulation of lipids, like subcutaneous adipose tissue, brown adipose tissue or bone marrow adipose tissue and can be found in human beings in a physiological state. Ectopic fat is often a displacement of fat in tissues that normally do not contain fat in healthy people, such as the liver or muscles. As fat has a high plasticity, changes in the amount and composition of fat can be used as markers in metabolic dysfunction, such as obesity, diabetes or cachexia. Measurement of fat can be used as a diagnostic tool, for risk stratification or as therapy monitoring.

This thesis focuses on new developments for non-invasively characterizing of fat in the liver and bone marrow.

Liver fat is an ectopic fat depot which is highly correlated with obesity [1]. It was shown that with reduction of weight, liver fat is also reduced [2, 3]. The first aim of this thesis is to characterize spatial distribution of liver fat during a lifestyle intervention.

Bone marrow adipose tissue is not correlated with obesity. On the contrary, bone marrow adipose tissue is increasing in anorectic patients [4]. Bone marrow adipose tissue seems to be good biomarker for the overall health of bone marrow and be related to the bone matrix health. The second aim of this thesis is to characterize bone marrow fatty acid composition.

Magnetic Resonance offers a powerful tool to measure and characterize fat across the human body. As a relatively new diagnostic modality in medicine there is still a lot of potential for further development. Nuclear magnetic resonance (NMR) was first applied in chemistry in the 1950s[5, 6], while imaging techniques were developed later in the 1970s by Paul C. Lauterbur[7] and Peter Mansfield[8]. The first scan of the human body was performed on the 3^{rd} July 1977[9]. With the invention of the first MRI product line in 1980 from GE the NMR technique became available for a more routine usage in medical applications. Since then, research in NMR techniques developed multiple applications in clinical routines and research is still continuing. Early imaging technologies mainly used the T_1 relaxation time and the T_2 relaxation time[10, 11, 12, 13], which produce qualitative images. Modern techniques focus on quantitative imaging allow a better comparison between subjects like spectroscopy or chemical-shift encoding imaging.

Spectroscopy and chemical-shift encoding imaging uses different resonance frequencies of the ^{1}H-protons within the molecules to generate contrast. Based on this, water and fat can be separated using MR. With these techniques, it is possible to measure specific quantities such as proton density fat fraction (PDFF), which became a robust and reliable biomarker. Therefore, it is used in clinical applications and better characterization of metabolic disorders. With improving the techniques based on chemical shift, the fat

unsaturation can be measured. Current research focuses on establishing unsaturation rate for metabolic disorders.

As fat is distributed all over the body, water-fat separating imaging can be used in multiple locations. This dissertation focuses on fat in the liver and bone marrow. Healthy subjects have close to no fat in the liver[14]. For early diagnosis of fat displacement in the liver even small amounts need to be detected. A main influence of the pathological displacement of fat in the liver is obesity and can be decreased by reducing body weight. Bone marrow fat is a special fat depot which behaves differently from other fat depots such as subcutaneous or liver fat. It seems that bone marrow fat is independent of nutritional state and seems more depending on bone marrow density[15, 16, 17] and other bone marrow diseases[18, 4, 16, 19] and therefore overall bone marrow health.

Continuous research in the field of quantitative imaging, development and establishment of biomarkers will improve the characterisation of diseases and will therefore help in early diagnosing diseases, planning individual therapies and monitoring those.

1.1 Technical Challenges and Clinical Relevance

As the MR is detecting mainly hydrogen (^{1}H-) protons and nearly all parts of the human body contain molecules partially persisting of ^{1}H-protons most parts can be assessed. Depending on the tissue and the respective amount of ^{1}H-protons, the strength of the signal varies. Therefore, in the early days of MR, imaging was mainly focused on soft tissues like organs and fat, as they have a high concentration of ^{1}H-protons due to high water and fat content. Other tissues such as bone marrow have very low concentration of ^{1}H-protons and therefore, imaging in those tissues is more complex.

Body MRI has the advantage of being a noninvasive method with high spatial resolution. As it is noninvasive, it can also be used for disease monitoring and longitudinal progression of diseases or treatments. These characteristics are also important for MR research as it can be performed on healthy subjects to establish metabolic biomarkers and understand physiological changes, e.g. with age or weight. These biomarkers can then be used to get a better understanding of pathologies and their respective treatment. The development of quantitative sequences in the last decades helped to develop biomarkers depending on the tissue and clinical question. The complexity of biomarkers also increased. Many biomarkers are based on water-fat-separation, such as determination of fat fraction to evaluate e.g. steatosis hepatis in obese subject and to monitor diets or other interventions[20, 21]. By improving the treatment of steatosis hepatis the risk of subjects to sicken of liver cirrhosis can be decreased. Modern MRI techniques are also used to classify hepatocellular carcinoma (HCC)[22] and help to decide the treatment of the disease. With very specific treatment depending on small differences in the carcinoma a better classification is needed to find the best treatment for individual subjects. Quantitative MR provides a method with high sensitivity and specificity to discriminate between small differences in the tumours.

Fat fraction was also established as biomarker in bone marrow[23, 24, 25]. A high correlation is known between a high fat fraction and low bone marrow density and os-

teoporosis[26, 27, 19, 28, 29]. MR Spectroscopy offers the ability to measure even more quantities and therefore biomarkers, which help to characterize different tissues and their compositions even further. In bone marrow fat unsaturation was shown[30, 16, 15] to be a predictive factor for osteoporosis. Up to this point, there is no gold standard for in vivo measurement of bone marrow unsaturation. Therefore, these techniques are still part of current investigations as different sequences exists to measure fat unsaturation with various advantages and disadvantages. Biomarkers like bone marrow fat fraction or bone marrow fat unsaturation rate could be used for an early detection of malignant changes in bone marrow such as bone metastasis and also for better description of these changes. With a better description of the lesions in bone marrow, a better classification can be applied and therefore a more adapted treatment can be performed for each individual subject. In clinical applications MR imaging is already used to differentiate between recent and active vertebral fractures compared to old non-active fractures[31]. Another important point in the clinical classification of fractures is the discrimination between malignant and benign fractures. Malignant fractures are caused by an underlying disease such as osteoporosis or metastasis. The treatment of malignant fractures differentiates from benign fractures. Quantitative MR offers the possibility of highly sensitive and specific biomarkers to differentiate between these fracture types and to optimize the treatment of patients. Bone marrow fat is especially interesting as it reacts differently from other fat depots. While in anorectic subjects the fat volume in e.g. subcutaneous adipose tissue or liver fat is decreasing it was shown by Bredella et al[4] that the fat fraction increases in bone marrow in these patients. MR offers a noninvasive method to get further understanding of the physiological reaction of bone marrow that seems not be influenced by the nutritional status of the subject like other fat depots[20]. Quantitative MR provides a noninvasive method of investigating fat depots in the whole body from simple depots like liver fat to more complex fat depots including bone marrow.

1.2 Thesis Purpose

The main purpose of the present thesis is the further development of MRI and MRS-based biomarkers of adipose tissue regarding imaging techniques and further understanding of adipose tissue composition. More specifically, the first purpose was to describe heterogenous changes of liver fat in subjects with in- and decreasing overall liver fat. This was achieved by creating a longitudinal study with measurement of liver fat with high spatial resolution. The second purpose was to find a method to make measurements of bone marrow unsaturation rate more feasible. This was achieved by defining and establishing a metric which separates bone marrow spectroscopies in two groups, where the unsaturation rate of the bone marrow is measured feasible in one group and not in the other.

1.2.1 Thesis Structure

The present cumulative thesis aims to describe the technical and clinical background of the two embedded journal publications and discusses the results in the context of existing

literature and current research.

Chapter 2 gives a brief overview of the main aspects of malnutrition and the consequences. Chapter 3 focuses on the different kinds of adipose tissue and the different fat depots across the body. In chapter 4 fundamentals of the MR physics are explained and a short description of the used sequences is given. Chapter 5 is a declaration of compliance with ethical standards. Chapter 6 summarizes the two embedded journal publications. The last chapter 7 gives a review of existing literature and current research, including the novelty, impact, limitations and perspective of the two journal publications.

2 Metabolic Dysfunction

Metabolic dysfunction is an umbrella term for disorders affecting the metabolism. The term covers a large range from undernutrition to overnutrition and internal and external reasons for the disorder.

Underweight is defined by the World Health Organization (WHO) as BMI ≤ 18.5 [32] and is a result of a lower metabolic intake or a higher metabolism. Lower metabolic intake is often an external reason caused by malnutrition, for example in subjects with anorexia nervosa or due to internal reasons for example with a low resorption of nutrient in the gastrointestinal tract. A higher metabolism is often caused by internal reasons like consuming diseases leading to cachexia or other diseases, for example thyroid hyperfunction.

Overweight is defined as BMI ≥ 25[32] and is often caused by a high metabolic intake due to a sedentary lifestyle or to a lower metabolism due to internal diseases,for example thyroid hypofunction. Obesity is the enhancement of overweight and is defined by a BMI ≥ 30.

Both, over- and underweight, can lead to various diseases and a reduction of quality of life. The next paragraphs discuss the complications of obesity and cachexia as a special case of underweight.

2.1 Obesity and diabetes

A sedentary lifestyle is leading to an increasing rate of obesity, especially in countries of the Western Hemisphere. Obesity is a risk factor for a lot of diseases such as diabetes mellitus type 2 (DM-II), hypertension and other cardiac diseases[33]. The WHO characterizes subjects with a BMI ≥ 25 as overweight and a BMI ≥ 30 as obese[32]. In 2016 over 1.9 billion adults were overweight and over 650 million obese[32]. As one of the main characteristics of the metabolic syndrome, obesity has a high risk for multiple diseases.

DM-II is highly associated with obesity[34] and its prevalence is increasing. DM-II itself is also a risk factor for various diseases, mainly focused on the cardiovascular disease such as hypertension, myocardial infarcts but also leads to diseases like diabetic neuropathy, retinopathy and nephropathy. Early detection and lifestyle changes can have a high impact on the course of the disease and can prevent long term complications if treated early and effectively. Next to the detriments of each individual subjects suffering from DM-II, the treatment of DM-II and its complications has a very high financial impact on the health care system. Better treatment in the early stages of the disease could reduce costs.

Obesity can also lead to fatty liver disease and in the progress to hepatis steatosis. Fatty liver disease can be differentiated in alcoholic liver disease and non-alcoholic fatty

liver disease (NAFLD). One of the highest risk factors for (NAFLD) is obesity and the metabolic syndrome[1, 35]. Early stages of fatty liver diseases are reversible without any residuals. Therapy includes a lifestyle changes with dieting, abstaining from alcohol and a more active lifestyle with increasing movements. Multiple studies have shown, that lifestyle interventions can lead to a decrease of liver fat [20, 36, 37]. Otherwise, later stages can turn into liver cirrhosis leading to liver insufficiency and a high risk for HCC. Therefore, early detection of fatty liver disease is important.

Cardiovascular diseases are the most frequent cause of death in the western world. They are strongly associated with a sedentary lifestyle with less movement and obesity. In therapy for these diseases next to medication, a reduction of weight is important to improve the outcome of the therapy. In hypertension for example, the blood pressure can be lowered even by small reduction of the body weight[38].

Obesity is a risk factor for many diseases in the western world caused by a sedentary lifestyle. Preventing obesity with lifestyle changes could lead to reduction of multiple diseases and could increase the life expectancy and quality of life.

2.2 Cachexia and anorexia

Cachexia is a form of a malignant underweight caused by consuming diseases like cancer, tuberculosis, autoimmune diseases or AIDS. The exact pathomechanism for the weight loss is very complex and multifactorial and not entire understood until today. Current research assumes that a chronic inflammation caused by the main disease leads to a change in the metabolism in the muscle and fat cells and also to a loss of appetite. These changes lead to a higher metabolic rate and simultaneously decreasing metabolic intake and, therefore, to a decreased volume of muscle and fat cells. Cachexia is defined as

- a weight loss of > 5 %
- a weight loss of > 2 % and a BMI < 20 kg/m^2
- a weight loss of > 2 % and sacropenia. [39]

A reduced nutritional status often leads to higher mortality rate in affected patients, for example due to higher risks in the operation room or changed therapy regimes. Pathomechanism, risk factors, early detection and optimized treatment are part of current research. Anorexia nervosa is another reason of serious underweight and is better researched. It was shown that fat depots like VAT, SAT are reduced in anorectic patients. In contrary, it was shown that the bone marrow fat fraction is increased in such patients[4, 40]. Furthermore, many anorectic patients develop a osteoporosis[41, 42].

3 Physiological Background of Human Fat

3.1 Different types of human fat

Fat in the human body can be classified in different ways. It is important to subdivide fat into adipose tissue (AT) and ectopic lipids. AT is a larger accumulation of fat in connective tissue containing mainly lipids. Ectopic lipids are smaller amounts of lipids in other tissues like the liver or muscles. These ectopic lipids are often displaced and show a pathological state like in fatty liver diseases or fat displacement in muscles. The adipose tissue in the human body can be distinguished into three different kinds of AT: white, brown and beige AT[43]. Mere brown AT is very rare in the human body, and the combination of white and brown AT is called beige adipose tissue. In mice mere brown adipose tissue (BAT) can be found[44]. MR can detect even small amounts of AT and can distinguish between those types of AT by measuring the composition of the adipose tissue, perfusion and other parameters.

White adipose tissue (WAT) is the main energy storage of humans. The cells persist of one droplet of triglycerides and very few other components such as water[45]. MRS of tissues mainly consisting of WAT show mainly fat peaks and very low amounts of water. Most of the fat depots in the body consist of WAT. As it is the main energy storage of the human body, WAT is reduced in metabolic disorders with reduced weight and is strongly increased in metabolic disorders with increased weight like obesity. Therefore, tracking the volume of WAT can be very important in the early detection of such diseases. WAT displacement in organs with no fat in healthy subjects may be an early marker of the long-term effects of malnutrition such as fatty liver disease. Efforts are also being made to establish newer biomarkers such as unsaturation rate to provide a better way to characterise WAT in different individuals. For example, a lower unsaturation rate in WAT is associated with lower insulin sensitivity [46] and therefore a higher risk for DM-II [47].

In comparison, BAT is a metabolic active tissue with the specialized function of generating thermal energy from chemical energy in the form of glucose and fatty acids. The cells of BAT have a higher blood perfusion compared to WAT and express a high amount of mitochondria. These mitochondria express a specialized enzyme called UCP-1 uncoupling the respiratory chain and generating heat instead of adenosine triphosphate[48]. Mere BAT can only be found in mice. In humans the brown fat is enclosed in WAT and is then called beige fat. Most BAT is found in the supraclavicular and paravertebral regions of the human body, but also in other regions[49]. BAT is mainly active in young children and the activity is decreasing with age[50]. However, active BAT is also found

in adults. As the volume of BAT is inversely correlated with BMI[51, 52] a big influence on metabolism is assumed. The activation of BAT is a widely discussed topic in the therapy of obesity and its secondary diseases[53, 54, 55]. The current gold standard of detecting BAT is the ^{18}F-fluorodeoxyglu-cose positron emission tomography (PET) with computed tomography (CT). However, this method lacks the reproducibility in subjects as the BAT can be activated by multiple factors like high calorie intake or cold[56]. Also, the radiation of PET and the CT causes issues with multiple scans. MR offers a non-invasive method to distinguish between BAT and WAT via multiple biomarkers. While WAT consists of nearly no water, BAT shows higher contents. This lower fat fraction can be used as a biomarker via chemical shift-encoding (CSE) based quantification methods to detect brown fat [57, 58, 59]. It was shown that MRS can detect differences between BAT and WAT. In comparison to WAT, BAT had a lower fat content and a lower unsaturation rate. Modern MRI techniques try to show the activation level of BAT. Several approaches in mice were applied, including blood perfusion of the BAT [60]. Accurate quantification of BAT with MRI is still limited due to motion artefacts, breathing and vessels in the region of interest.

3.2 Fat Accumulations in different Regions in the Human Body

3.2.1 Subcutaneous Adipose Tissue

Subcutaneous adipose tissue (SAT) is defined as the fat between the dermis and the aponeuroses and muscles including the mammary adipose tissue[61]. It consists mainly of WAT with low amounts of water. SAT is primarily an energy storage for the human body and can be easily accessed by the body if lower calorie intake occurs. A short dietary intervention of 4 weeks in obese women showed a reduction of SAT[20]. There is less of a consensus regarding the influence of SAT on risk for diseases like DM-II or cardiovascular diseases. Recent studies separate the SAT in superficial and deep SAT separated by the fascia superficialis[62]. Golan et al showed in subjects with DM-II that women have a higher superficial SAT compared to men with similar waist circumference[63]. They also showed that a higher amount of superficial SAT was correlated with lower blood pressure, higher heart rate variability, indicating a better cardiovascular health and improved HbA_{1C} and fasting glucose, indicating a better control of the insulin sensitivity. In contrast, a higher amount of deep SAT correlated with increased cardiovascular risk. This study is in line with other studies suggesting a correlation between the volume of deep SAT and higher insulin resistance[64, 65]. SAT also showed a high rate of polyunsaturated fatty acids compared to other fat depots of the body[46]. In particular, superficial SAT contains a higher amount of unsaturated fatty acids[66, 67].

3.2.2 Visceral Adipose Tissue

Visceral adipose tissue (VAT) is defined as the AT within the chest, abdomen and pelvis[61]. VAT mainly consists of WAT and surrounds the intraabdominal organs. Like

SAT, it is a main energy storage of the human body. Males tend to have higher abdominal VAT compared to females[68, 69]. In the study by Cordes et al the reduction of VAT volume during a four-week intervention was even stronger than the reduction of SAT[20]. However, VAT is also a hormonally active tissue releasing bioactive molecules and hormones such as adiponectin, leptin, tumour necrosis factor, interleukin 6[70] contributing to systemic inflammation[71]. Therefore, high amounts of VAT are associated with numerous pathological conditions like insulin resistance, cardiovascular diseases[72, 73] and increased predisposition for cancer of the colon[74], breast[75] and prostate[76]. VAT also contributes to the level of free fatty acids in the blood[77] interacting with the insulin balance and may explain the association between higher VAT volumes and insulin resistance[78] resulting in a higher risk for DM-II. Several studies showed high correlations between high VAT volumes and cardiovascular risk factors independent of the BMI[69, 79]. In addition to the volumetric quantification of VAT, the unsaturation rate of fatty acids is also becoming a focus of current research for a better characterization and probably better risk assessment for individual subjects[66, 80]. Here, MR offers a noninvasive method to investigate the unsaturation rate of different subjects. The unsaturation rate of the VAT is strongly effected by a high total amount of VAT. Machan et al showed that the fraction of unsaturated fatty acids in VAT was reduced in subjects with high total VAT volume[81]. VAT is remaining an interesting topic in research as it has high influence on the metabolism of the whole body and with an increasing prevalence of obesity a better understanding will be important for effective treatment.

3.2.3 Liver fat

Liver fat consists of ectopic lipids and results from a disposition of lipids in the liver. In healthy and lean subjects, fat is not accumulated in the liver. With the increased rate of overweight and the metabolic syndrome, the rate of NAFLD is also increasing[1]. NAFLD is a main cause of chronic liver disease[35]. Patient suffering from NAFLD have a high risk of development liver fibrosis leading to irreversible liver cirrhosis with liver dysfunction and a high risk for the developmnt of liver carcinoma, such as the HCC, or other lethal complications[82]. Different studies showed that early stages of NAFLD are reversible[2, 3]. Therefore, keeping track of liver fat changes in subjects suffering from NAFLD is important for measurement of the treatment and risk assessment. MRI offers the possibility to measure liver fat noninvasively using PDFF mapping based on CSE sequences. PDFF mapping also shows a very good spatial resolution and coverage of the entire organ. In multiple cross-sectional studies a heterogenous liver fat distribution was shown[83, 84, 85, 86]. This effect was also demonstrated in different longitudinal studies, including subjects within diets [21] and bariatric surgery[87]. Up to this point in time, a sufficient explanation of this phenomenon remains unclear. Some studies suggest a difference in perfusion of the liver segments, but the studies showed mixed results and missing a clear explanation for this phenomenon[88, 89, 90]. However, since liver fat is a good biomarker for diagnosing NASH and corresponding complications, PDFF mapping provides a powerful tool to measure the heterogeneity of liver fat in a noninvasive way.

3.2.4 Bone Marrow Adipose Tissue

Bone marrow mainly consists of trabecular, hematopoietic cells and white adipocytes. Hematopoietic cells mainly consisting of water and the white adipocytes tissue of triglycerides and both can be measured with the MR. Bone marrow can further be subclassified in red and yellow bone marrow. Yellow bone marrow is not involved in hematopoiesis and consists mainly of trabecular and adipocytes. In contrast, red bone marrow is heavily involved in hematopoiesis and therefore consists of a large water margin next to adipocytes. In adults, red bone marrow is mainly found in central skeleton like the pelvis, vertebrae and sternum[91]. These regions are also clinically relevant, as they are frequently affected by osteoporotic fractures. Multiple studies have shown a strong correlation between the amount of adipocytes in the bone marrow and osteoporosis[92, 93, 94]. Therefore, understanding the physiology of bone marrow adipose tissue is receiving more attention to understand the pathophysiology of osteoporosis. Bone marrow adipose tissue is independent of other fat resources of the body and is not correlated with the BMI. In infants, very low amounts of bone marrow adipose tissue is present and is increases with age. In subjects below the age of 50 men show higher bone marrow adipose tissue in the vertebral bones compared to age matched women. After the age of 50 women show higher amounts of bone marrow AT[23, 95, 96]. This might be explained by the menopause. It was also shown by Baum et al that bone marrow AT in vertebrae is increasing from the cervical spine to the lumbar spine[23]. Not only in osteoporotic patients the composition of bone marrow fat is changing. Patients suffering from anorexia nervosa show higher bone marrow fat content[4]. This also correlates with lower bone marrow mineral density (BMD) in these patients[97]. Fazeli et al also demonstrated a decreasing bone marrow AT in vertebrae of patients recovered from anorexia nervosa[98]. Therefore, it may be used as a biomarker for the success of treatment. As the correlation between anorexia nervosa and higher adipose tissue volume shows is bone marrow adipose tissue independent of BMI. It is also not affected by diets[98, 20]. PDFF mapping is mainly used to assess bone marrow adipose tissue with good spatial resolution. Due to the structure of bone marrow, the signal-to-noise ratio (SNR) is lower, and therefore the results are more inconsistent. Another method to access bone marrow AT is MRS. Here, bone marrow shows a much broader linewidth compared to other tissues with a higher SNR. With MRS the composition of bone marrow fat can be investigated. Multiple studies have shown a correlation between bone marrow matrix loss and bone marrow unsaturation rate[15, 99]. Especially in osteoporotic subjects show a decrease of bone marrow unsaturation rate compared to healthy subjects[15, 30, 19, 16]. However, as the olefinic peak is often overlapped by a strong water peak with broad linewidth in vertebrae the measurement of the unsaturation rate can be difficult. The publication *"Estimating vertebral bone marrow fat unsaturation based on short-TE STEAM MRS"* [100] included in this thesis proposes a method to separate subjects with a reliable extraction of the unsaturation rate compared to subjects in which the unsaturation can not be extracted reliable due to high amount of water and broad linewidth.

4 Magnetic Resonance in Medicine

The magnetic resonance technique excels in giving contrast in soft tissue. For generating a contrast between different tissues or physiological and pathological changes, multiple physical properties of ^{1}H-protons are used. These are dependent on surrounding tissues, but also on the location of the ^{1}H-protons within a specific molecule. In MR, signal is generated from magnetic spins. The spins are aligned with the main magnetic field and the spins lie along the longitudinal axis. After the excitation of the spins, they switch to the transversal axis. After this short impulse, they start to slowly return to the longitudinal axis - they relax. This longitudinal relaxation time is called T_1 relaxation time or spin-lattice-time as it is depended on the surrounding tissue, the lattice. The T_2 relaxation time is the transversal relaxation time and is mainly depending on spin-spin interaction and is also called the spin-spin-relaxation time. T_2 relaxation time is always faster or equal to the T_1 relaxation time. These two parameters mainly influence the measured signal measured with the MR. Another crucial phenomenon for understanding the next paragraphs is the concept of chemical shift encoding (CSE). As mentioned above, the chemical bindings of the ^{1}H-protons and the properties of their respective bonding partners also affect the ^{1}H-protons. The surrounding electron clouds of these bounds are shielding the nucleus of the hydrogen protons and therefore have a small influence on the resonant frequencies. This effect is called chemical shift. At first, it was used to generate a water and a fat image by measuring one image with water and fat in-phase and one image with water and fat out-of-phase. With these two images you can calculate a water and a fat image. In addition, it is possible to calculate the fat fraction by dividing the fat signal by the sum of the water and fat signal. Over time, multiple physical effects like T_2^* decay or B_0 inhomogeneities were discovered and can be measured via CSE imaging. The chemical shift is stated as part per millions (ppm) as a fraction of the normal resonance frequency. Water is located at 4.70 ppm. Triglycerides have multiple different ^{1}H-protons and they all have small different resonant frequencies and with modern sequences these differences can be measured. Fig. 4.1 shows the model of triglyceride molecule. The letters represent ^{1}H-protons with different resonant frequencies. A stands for the methyl protons located at 0.90 ppm, B for methylene protons located at 1.30 ppm, C for *beta*-carboxyl protons located at 1.60 ppm, D for *alpha*-olefinic protons located at 2.02 ppm, E for *alpha*-carboxyl protons located at 2.24 ppm, F for diallylic protons located at 2.75 ppm, G, H and I represent glycerol protons located at 4.10 ppm, 4.30 ppm and 5.19 ppm, respectively and J stands for olefinic protons located at 5.29 pm. By differentiating individual protons within triglycerides, it is possible to extract further information about the respective fat tissue, e.g. the unsaturation rate.

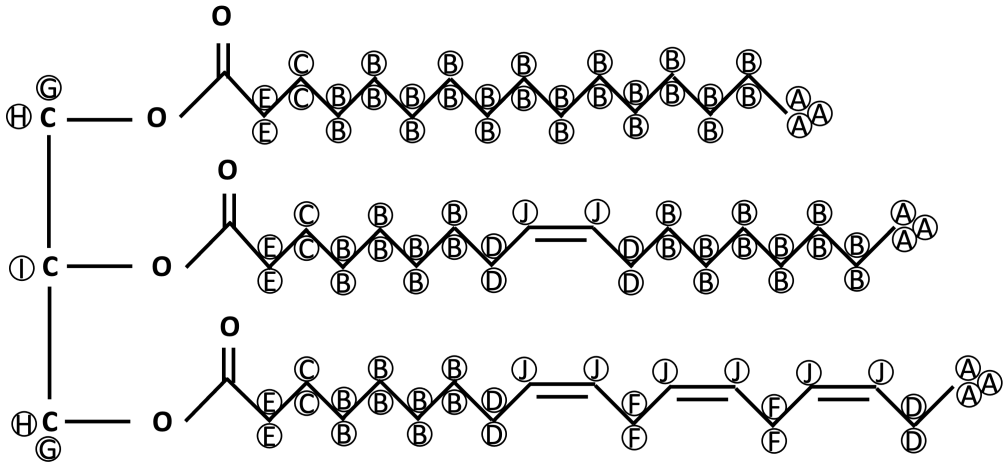

Figure 4.1: Example of a triglyceride composed of glycerol (left part), palmitic acid (top part), oleic acid (middle part) and alpha-linolenic acid (bottom part). The letters correspond to the respecting peaks in the spectroscopy.

4.1 Qualitative Imaging

Qualitative imaging is often used in clinical applications and provides good contrast between tissues and shows differences between physiological and pathological tissues. The generated images are called weighted-images and the contrast is only given by the signal difference within the voxels of the specific image and can not be compared between different time points or different subjects. The values behind the voxels do not represent a defined quantity and can only be assessed by the reader. The most commonly used sequences are T_1-weighted and T_2-weighted images. T_1-weighted images using different longitudinal relaxation times to get a contrast between different tissues. Fat has a short T_1 time and is therefore brighter on T_1-weighted images compared to water, which has a slower T_1 time. These sequences can be used to show fatty infiltration, e.g. in muscles[101] or in the liver[102]. It can also be used to specify bone marrow lesions in the spine [103]. Red bone marrow contains a lot of fatty acids and is therefore bright in T_1-weighted images. Malignant lesions like metastasis contains a much higher amount of water and will have lower signal. Another important use of T_1-weighted images is the use with contrast agent. Gadolinium has a very quick T_1 time and is therefore very bright in these images. It can indicate hypervascularization in e.g. areas of inflammation. T_2-weighted images rely on the vertical relaxation, the spin-spin-relaxation, to generate contrast. Tissues with longer T_2 relaxation time appear brighter in T_2-weighted images compared to tissues with a shorter T_2 time. Water and fat both have longer T_2-relaxation times, and therefore they appear brighter in these images. With T_2-weighted images fat suppression sequences are often used to get higher contrast in tissues with larger amounts of water, e.g. in oedema.

4.2 Quantitative Imaging

Quantitative imaging has become increasingly more popular in recent years and there is a large focus in research on the development of quantitative sequences. It offers the advantage of robust and objective parameters. While in qualitative imaging the value of a voxel is not specific and only shows a contrast to surrounding tissue, quantitative imaging shows absolute quantities of a tissue representing a physical property of the tissue. These values are comparable between multiple time points of the same subject or even between different subjects. This makes it easier to define scores and cut-off values within the framework of evidence-based medicine. This leads to a more personalized treatment of each individual subject. It also provides the opportunity to monitor the treatment process in a very objective way. Two commonly used sequences are the chemical-shift encoding water-fat imaging sequences which are described in section 4.2.1 and single-voxel MR spectroscopy which are described in section 4.2.2. These sequences were also used in this thesis.

4.2.1 Quantitative chemical-shift encoding water-fat Imaging

The water-fat imaging technique was developed by Thomas Dixon and described a sequence acquiring two echoes generating two images[104]. In one image the water and the fat signals were in-phase and in the other image the water and the fat signals were out-of-phase. The fat signal was assumed as only one peak, the methylene peak at 1.30 ppm. With these two images a water and a fat image could be generated, and also the fat fraction as a ratio of fat signal to the sum of water and fat signal could be calculated. With increasing knowledge about the MRI, e.g. B_0-inhomogeneity, T_2^*-decay or complex fat models as described in section 4, this technique was developed even further. Distinct measurement of T_2^* and the usage of more complex fat spectrums are confounding effects for PDFF quantification. Multiple echoes at different water-fat angles were acquired, which also opened the possibility to generate more different images. Modern quantitative multi-echo-based chemical-shift encoding sequences generate a fat image, a water image, a proton density fat-fraction image - which will be further discussed in more detail in section 4.3.1 -, a T_2^*-map and a B_0-map as it is shown in Fig. 4.2.

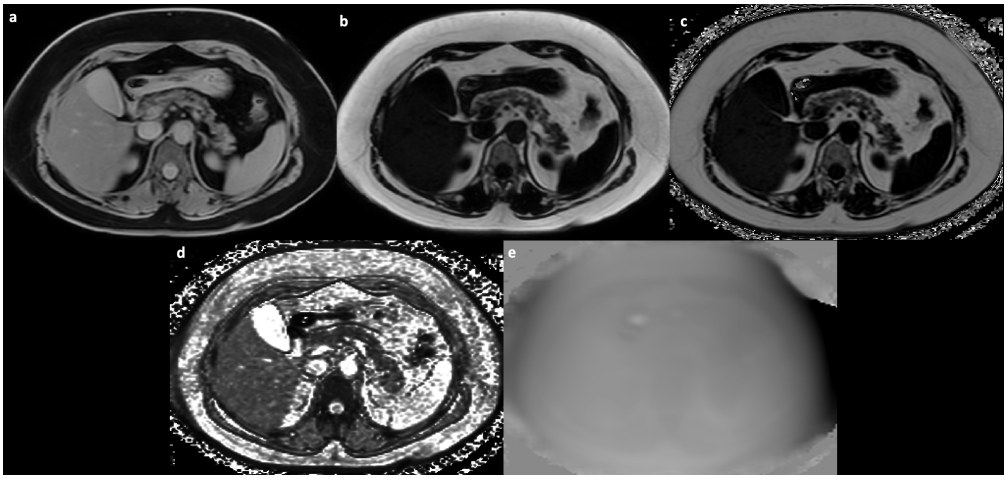

Figure 4.2: Example of a quantitative chemical-shift encoding based water-fat image with a) the water image, b) the fat image, c) the PDFF-map, d) the T_2^*-map and e) the B_0-map.

4.2.2 Single-voxel Magnetic Resonance Spectroscopy

^1H-MRS is a method to differentiate between the signal of different ^{1}H-protons depending on chemical-shift, as described in section 4. It helps to analyse the composition of a tissue in a homogenous well-defined volume of interest (VOI). In this thesis it was used to analyse the composition of fatty acids in bone marrow, but it can also be used to quantify various metabolites, such as neurotransmitters in the brain and choline in the liver. The major disadvantage of single-voxel MRS is that it has a very low spatial resolution. An example of a signal extracted from such a sequence is shown in Fig. 4.3. Each peak represents a different type of hydrogen proton. For example, the broad peak labelled A represents the signal of the methylene peak, the peak labelled B represents the water peak, and the peak labelled C represents the olefinic peak. Multiple peaks can be fitted into the MR spectrum and can be used for a detailed analysis of the corresponding volume of interest.

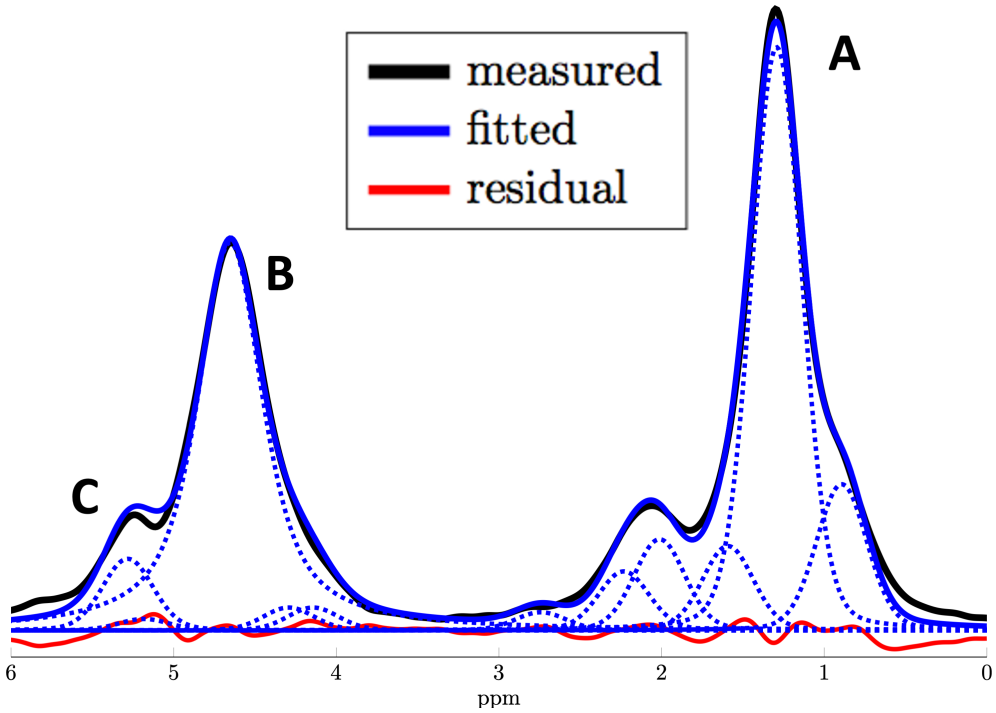

Figure 4.3: Example of a spectroscopie of a Stimulated Echo Acquisition Model sequence of the vertebra L5 with the black line representing the measured signal, the blue line the fitted signal and the red line the residuals. The letter A shows the main fat peak representing the methylene hydrogen protons, B the water peak and C the olefinic peak.

The most commonly used sequences are the point-resolved spectroscopy (PRESS) and the Stimulated echo acquisition mode (STEAM). While PRESS has the advantage of higher SNR and the possibility to acquire larger volume of interests, STEAM can be used with shorter echo times. In this thesis STEAM-MRS was performed.

4.3 Developing of Imaging Biomarkers

Based on quantitative sequences, imaging biomarkers can be developed. Biomarkers represent specific quantities in tissues. A biomarker is useful for clinical application if it measures a clinically relevant quantity. There are several conditions that a biomarker must meet. First, the biomarker must match the gold standard and therefore measure the correct quantity. That means the biomarker must be accurate. Second, the biomarker has to be robust to small changes in the setup. Third, the biomarker has to be precise, meaning it has to be repeatable between multiple time points and between multiple subjects. Fourth, the measurement has to be reproducible independent of scanner, operator or reader. A biomarker matching these conditions can be used in clinical application.

Initially, average values for these quantities can then be developed in healthy subjects

to provide a baseline and to show changes in healthy subjects, for example with age. In a next step, patients with diseases that have an impact on the tissues then can be compared with the healthy subjects and therefore diagnostic tools and sequences for specific diseases can be defined. Early changes can be seen with the MR and earlier diagnoses might be possible. If the changes are reversible, therapy monitoring is also possible.

The developing of biomarkers and their respective boundary values is a main focus of ongoing research. The quantitative imaging approach has the great advantage that the images of subjects can be evaluated objectively. Also, the amount of difference between subjects can be determined. Especially patients with changes in tissue affecting the suitable biomarkers benefit from the quantitative imaging as the degree of the changes can be determined. Depending on this information from studies, the degree of tissue alternations can be used to develop scores and classifications and then lead to a more personalized treatment. The research of automated build analysis using artificial intelligence also benefits from the use of quantitative imaging. In the following two sections the biomarkers proton density fat fraction (PDFF) and fat unsaturation range as these were used in this thesis.

4.3.1 Proton Density Fat Fraction

PDFF is a very reliable biomarker for measuring the fat concentration in a tissue. It is broadly used in the clinical environment as a diagnostic tool. It defined as density of the ^{1}H-protons in triglycerides divided by the sum of the density from triglycerides and water. The density is measured by CSE as described in section 4. PDFF can be measured with MRI as well as with MRS. The determination of PDFF can be very useful for monitoring different diseases. For example, it is used in the liver as a biomarker for early detection and therapy monitoring of NAFLD or other diseases with increase liver fat. As a healthy subject has close to no fat in the liver, even very small changes can be tracked using this method. An example of a liver with high and one with low PDFF are shown in Fig. 4.4.

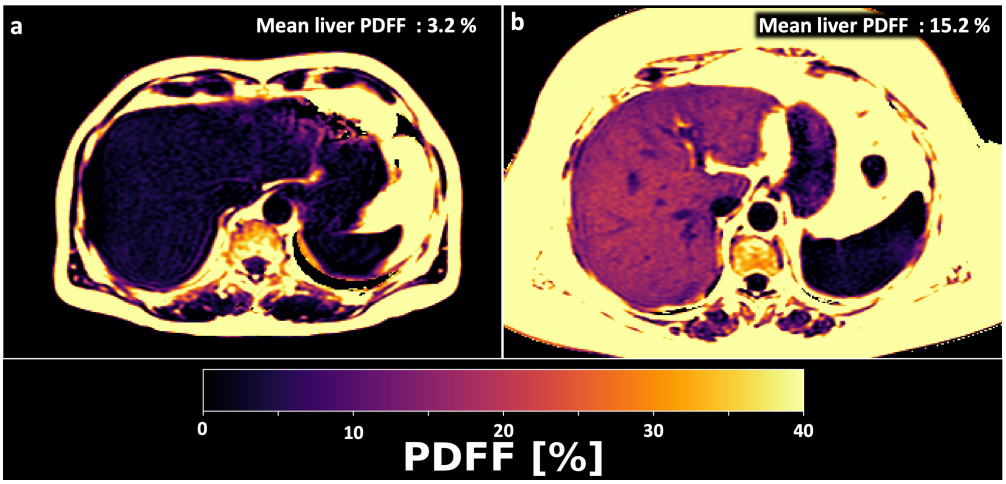

Figure 4.4: Example of two subjects with a) low liver PDFF and b) high liver PDFF.

Another example is the measurement of PDFF in the spine as a biomarker for the risk of osteoporosis. Here it is well established as a biomarker and shows strong correlation with Dual-Energy X-Ray Absorptiometry measurements. PDFF is known to increase with age and in the lower vertebrae.

4.3.2 Fat unsaturation rate

Fat unsaturation is measured with MRS by extracting the olefinic peak. With MR it is measured via MRS. It is defined as the signal of the olefinic peak at 5.30 ppm divided by the sum of the signal of all fat peaks. The accuracy is very much depending on the tissue. The main problem is the broad linewidth due to the low signal. As the water peak at 4.70 ppm is close to the olefinic peak, the water peak can overlay the olefinic peak. An example is shown in Fig. 4.5. In tissues without water the unsaturation rate is very well extractable, but in tissues with high amount of water, like the bone marrow in the spine it is more difficult. Overall, unsaturation rate is a more challenging biomarker compared to PDFF.

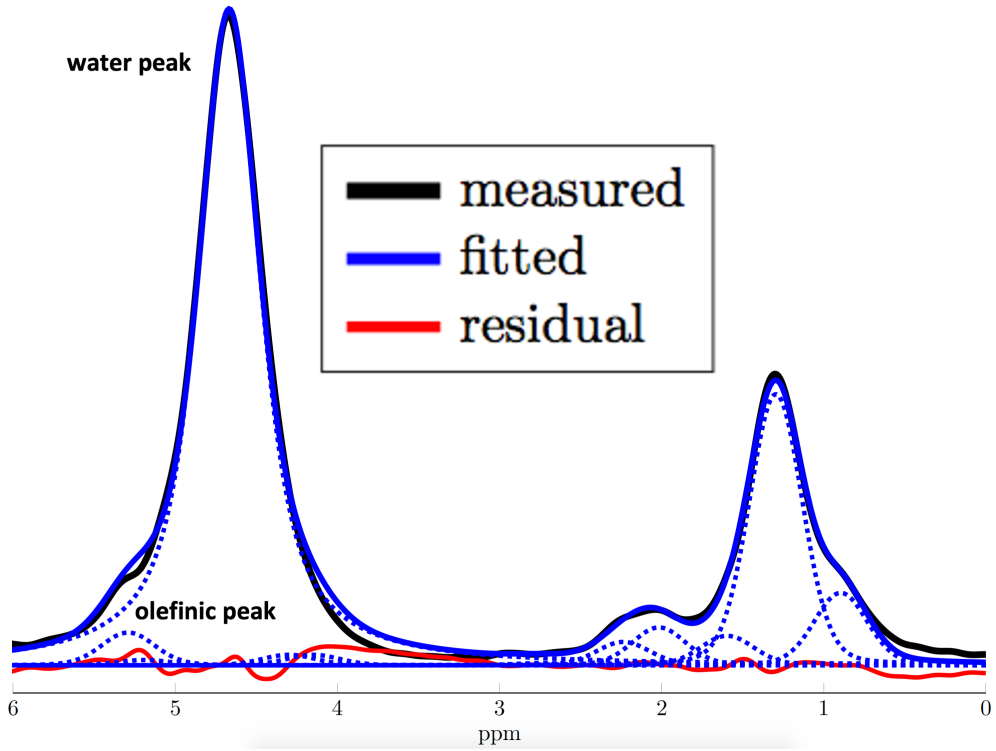

Figure 4.5: Example of a spectroscopy of a Stimulated echo acquisition model sequence of the vertebra L5 with the black line representing the measured signal, the blue line the fitted signal and the red line the residuals. The olefinic peak is mainly overlapped by the water peak and fitting results can vary depending on the fitting method.

5 Compliance with Ethical Standards

All investigations performed in studies involving human participants were in accordance with the ethical standards of the institutional and/or national research committee as well as the 1964 Helsinki declaration and its later amendments or comparable ethical standards. The included studies also were approved by the ethics comitee of the Technical University Munich (Ethik Votum 5802/13 S-AS). Informed consent was obtained from all individual participants included in the studies.

6 Journal Publications

6.1 Longitudinal changes on liver proton density fat fraction differ between liver segments

The publication entitled *Longitudinal changes on liver proton density fat fraction differ between liver segments* was published in Quantitative Imaging in Medicine and Surgery (Volume 11(5):1701-1709). The manuscript was authored by Jan Syväri, Daniela Junker, Lisa Patzelt, Katharina Kappo, Loubna Al Sadat, Sonia Erfanian, Marcus R. Makowski, Hans H. Hauner, Dimitrios C. Karampinos

6.1.1 Abstract

Background To study the spatial heterogeneity of liver fat fraction changes during a long-term lifestyle intervention study using magnetic resonance imaging (MRI).

Methods Thirty-two subjects underwent two MRI-scans in a span of one year. A chemical shift encoding-based water-fat separation method was applied to measure liver proton density fat fraction (PDFF) maps. The PDFF changes in the two liver lobes and the Couinaud segments were compared with the mean liver PDFF change.

Results The slope of the relationship between mean liver PDFF changes and PDFF liver lobe changes was higher in the right compared to the left lobe
($slope_{meanPDFF_{wholeliver} \sim meanPDFF_{rightlobe}} = 1.08$,
$slope_{meanPDFF_{wholeliver} \sim meanPDFF_{leftlobe}} = 0.93$, $P < 0.001$). The highest slope of agreement between PDFF changes in each specific liver segment and mean liver PDFF changes was observed in segment VII (slope = 1.12). The lowest slope of agreement between PDFF changes in each specific liver segment and mean liver PDFF changes was observed in segment I (slope = 0.77).

Conclusion Larger PDFF changes in the right liver lobe were observed compared to PDFF changes in the left liver lobe (LLL) in subjects with both increasing and decreasing mean liver PDFF after one year. The results are in line with the existing literature reporting a heterogeneous spatial distribution of liver fat and highlight the need to spatially resolve liver fat fraction changes in longitudinal studies.

6.1.2 Author contributions

I performed the recruitment and MRI scans of the study participants, manual segmentation of ROIs within each Couinaud segment of the liver as well as the post-processing, quantification and statistical analysis of MRI data using Python and R. In collaboration with the co-authors I designed the analyzed and interpreted the data and wrote the manuscript of the publication.

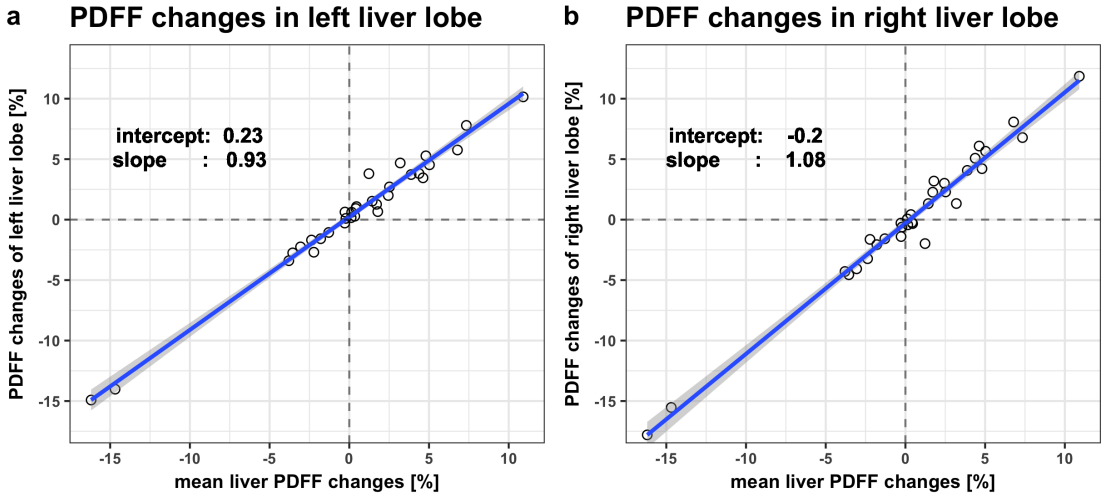

Figure 6.1: Changes of the liver PDFF in the LLL (A) and the RLL (B) as a function of mean liver PDFF change. The right lobe shows larger liver PDFF changes compared to the left lobe, visualized by the slopes of the regression line. PDFF, proton density fat fraction; LLL, left liver lobe; RLL, right liver lobe.

6.1.3 Copyright

Order Date	15-Dec-2022	**Type of Use**	Republish in a thesis/dissertation
Order License ID	1301177-1	**Publisher**	AME Publishing Company
ISSN	2223-4292	**Portion**	Chapter/article

LICENSED CONTENT

Publication Title	Quantitative imaging in medicine and surgery	**Publication Type**	Journal
Article Title	Longitudinal changes on liver proton density fat fraction differ between liver segments	**Start Page**	1701
		End Page	1709
		Issue	5
Date	01/01/2011	**Volume**	11
Language	English		
Country	China		
Rightsholder	Nancy International Ltd Subsidiary AME Publishing Company		

REQUEST DETAILS

Portion Type	Chapter/article	**Rights Requested**	Main product, any product related to main product, and other compilations/derivative products
Page Range(s)	1-9		
Total Number of Pages	9	**Distribution**	Worldwide
Format (select all that apply)	Print, Electronic	**Translation**	Original language of publication
Who Will Republish the Content?	Publisher, not-for-profit	**Copies for the Disabled?**	Yes
Duration of Use	Life of current and all future editions	**Minor Editing Privileges?**	Yes
Lifetime Unit Quantity	Up to 4,999	**Incidental Promotional Use?**	Yes
		Currency	EUR

NEW WORK DETAILS

Title	Magnetic Resonance Imaging and Spectroscopy based Quantification of Proton Density Fat Fraction and Fatty Acid Composition	**Institution Name**	Technical University Munich
		Expected Presentation Date	2023-02-01
Instructor Name	Jan Syväri		

ADDITIONAL DETAILS

Order Reference Number	N/A	**The Requesting Person/Organization to Appear on the License**	Jan Syväri

REUSE CONTENT DETAILS

Title, Description or Numeric Reference of the Portion(s)	Longitudinal changes on liver proton density fat fraction differ between liver segments	**Title of the Article/Chapter the Portion Is From**	Longitudinal changes on liver proton density fat fraction differ between liver segments
Editor of Portion(s)	Syväri, Jan; Junker, Daniela; Patzelt, Lisa; Kappo, Katharina; Al Sadat, Loubna; Erfanian, Sonia; Makowski, Marcus R.; Hauner, Hans; Karampinos, Dimitrios C.	**Author of Portion(s)**	Syväri, Jan; Junker, Daniela; Patzelt, Lisa; Kappo, Katharina; Al Sadat, Loubna; Erfanian, Sonia; Makowski, Marcus R.; Hauner, Hans; Karampinos, Dimitrios C.
Volume of Serial or Monograph	11	**Issue, if Republishing an Article From a Serial**	5
Page or Page Range of Portion	1701-1709	**Publication Date of Portion**	2021-05-01

RIGHTSHOLDER TERMS AND CONDITIONS

It is the responsibility of the users' to identify the copyright holder of any materials. If the user has any doubts, please contact the publisher at permissions@amegrouops.com. For illustrations owned by Ms. Croce, please contact beth@bioperspective.com.

Marketplace Order General Terms and Conditions

The following terms and conditions ("General Terms"), together with any applicable Publisher Terms and Conditions, govern User's use of Works pursuant to the Licenses granted by Copyright Clearance Center, Inc. ("CCC") on behalf of the applicable Rightsholders of such Works through CCC's applicable Marketplace transactional licensing services (each, a "Service").

1) **Definitions.** For purposes of these General Terms, the following definitions apply:

"License" is the licensed use the User obtains via the Marketplace platform in a particular licensing transaction, as set forth in the Order Confirmation.

"Order Confirmation" is the confirmation CCC provides to the User at the conclusion of each Marketplace transaction. "Order Confirmation Terms" are additional terms set forth on specific Order Confirmations not set forth in the General Terms that can include terms applicable to a particular CCC transactional licensing service and/or any Rightsholder-specific terms.

"Rightsholder(s)" are the holders of copyright rights in the Works for which a User obtains licenses via the Marketplace platform, which are displayed on specific Order Confirmations.

"Terms" means the terms and conditions set forth in these General Terms and any additional Order Confirmation Terms collectively.

"User" or "you" is the person or entity making the use granted under the relevant License. Where the person accepting the Terms on behalf of a User is a freelancer or other third party who the User authorized to accept the General Terms on the User's behalf, such person shall be deemed jointly a User for purposes of such Terms.

"Work(s)" are the copyright protected works described in relevant Order Confirmations.

2) **Description of Service.** CCC's Marketplace enables Users to obtain Licenses to use one or more Works in accordance with all relevant Terms. CCC grants Licenses as an agent on behalf of the copyright rightsholder identified in the relevant Order Confirmation.

3) **Applicability of Terms.** The Terms govern User's use of Works in connection with the relevant License. In the event of any conflict between General Terms and Order Confirmation Terms, the latter shall govern. User acknowledges that Rightsholders have complete discretion whether to grant any permission, and whether to place any limitations on any grant, and that CCC has no right to supersede or to modify any such discretionary act by a Rightsholder.

4) **Representations; Acceptance.** By using the Service, User represents and warrants that User has been duly authorized by the User to accept, and hereby does accept, all Terms.

5) **Scope of License; Limitations and Obligations.** All Works and all rights therein, including copyright rights, remain the sole and exclusive property of the Rightsholder. The License provides only those rights expressly set forth in the terms and conveys no other rights in any Works

6) **General Payment Terms.** User may pay at time of checkout by credit card or choose to be invoiced. If the User chooses to be invoiced, the User shall: (i) remit payments in the manner identified on specific invoices, (ii) unless otherwise specifically stated in an Order Confirmation or separate written agreement, Users shall remit payments upon receipt of the relevant invoice from CCC, either by delivery or notification of availability of the invoice via the Marketplace platform, and (iii) if the User does not pay the invoice within 30 days of receipt, the User may incur a service charge of 1.5% per month or the maximum rate allowed by applicable law, whichever is less. While User may exercise the rights in the License immediately upon receiving the Order Confirmation, the License is automatically revoked and is null and void, as if it had never been issued, if CCC does not receive complete payment on a timely basis.

7) **General Limits on Use.** Unless otherwise provided in the Order Confirmation, any grant of rights to User (i) involves only the rights set forth in the Terms and does not include subsequent or additional uses, (ii) is non-exclusive and non-transferable, and (iii) is subject to any and all limitations and restrictions (such as, but not limited to, limitations on duration of use or circulation) included in the Terms. Upon completion of the licensed use as set forth in the Order Confirmation, User shall either secure a new permission for further use of the Work(s) or immediately cease any new use of the Work(s) and shall render inaccessible (such as by deleting or by removing or severing links or other locators) any further copies of the Work. User may only make alterations to the Work if and as expressly set forth in the Order Confirmation. No Work may be used in any way that is defamatory, violates the rights of third parties (including such third parties' rights of copyright, privacy, publicity, or other tangible or intangible property), or is otherwise illegal, sexually explicit, or obscene. In addition, User may not conjoin a Work with any other material that may result in damage to the reputation of the Rightsholder. User agrees to inform CCC if it becomes aware of any infringement of any rights in a Work and to cooperate with any reasonable request of CCC or the Rightsholder in connection therewith.

8) **Third Party Materials.** In the event that the material for which a License is sought includes third party materials (such as photographs, illustrations, graphs, inserts and similar materials) that are identified in such material as having been used by permission (or a similar indicator), User is responsible for identifying, and seeking separate licenses (under this Service, if available, or otherwise) for any of such third party materials; without a separate license, User may not use such third party materials via the License.

9) **Copyright Notice.** Use of proper copyright notice for a Work is required as a condition of any License granted under the Service. Unless otherwise provided in the Order Confirmation, a proper copyright notice will read substantially as follows: "Used with permission of [Rightsholder's name], from [Work's title, author, volume, edition number and year of copyright]; permission conveyed through Copyright Clearance Center, Inc." Such notice must be provided in a reasonably legible font size and must be placed either on a cover page or in another location that any person, upon gaining access to the material which is the subject of a permission, shall see, or in the case of republication Licenses, immediately adjacent to the Work as used (for example, as part of a by-line or footnote) or in the place where substantially all other credits or notices for the new work containing the republished Work are located. Failure to include the required notice results in loss to the Rightsholder and CCC, and the User shall be liable to pay liquidated damages for each such failure equal to twice the use fee specified in the Order Confirmation, in addition to the use fee itself and any other fees and charges specified.

10) **Indemnity.** User hereby indemnifies and agrees to defend the Rightsholder and CCC, and their respective employees and directors, against all claims, liability, damages, costs, and expenses, including legal fees and expenses, arising out of any use of a Work beyond the scope of the rights granted herein and in the Order Confirmation, or any use of a Work which has been altered in any unauthorized way by User, including claims of defamation or infringement of rights of copyright, publicity, privacy, or other tangible or intangible property.

11) **Limitation of Liability.** UNDER NO CIRCUMSTANCES WILL CCC OR THE RIGHTSHOLDER BE LIABLE FOR ANY DIRECT, INDIRECT, CONSEQUENTIAL, OR INCIDENTAL DAMAGES (INCLUDING WITHOUT LIMITATION DAMAGES FOR LOSS OF BUSINESS PROFITS OR INFORMATION, OR FOR BUSINESS INTERRUPTION) ARISING OUT OF THE USE OR INABILITY TO USE A WORK, EVEN IF ONE OR BOTH OF THEM HAS BEEN ADVISED OF THE POSSIBILITY OF SUCH DAMAGES. In any event, the total liability of the Rightsholder and CCC (including their respective employees and directors) shall not exceed the total amount actually paid by User for the relevant License. User assumes full liability for the actions and omissions of its principals, employees, agents, affiliates, successors, and assigns.

12) **Limited Warranties.** THE WORK(S) AND RIGHT(S) ARE PROVIDED "AS IS." CCC HAS THE RIGHT TO GRANT TO USER THE RIGHTS GRANTED IN THE ORDER CONFIRMATION DOCUMENT. CCC AND THE RIGHTSHOLDER DISCLAIM ALL OTHER WARRANTIES RELATING TO THE WORK(S) AND RIGHT(S), EITHER EXPRESS OR IMPLIED, INCLUDING WITHOUT LIMITATION IMPLIED WARRANTIES OF MERCHANTABILITY OR FITNESS FOR A PARTICULAR PURPOSE. ADDITIONAL RIGHTS MAY BE REQUIRED TO USE ILLUSTRATIONS, GRAPHS, PHOTOGRAPHS, ABSTRACTS, INSERTS, OR OTHER PORTIONS OF THE WORK (AS OPPOSED TO THE ENTIRE WORK) IN A MANNER CONTEMPLATED BY USER; USER UNDERSTANDS AND AGREES THAT NEITHER CCC NOR THE RIGHTSHOLDER MAY HAVE SUCH ADDITIONAL RIGHTS TO GRANT.

13) **Effect of Breach.** Any failure by User to pay any amount when due, or any use by User of a Work beyond the scope of the License set forth in the Order Confirmation and/or the Terms, shall be a material breach of such License. Any breach not cured within 10 days of written notice thereof shall result in immediate termination of such License without further notice. Any unauthorized (but licensable) use of a Work that is terminated immediately upon notice thereof may be liquidated by payment of the Rightsholder's ordinary license price therefor; any unauthorized (and unlicensable) use that is not terminated immediately for any reason (including, for example, because materials containing the Work cannot reasonably be recalled) will be subject to all remedies available at law or in equity, but in no event to a payment of less than three times the Rightsholder's ordinary license price for the most closely analogous licensable use plus Rightsholder's and/or CCC's costs and expenses incurred in collecting such payment.

14) **Additional Terms for Specific Products and Services.** If a User is making one of the uses described in this Section 14, the additional terms and conditions apply:

a) ***Print Uses of Academic Course Content and Materials (photocopies for academic coursepacks or classroom handouts).*** For photocopies for academic coursepacks or classroom handouts the following additional terms apply:

i) The copies and anthologies created under this License may be made and assembled by faculty members individually or at their request by on-campus bookstores or copy centers, or by off-campus copy shops and other similar entities.

ii) No License granted shall in any way: (i) include any right by User to create a substantively non-identical copy of the Work or to edit or in any other way modify the Work (except by means of deleting material immediately preceding or following the entire portion of the Work copied) (ii) permit "publishing ventures" where any particular anthology would be systematically marketed at multiple institutions.

iii) Subject to any Publisher Terms (and notwithstanding any apparent contradiction in the Order Confirmation arising from data provided by User), any use authorized under the academic pay-per-use service is limited as follows:

A) any License granted shall apply to only one class (bearing a unique identifier as assigned by the institution, and thereby including all sections or other subparts of the class) at one institution;

B) use is limited to not more than 25% of the text of a book or of the items in a published collection of essays, poems or articles;

C) use is limited to no more than the greater of (a) 25% of the text of an issue of a journal or other periodical or (b) two articles from such an issue;

D) no User may sell or distribute any particular anthology, whether photocopied or electronic, at more than one institution of learning;

E) in the case of a photocopy permission, no materials may be entered into electronic memory by User except in order to produce an identical copy of a Work before or during the academic term (or analogous period) as to which any particular permission is granted. In the event that User shall choose to retain materials that are the subject of a photocopy permission in electronic memory for purposes of producing identical copies more than one day after such retention (but still within the scope of any permission granted), User must notify CCC of such fact in the applicable permission request and such retention shall constitute one copy actually sold for purposes of calculating permission fees due; and

F) any permission granted shall expire at the end of the class. No permission granted shall in any way include any right by User to create a substantively non-identical copy of the Work or to edit or in any other way modify the Work (except by means of deleting material immediately preceding or following the entire portion of the Work copied).

iv) Books and Records; Right to Audit. As to each permission granted under the academic pay-per-use Service, User shall maintain for at least four full calendar years books and records sufficient for CCC to determine the numbers of copies made by User under such permission. CCC and any representatives it may designate shall have the right to audit such books and records at any time during User's ordinary business hours, upon two days' prior notice. If any such audit shall determine that User shall have underpaid for, or underreported, any photocopies sold or by three percent (3%) or more, then User shall bear all the costs of any such audit; otherwise, CCC shall bear the costs of any such audit. Any amount determined by such audit to have been underpaid by User shall immediately be paid to CCC by User, together with interest thereon at the rate of 10% per annum from the date such amount was originally due. The provisions of this paragraph shall survive the termination of this License for any reason.

b) ***Digital Pay-Per-Uses of Academic Course Content and Materials (e-coursepacks, electronic reserves, learning management systems, academic institution intranets).*** For uses in e-coursepacks, posts in electronic reserves, posts in learning management systems, or posts on academic institution intranets, the following additional terms apply:

i) The pay-per-uses subject to this Section 14(b) include:

A) **Posting e-reserves, course management systems, e-coursepacks for text-based content,** which grants authorizations to import requested material in electronic format, and allows electronic access to this material to members of a designated college or university class, under the direction of an instructor designated by the college or university, accessible only under appropriate electronic controls (e.g., password);

B) **Posting e-reserves, course management systems, e-coursepacks for material consisting of photographs or other still images not embedded in text,** which grants not only the authorizations described in Section 14(b)(i)(A) above, but also the following authorization: to include the requested material in course materials for use consistent with Section 14(b)(i)(A) above, including any necessary resizing, reformatting or modification of the resolution of such requested material (provided that such modification does not alter the underlying editorial content or meaning of the requested material, and provided that the resulting modified content is used solely within the scope of, and in a manner consistent with, the particular authorization described in the Order Confirmation and the Terms), but not including any other form of manipulation, alteration or editing of the requested material;

C) **Posting e-reserves, course management systems, e-coursepacks or other academic distribution for audiovisual content,** which grants not only the authorizations described in Section 14(b)(i)(A) above, but also the following authorizations: (i) to include the requested material in course materials for use consistent with Section 14(b)(i)(A) above; (ii) to display and perform the requested material to such members of such class in the physical classroom or remotely by means of streaming media or other video formats; and (iii) to "clip" or reformat the requested material for purposes of time or content management or ease of delivery, provided that such "clipping" or reformatting does not alter the underlying editorial content or meaning of the requested material and that the resulting material is used solely within the scope of, and in a manner consistent with, the particular authorization described in the Order Confirmation and the Terms. Unless expressly set forth in the relevant Order Conformation, the License does not

authorize any other form of manipulation, alteration or editing of the requested material.

ii) Unless expressly set forth in the relevant Order Confirmation, no License granted shall in any way: (i) include any right by User to create a substantively non-identical copy of the Work or to edit or in any other way modify the Work (except by means of deleting material immediately preceding or following the entire portion of the Work copied or, in the case of Works subject to Sections 14(b)(1)(B) or (C) above, as described in such Sections) (ii) permit "publishing ventures" where any particular course materials would be systematically marketed at multiple institutions.

iii) Subject to any further limitations determined in the Rightsholder Terms (and notwithstanding any apparent contradiction in the Order Confirmation arising from data provided by User), any use authorized under the electronic course content pay-per-use service is limited as follows:

A) any License granted shall apply to only one class (bearing a unique identifier as assigned by the institution, and thereby including all sections or other subparts of the class) at one institution;

B) use is limited to not more than 25% of the text of a book or of the items in a published collection of essays, poems or articles;

C) use is limited to not more than the greater of (a) 25% of the text of an issue of a journal or other periodical or (b) two articles from such an issue;

D) no User may sell or distribute any particular materials, whether photocopied or electronic, at more than one institution of learning;

E) electronic access to material which is the subject of an electronic-use permission must be limited by means of electronic password, student identification or other control permitting access solely to students and instructors in the class;

F) User must ensure (through use of an electronic cover page or other appropriate means) that any person, upon gaining electronic access to the material, which is the subject of a permission, shall see:

- a proper copyright notice, identifying the Rightsholder in whose name CCC has granted permission,
- a statement to the effect that such copy was made pursuant to permission,
- a statement identifying the class to which the material applies and notifying the reader that the material has been made available electronically solely for use in the class, and
- a statement to the effect that the material may not be further distributed to any person outside the class, whether by copying or by transmission and whether electronically or in paper form, and User must also ensure that such cover page or other means will print out in the event that the person accessing the material chooses to print out the material or any part thereof.

G) any permission granted shall expire at the end of the class and, absent some other form of authorization, User is thereupon required to delete the applicable material from any electronic storage or to block electronic access to the applicable material.

iv) Uses of separate portions of a Work, even if they are to be included in the same course material or the same university or college class, require separate permissions under the electronic course content pay-per-use Service. Unless otherwise provided in the Order Confirmation, any grant of rights to User is limited to use completed no later than the end of the academic term (or analogous period) as to which any particular permission is granted.

v) Books and Records; Right to Audit. As to each permission granted under the electronic course content Service, User shall maintain for at least four full calendar years books and records sufficient for CCC to determine the numbers of copies made by User under such permission. CCC and any representatives it may designate shall have the right to audit such books and records at any time during User's ordinary business hours, upon two days' prior notice. If any such audit shall determine that User shall have underpaid for, or underreported, any electronic copies used by three percent (3%) or more, then User shall bear all the costs of any such audit; otherwise, CCC shall bear the costs of any such audit. Any amount determined by such audit to have been underpaid by User shall immediately be paid to CCC by User, together with interest thereon at the rate of 10% per annum from the date such amount was originally due. The provisions of this paragraph shall survive the termination of this license for any reason.

c) ***Pay-Per-Use Permissions for Certain Reproductions (Academic photocopies for library reserves and interlibrary loan reporting) (Non-academic internal/external business uses and commercial document delivery).*** The License expressly excludes the uses listed in Section (c)(i)-(v) below (which must be subject to separate license from the applicable Rightsholder) for: academic photocopies for library reserves and interlibrary loan reporting; and non-academic internal/external business uses and commercial document delivery.

i) electronic storage of any reproduction (whether in plain-text, PDF, or any other format) other than on a transitory basis;

ii) the input of Works or reproductions thereof into any computerized database;

iii) reproduction of an entire Work (cover-to-cover copying) except where the Work is a single article;

iv) reproduction for resale to anyone other than a specific customer of User;

v) republication in any different form. Please obtain authorizations for these uses through other CCC services or directly from the rightsholder.

Any license granted is further limited as set forth in any restrictions included in the Order Confirmation and/or in these Terms.

d) ***Electronic Reproductions in Online Environments (Non-Academic-email, intranet, internet and extranet).*** For "electronic reproductions", which generally includes e-mail use (including instant messaging or other electronic transmission to a defined group of recipients) or posting on an intranet, extranet or Intranet site (including any display or performance incidental thereto), the following additional terms apply:

i) Unless otherwise set forth in the Order Confirmation, the License is limited to use completed within 30 days for any use on the Internet, 60 days for any use on an intranet or extranet and one year for any other use, all as measured from the "republication date" as identified in the Order Confirmation, if any, and otherwise from the date of the Order Confirmation.

ii) User may not make or permit any alterations to the Work, unless expressly set forth in the Order Confirmation (after request by User and approval by Rightsholder); provided, however, that a Work consisting of photographs or other still images not embedded in text may, if necessary, be resized, reformatted or have its resolution modified without additional express permission, and a Work consisting of audiovisual content may, if necessary, be "clipped" or reformatted for purposes of time or content management or ease of delivery (provided that any such resizing, reformatting, resolution modification or “clipping” does not alter the underlying editorial content or meaning of the Work used, and that the resulting material is used solely within the scope of, and in a manner consistent with, the particular License described in the Order Confirmation and the Terms.

15) **Miscellaneous.**

a) User acknowledges that CCC may, from time to time, make changes or additions to the Service or to the Terms, and that Rightsholder may make changes or additions to the Rightsholder Terms. Such updated Terms will replace the prior terms and conditions in the order workflow and shall be effective as to any subsequent Licenses but shall not apply to Licenses already granted and paid for under a prior set of terms.

b) Use of User-related information collected through the Service is governed by CCC's privacy policy, available online at www.copyright.com/about/privacy-policy/.

c) The License is personal to User. Therefore, User may not assign or transfer to any other person (whether a natural person or an organization of any kind) the License or any rights granted thereunder; provided, however, that, where applicable, User may assign such License in its entirety on written notice to CCC in the event of a transfer of all or substantially all of User's rights in any new material which includes the Work(s) licensed under this Service.

d) No amendment or waiver of any Terms is binding unless set forth in writing and signed by the appropriate parties, including, where applicable, the Rightsholder. The Rightsholder and CCC hereby object to any terms contained in any writing prepared by or on behalf of the User or its principals, employees, agents or affiliates and purporting to govern or otherwise relate to the License described in the Order Confirmation, which terms are in any way inconsistent with any Terms set forth in the Order Confirmation, and/or in CCC's standard operating procedures, whether such writing is prepared prior to, simultaneously with or subsequent to the Order Confirmation, and whether such writing appears on a copy of the Order Confirmation or in a separate instrument.

e) The License described in the Order Confirmation shall be governed by and construed under the law of the State of New York, USA, without regard to the principles thereof of conflicts of law. Any case, controversy, suit, action, or proceeding arising out of, in connection with, or related to such License shall be brought, at CCC's sole discretion, in any federal or state court located in the County of New York, State of New York, USA, or in any federal or state court whose geographical jurisdiction covers the location of the Rightsholder set forth in the Order Confirmation. The parties expressly submit to the personal jurisdiction and venue of each such federal or state court.

Original Article

Longitudinal changes on liver proton density fat fraction differ between liver segments

Jan Syväri[1], Daniela Junker[1], Lisa Patzelt[1], Katharina Kappo[2], Loubna Al Sadat[2], Sonia Erfanian[2], Marcus R. Makowski[1], Hans Hauner[2,3], Dimitrios C. Karampinos[1]

[1]Department of Diagnostic and Interventional Radiology, School of Medicine, Technical University of Munich, Munich, Germany; [2]Institute for Nutritional Medicine, Else Kroener-Fresenius-Center of Nutritional Medicine, School of Medicine, Technical University of Munich, Munich, Germany; [3]German Center for Diabetes Research, Helmholtz Diabetes Center, Neuherberg, Germany

Correspondence to: Jan Syväri. Department of Diagnostic and Interventional Radiology, Klinikum rechts der Isar, Technische Universität München, Ismaninger Str. 22, 81675 Munich, Germany. Email: jan.syvaeri@tum.de.

Background: To study the spatial heterogeneity of liver fat fraction changes during a long-term lifestyle intervention study using magnetic resonance imaging (MRI).

Methods: Thirty-two subjects underwent two MRI-scans in a span of one year. A chemical shift encoding-based water-fat separation method was applied to measure liver proton density fat fraction (PDFF) maps. The PDFF changes in the two liver lobes and the Couinaud segments were compared with the mean liver PDFF change.

Results: The slope of the relationship between mean liver PDFF changes and PDFF liver lobe changes was higher in the right compared to the left lobe ($slope_{\text{mean PDFF whole liver ~ mean PDFF right lobe}}$ =1.08, $slope_{\text{mean PDFF whole liver ~ mean PDFF left lobe}}$ =0.93, P<0.001). The highest slope of agreement between PDFF changes in each specific liver segment and mean liver PDFF changes was observed in segment VII (slope =1.12). The lowest slope of agreement between PDFF changes in each specific liver segment and mean liver PDFF changes was observed in segment I (slope =0.77).

Conclusions: Larger PDFF changes in the right liver lobe were observed compared to PDFF changes in the left liver lobe (LLL) in subjects with both increasing and decreasing mean liver PDFF after one year. The results are in line with the existing literature reporting a heterogeneous spatial distribution of liver fat and highlight the need to spatially resolve liver fat fraction changes in longitudinal studies.

Keywords: Lifestyle intervention study; liver fat fraction spatial heterogeneity; quantitative MRI; Dixon MRI; proton density fat fraction (PDFF)

Submitted Jul 15, 2020. Accepted for publication Nov 19, 2020.
doi: 10.21037/qims-20-873
View this article at: http://dx.doi.org/10.21037/qims-20-873

Introduction

A sedentary lifestyle and chronic over-nutrition are the leading causes for the increasing rates of overweight, metabolic syndrome and subsequently type 2 diabetes in many countries around the globe (1-3). The metabolic syndrome is associated with fat deposition in the liver, and eventually with the occurrence of nonalcoholic fatty liver disease (NAFLD) (4), which is a main cause of chronic liver disease (5). Specifically, patients with NAFLD are at high risk of developing liver fibrosis and liver cirrhosis leading to irreversible liver dysfunction and eventually are at high risk for liver carcinoma or other fatal complications (6). It is well known that early fat deposition in the liver caused by over-nutrition and the lack of exercise is reversible (7,8). Therefore, tracking liver fat changes in patients with NAFLD is important for both risk assessment and treatment.

Measuring liver fat is feasible using either invasive or

non-invasive methods. Liver biopsy is considered the gold standard for measuring liver fat in single locations (9). However, since liver biopsy is highly invasive, its use in longitudinal studies can be associated with strong discomfort for the patient and other complications. Single-voxel magnetic resonance spectroscopy (MRS) has been shown to be a very reliable way of non-invasively measuring the liver proton density fat fraction (PDFF) (10). However, single-voxel MRS has limited spatial coverage as it typically reports the result on one specific area of the liver per measurement. Therefore, neither biopsy nor single-voxel MRS can cover the whole liver and therefore cannot detect any heterogeneity in liver fat deposition. In addition, repetitive measurements could become difficult to perform using techniques with limited spatial coverage, since the selection of the exact same region during the measurement at different timepoints is more difficult to execute.

Magnetic resonance imaging (MRI)-based PDFF mapping has been alternatively emerging as a reliable and accurate technique for spatially resolving liver fat fraction non-invasively. MRI-based PDFF has been validated as a biomarker in comparison with MRS and biopsies (11,12). MRI-based liver PDFF mapping adds the advantage of spatially covering the whole organ with adequate resolution and therefore enables the investigation of liver fat distribution throughout the whole organ taking into consideration any differences between the individual Couinaud liver segments. In addition, as the whole liver is covered during the scan, placing of regions of interests (ROI) after the scan can be easily compared to previous measurements of the same subject, which is important for longitudinal measurements.

Multiple cross-sectional studies have reported heterogeneous liver fat distribution across different lobes and segments (13-16). Recently, Fazeli Dehkordy *et al.* (17) showed, based on PDFF mapping, a heterogeneity in liver fat distribution both at baseline and after bariatric weight-loss surgery and reported right lobe segments having higher PDFF at baseline and a more rapid reduction in liver PDFF than left lobe segments. In this study, all subjects lost weight after surgery and showed a decreasing PDFF across all liver segments and lobes. However, it is not known how the spatial distribution of the PDFF is changing in a longitudinal setting, where subjects participating in a long-term lifestyle intervention study might either gain or lose weight during the intervention.

The purpose of our study was to study the spatial heterogeneity of PDFF changes in subjects participating in a long-term lifestyle intervention study and show variable changes in body weight.

Methods

Subjects

Thirty-two subjects (18 women and 14 men) participating in a German wide prospective, randomized, multicenter lifestyle intervention study at the Else Kröner-Fresenius-Center for Nutritional Medicine, Technical University of Munich, with MRI scans at two different time points within a time interval of one year were included in the present analysis. Inclusion criteria were age between 18 and 75 years and a high risk of developing diabetes mellitus type 2 by scoring more than 50 points in the screening questionnaire "German Diabetes Risk Test" (18). The subjects received nutritional counseling for one year covering multiple appointments. It included discussing nutritional protocols, information and recommendations on healthy eating and moderate energy restriction for losing weight, and individual guidance for more exercise. Further inclusion and exclusion criteria and more details about the intervention can be found at (19). The present dataset includes 17 subjects scanned before the beginning of the intervention and after 1 year and 15 subjects scanned after the end of the intervention at two time points with an interval of 1 year when weight regain was frequently occurring.

MRI measurements

The study was approved by an ethics committee and all subjects gave written informed consent before participation in the study including repeated MRI scanning. MRI was performed on a whole-body-MRI-scanner (Ingenia, 3.0T, Philips Healthcare, Best, The Netherlands) using the built in 12-channel posterior and 16-channel anterior coil.

The MRI acquisition consisted of an axial six-echo multi-echo 3D spoiled gradient echo sequence for chemical shift-encoding based water-fat separation of the abdomen using bipolar gradient readouts. The acquisition time was 14.1 s and was performed with a single breath hold and covered the liver, with the following parameters: TR/TE1/ΔTE =7.8/1.3/1.1 ms, echoes =6, FOV =300×402.6×150 mm^3, acquisition voxel size =1.97×3.01×6.00 mm^3, acquisition matrix =152×133, SENSE reduction factor =2.2 (RL) ×1.2 (FH), frequency direction = A/P, bandwidth =1,522.8 Hz, NSA =1, flip angle =3°.

Complex multi-echo gradient-echo images were generated and provided as input to the fat quantification algorithm provided by the vendor (mDixon Quant, Philips Healthcare), including the following steps: a phase correction step was performed first to address eddy current-induced phase errors. Field inhomogeneity-induced misregistration effects and chemical shift-induced mis-registration effects were minimized by using the maximum receiver bandwidth. A complex-based water-fat decomposition was performed next using a single T_2* correction and a pre-calibrated fat spectrum accounting for the multi-peak nature of the fat spectrum. A seven-peak fat spectrum model was used (20). The PDFF map was computed as the ratio of the fat signal over the sum of fat and water signals and the magnitude discrimination approach was used to reduce noise bias effects (21).

Segmentation of liver PDFF

In each Couinaud segment (22) of the liver, a circular ROI with a diameter of 20 mm (volume of ~1,885 mm^3) was placed by a researcher (JS) with 2 years of experience in liver segmentation with 3D Slicer as described by Tang (23). Liver PDFF was calculated per ROI in each segment. Mean liver PDFF was calculated as the mean of all ROIs from each segment. For mean PDFF of left liver lobe (LLL), the mean PDFF of the ROIs of segments I, II, III, IVa and IVb, and for the right liver lobe (RLL) of the segments V, VI, VII and VIII, respectively, were calculated.

For inter-observer analysis, 7 subjects (21.9%) were segmented by a second observer (LP, 1 year of experience in liver segmentation) and the inter-observer correlations for mean PDFF of whole liver, liver lobes and liver segments were calculated to study the reproducibility of the segmentation.

Statistical analysis

Statistical analyses were performed with RStudio [RStudio Team (2016). RStudio: Integrated Development for R. RStudio, Inc., Boston, MA, URL http://www.rstudio.com/]. Linear regression was calculated with Pearson correlation coefficient analysis with 0.05 level of significance. Two-sided paired *t*-test was used to calculate differences in fat content between liver lobes with 0.05 level of significance. A statistical test was performed to compare the slope between PDFF changes in the LLL and mean PDFF changes and the slope between PDFF changes in the RLL and mean PDFF changes, using a z statistic defined by the difference between the slopes of the regression lines divided by the standard error of the differences between the slopes (24). The intraclass correlation coefficient (ICC) was used to calculate inter-observer agreement.

Results

Subjects' characteristics

The age range of the scanned subjects was from 24 to 76 (mean: 54.3) years at the timepoint of the first MRI scan. Subjects showed weight changes ranging from +11.1 kg (+11.4%) to –11.4 kg (–10.1%) with a mean absolute change of 3.8 kg; 17 subjects showed weight gain (mean weight increase: +3.8±2.9 kg) and 15 subjects showed weight loss over the period of 1 year (mean weight decrease: –4.0±3.5 kg). The subjects did not show different changes in weight depending on the starting point (starting point before intervention: –1.2±4.9 kg, starting point after intervention: +1.4±5.0 kg).

Inter-observer analysis

The ICC for PDFF values between the two observers per liver segment was 0.998 for segment I, 0.994 for segment II, 0.994 for segment III, 0.989 for segment IVa, 0.998 for segment IVb, 0.986 for segment V, 0.997 for segment VI, 0.998 for segment VII and 0.999 for segment VIII. The ICC for the total mean liver PDFF change was 0.998, for the PDFF change of the RLL was 0.998 and for the PDFF change of the LLL was 0.998.

PDFF spatial variation at baseline and follow-up

At baseline, the median PDFF was 7.5% in the RLL (range, 0.6–43.8%) and 5.5% in the LLL (range, 0.8–39.9%) (paired *t*-test: P<0.001). At 1-year follow-up, the median PDFF was 9.2% in the RLL (range, 2.8–42.4%) and 6.7% in the LLL (range, 1.6–41.6%) (paired *t*-test: P<0.001). All results of the individual segments are shown in *Table 1*.

Correlation between mean liver PDFF and PDFF of specific lobes and segments at baseline

Strong correlations were observed between the mean liver PDFF and the PDFFs for the different lobes and segments (P<0.001 for both lobes and all segments). The liver PDFF

Table 1 Values of mean, standard deviation (SD), median and range of PDFF in % of total liver mass, left liver lobe, right liver lobe and specific liver segments at baseline and follow-up scans

Region	Baseline (I)/follow-up (II)	Mean (%)	SD (%)	Median (%)	Min (%)	Max (%)
Total liver	I	9.8	9.7	6.4	0.7	41.7
	II	10.2	9.5	7.7	2.1	41.4
Right lobe	I	10.9	10.1	7.6	0.6	43.8
	II	11.1	9.5	9.2	2.8	42.4
Left love	I	8.8	9.4	5.5	0.8	39.9
	II	9.5	9.5	6.7	1.6	41.6
Seg I	I	7.7	9.2	5.1	–1.2	37.7
	II	8.3	9.2	5.8	1.0	39.7
Seg II	I	9.4	9.7	6.2	–0.3	42.1
	II	10.1	9.9	7.9	1.6	45.5
Seg III	I	8.9	10.1	5.4	0.1	43.2
	II	10.0	10.2	7.2	0.9	45.2
Seg IVa	I	9.0	8.9	5.6	1.4	36.4
	II	9.4	8.7	6.6	0.7	37.9
Seg IVb	I	9.2	9.8	5.7	0.7	40.1
	II	9.5	10.0	6.3	1.3	43.2
Seg V	I	10.1	10.4	6.3	0.3	42.2
	II	10.2	9.0	7.4	1.6	39.7
Seg VI	I	10.9	9.7	8.2	–0.1	43.0
	II	10.7	8.4	9.5	3.0	38.7
Seg VII	I	10.9	10.2	7.1	0.5	44.9
	II	11.7	10.3	9.2	2.6	46.6
Seg VIII	I	11.6	10.6	8.3	1.9	45.3
	II	11.7	10.7	8.8	2.2	44.7

PDFF, proton density fat fraction.

of both lobes showed a close correlation with mean liver PDFF ($R^2_{\text{left lobe}}$ =0.99, $R^2_{\text{right lobe}}$ =0.98, respectively). Highest R^2 values of agreement with the mean PDFF were observed in segments IVa (R^2 =0.99), IVb (R^2 =0.99) and VI (R^2 =0.98). The lowest R^2 values were observed in the segments I (R^2 =0.96), II (R^2 =0.96) and IX (R^2 =0.96).

Comparison of individual lobe PDFF changes

Figure 1 shows two examples of liver PDFF maps at baseline and follow-up for a subject with increasing liver PDFF (*Figure 1A*,*B*) and for a subject with decreasing liver PDFF (*Figure 1C*,*D*). In both subjects, the absolute PDFF changes in the RLL (white circle) were larger, compared to the absolute PDFF changes in LLL (green circle).

Figure 2 shows the correlation of the changes of PDFF in the left and the right lobe with mean liver PDFF change. The regression line of the LLL PDFF change with the mean liver PDFF change (*Figure 2A*) had a slope m of 0.93 and an intercept of –0.23%. The regression line of the RLL PDFF change with the mean liver PDFF change (*Figure 2B*) had a slope m of 1.08 and an intercept of –0.29.

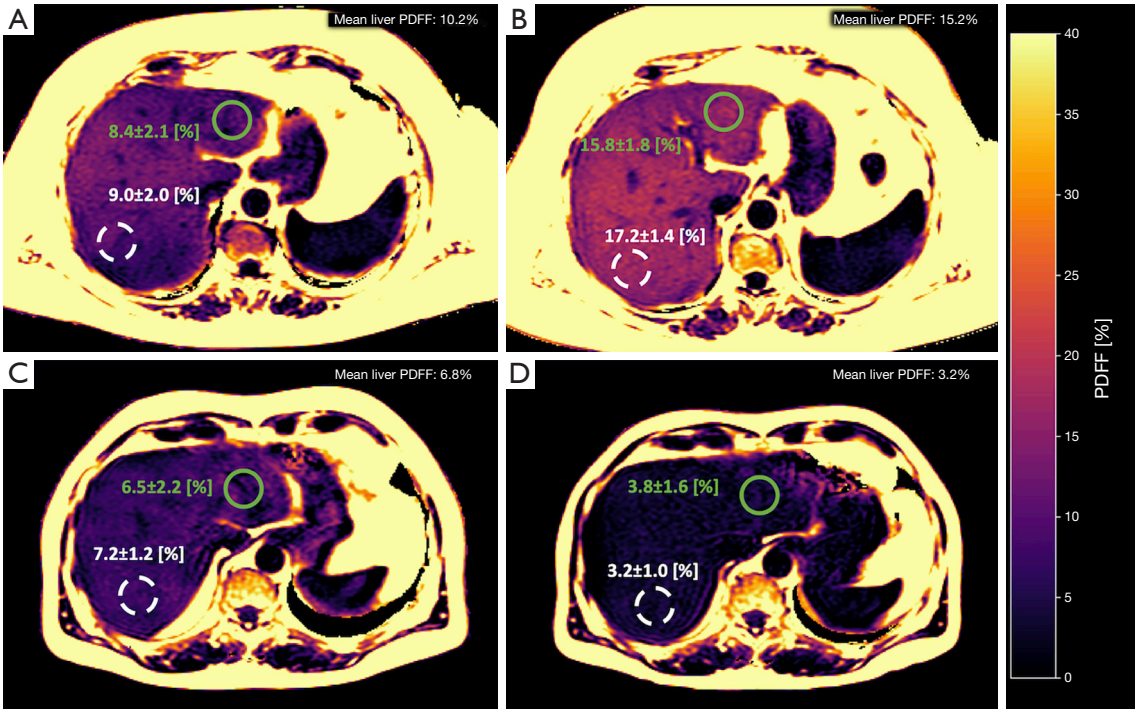

Figure 1 Liver PDFF maps at two time points (A, C at baseline and B, D after one year) for (A,B) one subject with increasing liver PDFF (weight gain of 5.9 kg) and (C,D) one subject with decreasing liver PDFF (weight loss of 7.1 kg). (A) shows higher PDFF in the right lobe compared to the left lobe. (B) shows the same subject after one year with strongly increasing mean liver PDFF and a larger PDFF change in the right lobe compared to the left lobe ($\Delta PDFF_{left\ lobe}$ =7.4%, $\Delta PDFF_{right\ lobe}$ =8.2%). The same effect of larger changes of liver PDFF in the right lobe compared to the left lobe can also be detected in the subject with decreasing mean liver PDFF ($\Delta PDFF_{left\ lobe}$ =−2.7%, $\Delta PDFF_{right\ lobe}$ =−4.0%) (C,D). PDFF, proton density fat fraction.

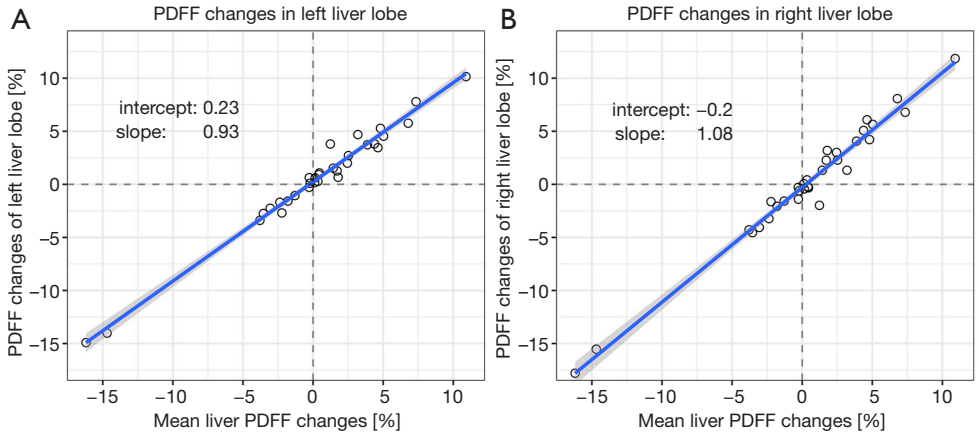

Figure 2 Changes of the liver PDFF in the LLL (A) and the RLL (B) as a function of mean liver PDFF change. The right lobe shows larger liver PDFF changes compared to the left lobe, visualized by the slopes of the regression line. PDFF, proton density fat fraction; LLL, left liver lobe; RLL, right liver lobe.

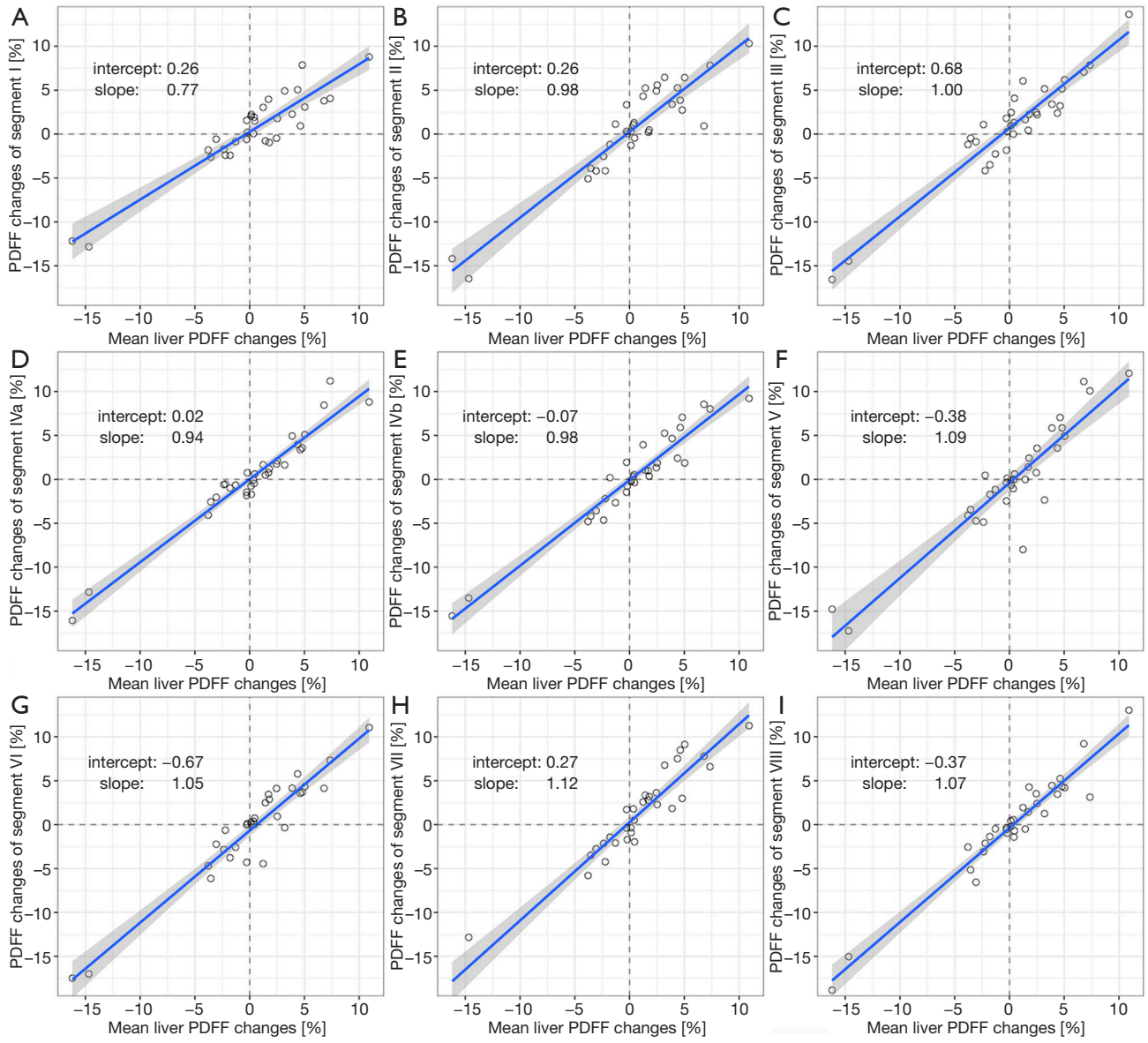

Figure 3 Changes of the liver PDFF for each by Couinaud segment (A,B,C,D,E,F,G,H,I) as a function of mean liver PDFF change. PDFF changes in segments V and VII show the strongest influence on the mean liver PDFF change (highest slope). PDFF changes in segment I show the weakest influence on the mean liver PDFF change (lowest slope). PDFF, proton density fat fraction.

The slope of the regression line for the correlation of RLL PDFF change versus the mean liver PDFF change was significantly higher (P<0.01) when compared to the slope of the agreement for the LLL PDFF change versus the mean liver PDFF change.

Comparison of specific segment PDFF changes

Figure 3 shows the correlation of PDFF changes in each Couinaud segment compared with the mean liver PDFF changes. The highest slope of agreement between PDFF changes in each specific liver segment and mean liver PDFF changes was observed in segment VII (m_{slope} =1.12). The lowest slope of agreement between PDFF changes in each specific liver segment and mean liver PDFF changes was observed in segment I (m_{slope} =0.77). The segments with higher agreement slopes were in the RLL and the segments with lower agreement were in the LLL.

Discussion

The present work performed a longitudinal analysis of PDFF changes in subjects participating in a long-term lifestyle intervention study for weight loss to investigate regional changes in liver PDFF over a period of one year. The main finding was a larger change of PDFF in the RLL compared to the LLL for a given mean liver PDFF change. In addition, the RLL had a stronger influence on mean liver PDFF than the LLL. For a given mean liver PDFF change (including both subjects with increasing and subjects with decreasing mean liver PDFF), differences in regional changes of liver PDFF per liver segment were also observed, with highest absolute changes in segments V and VII—both in the RLL—and lowest absolute changes in segments I and III—both in the LLL.

Liver fat deposition assessed by biopsy is known to be spatially heterogeneous (15,16) and liver PDFF has been reported as being spatially heterogeneous in previous studies (13,14). To address the above spatial heterogeneity of liver PDFF, different ROI sampling methods have been reported in the literature (25,26). The present method adopted the ROI sampling method introduced in (23). Inter-observer analysis in the present work showed high agreement between the two observers.

Despite some evidence for spatial heterogeneity of liver PDFF in a cross-sectional setting (15,16), only a few studies have characterized how heterogeneous PDFF changes may behave in longitudinal studies. In a previous study by Fazeli Dehkordy *et al.* (17), it was shown that subjects with decreasing liver PDFF following bariatric surgery have a larger liver PDFF decrease in the right lobe compared to the left lobe. The results of the present study are in agreement with the study by Fazeli Dehkordy *et al.* Additionally, the present study shows that liver PDFF changes in the RLL contribute stronger to mean liver PDFF changes in subjects with both increasing and decreasing liver PDFF.

The exact reasons for the observed heterogeneous changes in liver PDFF remain unclear. A common explanation suggested by other studies reporting on heterogeneous liver PDFF distribution is the difference in perfusion of the respective liver segments (13,17). Specifically, different studies have tried to explain the heterogeneous liver fat distribution by differences in venous blood flow in the portal vein depending if the blood's origin was mesenteric or splenic. However, the above studies show mixed results and do not offer a clear explanation for the heterogeneous PDFF distribution in the liver (27-29). Despite the lack of a definite explanation for the observed spatial heterogeneity in liver PDFF changes, the present study is in line with previous studies reporting an inhomogeneous segmental and lobar liver fat distribution in subjects with NAFLD (13,14) and advocates for a high spatial resolution PDFF measurement with whole liver coverage to more accurately assess liver fat changes.

The present study has several limitations. First, the present study included participants with different levels of compliance during and after the lifestyle intervention, resulting in subjects with both increasing and decreasing mean liver PDFF over the one-year observation period. However, the key intention of the present study was to investigate regional liver PDFF changes in subjects with longitudinal mean liver PDFF changes. An additional analysis of the weight changes between the group scanned before the beginning of the intervention and after 1 year and the group scanned after the end of the intervention at two time points with an interval of one year showed no statistical differences in the extent of weight change between the two groups. Second, regional liver analysis was based on ROI drawing as suggested in previous studies (25,26) and no whole liver segmentation was performed. Third, the sample size of the present study was small and further studies are required to verify the results in larger cohorts.

Conclusions

Heterogeneous long-term liver PDFF changes in the left and right lobe and the liver Couinaud segments were observed in subjects scanned longitudinally during and after a long-term lifestyle intervention study with significant weight fluctuations. Given a mean liver PDFF change, the RLL, and segments in this area, showed larger PDFF changes compared to the LLL and the respective segments. Therefore, liver PDFF measurement methods with high spatial resolution and whole liver coverage should be used to track liver fat fraction heterogeneity changes in longitudinal studies.

Acknowledgments

Funding: The present work was supported by the European Research Council (grant agreement No. 677661, ProFatMRI), the German Research Foundation (DFG-SFB824/A9) and Philips Healthcare. Additional funding

was provided by the German Center for Diabetes Research (BMBF: 01GI0925).

Footnote

Conflicts of Interest: All authors have completed the ICMJE uniform disclosure form (available at http://dx.doi.org/10.21037/qims-20-873). Dr. HH reports grants from German Ministry of Education and Research, during the conduct of the study; Dr. DCK reports grants from European Research Council, grants from Philips Healthcare, during the conduct of the study; Dr. DCK reports grants from European Research Council (No. 677661), grants from Philips Healthcare, grants from German Research Foundation (DFG-SFB824/A9), during the conduct of the study; grants from Philips Healthcare, outside the submitted work. The other authors have no conflicts of interest to declare.

Ethical Statement: The study was approved by an ethics committee and all subjects gave written informed consent before participation in the study including repeated MRI scanning.

References

1. Holman N, Forouhi NG, Goyder E, Wild SH. The Association of Public Health Observatories (APHO) Diabetes Prevalence Model: estimates of total diabetes prevalence for England, 2010-2030. Diabet Med 2011;28:575-82.
2. World-Health-Organization. Diabetes. 2018. Available online: https://www.who.int/news-room/fact-sheets/detail/diabetes. Accessed 07.08.2020.
3. World-Health-Organization. Obesity and Overweight. 2018. Available online: https://www.who.int/news-room/fact-sheets/detail/obesity-and-overweight. Accessed 07.8.2020.
4. Estes C, Razavi H, Loomba R, Younossi Z, Sanyal AJ. Modeling the epidemic of nonalcoholic fatty liver disease demonstrates an exponential increase in burden of disease. Hepatology 2018;67:123-33.
5. Loomba R, Sanyal AJ. The global NAFLD epidemic. Nat Rev Gastroenterol Hepatol 2013;10:686.
6. Byrne CD, Targher G. NAFLD: a multisystem disease. J Hepatol 2015;62:S47-64.
7. Tock L, Prado WL, Caranti DA, Cristofalo DM, Lederman H, Fisberg M, Siqueira KO, Stella SG, Antunes HK, Cintra IP, Tufik S, de Mello MT, Damaso AR. Nonalcoholic fatty liver disease decrease in obese adolescents after multidisciplinary therapy. Eur J Gastroenterol Hepatol 2006;18:1241-5.
8. Bacchi E, Negri C, Targher G, Faccioli N, Lanza M, Zoppini G, Zanolin E, Schena F, Bonora E, Moghetti P. Both resistance training and aerobic training reduce hepatic fat content in type 2 diabetic subjects with nonalcoholic fatty liver disease (the RAED2 Randomized Trial). Hepatology 2013;58:1287-95.
9. Adams LA, Sanderson S, Lindor KD, Angulo P. The histological course of nonalcoholic fatty liver disease: a longitudinal study of 103 patients with sequential liver biopsies. J Hepatol 2005;42:132-8.
10. Reeder SB, Cruite I, Hamilton G, Sirlin CB. Quantitative Assessment of Liver Fat with Magnetic Resonance Imaging and Spectroscopy. J Magn Reson Imaging 2011;34:729-49.
11. Middleton MS, Heba ER, Hooker CA, Bashir MR, Fowler KJ, Sandrasegaran K, Brunt EM, Kleiner DE, Doo E, Van Natta ML, Lavine JE, Neuschwander-Tetri BA, Sanyal A, Loomba R, Sirlin CB, Network NCR. Agreement Between Magnetic Resonance Imaging Proton Density Fat Fraction Measurements and Pathologist-Assigned Steatosis Grades of Liver Biopsies From Adults With Nonalcoholic Steatohepatitis. Gastroenterology 2017;153:753-61.
12. Wildman-Tobriner B, Middleton MM, Moylan CA, Rossi S, Flores O, Chang ZA, Abdelmalek MF, Sirlin CB, Bashir MR. Association Between Magnetic Resonance Imaging-Proton Density Fat Fraction and Liver Histology Features in Patients With Nonalcoholic Fatty Liver Disease or Nonalcoholic Steatohepatitis. Gastroenterology 2018;155:1428-35.e2.
13. Bonekamp S, Tang A, Mashhood A, Wolfson T, Changchien C, Middleton MS, Clark L, Gamst A, Loomba R, Sirlin CB. Spatial distribution of MRI-determined hepatic proton density fat fraction in adults with nonalcoholic fatty liver disease. J Magn Reson Imaging 2014;39:1525-32.

14. Sofue K, Mileto A, Dale BM, Zhong X, Bashir MR. Interexamination repeatability and spatial heterogeneity of liver iron and fat quantification using MRI-based multistep adaptive fitting algorithm. J Magn Reson Imaging 2015;42:1281-90.
15. Larson SP, Bowers SP, Palekar NA, Ward JA, Pulcini JP, Harrison SA. Histopathologic variability between the right and left lobes of the liver in morbidly obese patients undergoing Roux-en-Y bypass. Clin Gastroenterol Hepatol 2007;5:1329-32.
16. Ratziu V, Charlotte F, Heurtier A, Gombert S, Giral P, Bruckert E, Grimaldi A, Capron F, Poynard T, Group LS. Sampling variability of liver biopsy in nonalcoholic fatty liver disease. Gastroenterology 2005;128:1898-906.
17. Fazeli Dehkordy S, Fowler KJ, Mamidipalli A, Wolfson T, Hong CW, Covarrubias Y, Hooker JC, Sy EZ, Schlein AN, Cui JY, Gamst AC, Hamilton G, Reeder SB, Sirlin CB. Hepatic steatosis and reduction in steatosis following bariatric weight loss surgery differs between segments and lobes. Eur Radiol 2019;29:2474-80.
18. Schulze MB, Hoffmann K, Boeing H, Linseisen J, Rohrmann S, Mohlig M, Pfeiffer AF, Spranger J, Thamer C, Haring HU, Fritsche A, Joost HG. An accurate risk score based on anthropometric, dietary, and lifestyle factors to predict the development of type 2 diabetes. Diabetes Care 2007;30:510-5.
19. ClinicalTrials.gov. Individualized Lifestyle Intervention in Subjects with Prediabetes (PLIS). ClinicalTrials.gov. 2013. Available online: https://www.clinicaltrials.gov/ct2/show/NCT01947595?term=PLIS. Accessed September 22, 2020 2020.
20. Ren J, Dimitrov I, Sherry AD, Malloy CR. Composition of adipose tissue and marrow fat in humans by 1H NMR at 7 Tesla. J Lipid Res 2008;49:2055-62.
21. Liu CY, McKenzie CA, Yu H, Brittain JH, Reeder SB. Fat quantification with IDEAL gradient echo imaging: correction of bias from T(1) and noise. Magn Reson Med 2007;58:354-64.
22. Juza RM, Pauli EM. Clinical and surgical anatomy of the liver: a review for clinicians. Clin Anat 2014;27:764-9.
23. Tang A, Tan J, Sun M, Hamilton G, Bydder M, Wolfson T, Gamst AC, Middleton M, Brunt EM, Loomba R, Lavine JE, Schwimmer JB, Sirlin CB. Nonalcoholic fatty liver disease: MR imaging of liver proton density fat fraction to assess hepatic steatosis. Radiology 2013;267:422-31.
24. Kleinbaum DG, Kupper LL, Nizam A, Rosenberg ES. Applied regression analysis and other multivariable methods. Nelson Education; 2013.
25. Vu KN, Gilbert G, Chalut M, Chagnon M, Chartrand G, Tang A. MRI-determined liver proton density fat fraction, with MRS validation: Comparison of regions of interest sampling methods in patients with type 2 diabetes. J Magn Reson Imaging 2016;43:1090-9.
26. Hong CW, Wolfson T, Sy EZ, Schlein AN, Hooker JC, Fazeli Dehkordy S, Hamilton G, Reeder SB, Loomba R, Sirlin CB. Optimization of region-of-interest sampling strategies for hepatic MRI proton density fat fraction quantification. J Magn Reson Imaging 2018;47:988-94.
27. Groszmann RJ, Kotelanski B, Cohn JN. Hepatic lobar distribution of splenic and mesenteric blood flow in man. Gastroenterology 1971;60:1047-52.
28. Copher GH, Dick BM. Stream line phenomena in the portal vein and the selective distribution of portal blood in the liver. Arch Surg 1928;17:408-19.
29. Tsukuda T, Ito K, Koike S, Sasaki K, Shimizu A, Fujita T, Miyazaki M, Kanazawa H, Jo C, Matsunaga N. Pre- and postprandial alterations of portal venous flow: evaluation with single breath-hold three-dimensional half-Fourier fast spin-echo MR imaging and a selective inversion recovery tagging pulse. J Magn Reson Imaging 2005;22:527-33.

Cite this article as: Syväri J, Junker D, Patzelt L, Kappo K, Al Sadat L, Erfanian S, Makowski MR, Hauner H, Karampinos DC. Longitudinal changes on liver proton density fat fraction differ between liver segments. Quant Imaging Med Surg 2021;11(5):1701-1709. doi: 10.21037/qims-20-873

6.2 Estimating vertebral bone marrow fat unsaturation based on short-TE STEAM MRS

The publication entitled *Estimating vertebral bone marrow fat unsaturation based on short-TE STEAM MRS* was published in Magnetic Resonance in Medicine (Volume 85, Issue 2, p 615-626). The manuscript was authored by Jan Syväri, Stefan Ruschke, Michael Dieckmeyer, Hans H. Hauner, Daniela Junker, Marcus R. Makowski, Thomas Baum, Dimitrios C. Karampinos.

6.2.1 Abstract

Purpose To define a metric for the separability between water and olefinic fat peaks that defines a threshold beyond which the extraction of the olefinic fat peak from vertebral bone marrow short-echo time-stimulated echo acquisition mode MRS at 3T is feasible when using a constrained peak fitting based on the triglyceride fat model.

Methods The water and olefinic peak height difference was defined as a metric for quantifying the separability of water and olefinic fat peaks. Fat unsaturation was determined using an unconstrained olefinic peak fitting and a constrained fitting of all fat peaks to the triglyceride model. The agreement between the two peak-fitting methods was used to define a threshold on water and olefinic peak height difference separating two groups (A and B), based on L5 short-echo time-stimulated echo acquisition mode (TE = 11 ms) spectra from 252 subjects measured at 3T.

Results A threshold on water and olefinic peak height difference was defined. Group A with a good agreement of the olefinic fat peak between the two peak-fitting methods showed a mean number of double bounds = 2.95 ± 0.21, a mean number of methylene-interrupted double bounds = 0.94 ± 0.16 and also a significantly lower coefficient of variation for all fatty acid composition parameters compared to group B ($p < .001$). The water and olefinic peak height difference value showed an inverse association with fat fraction.

Conclusion A threshold of a metric quantifying the separability of the water peak and the olefinic fat peaks was defined for the estimation of the vertebral bone marrow fat unsaturation from short-echo time-stimulated echo acquisition mode MRS. The proposed methodology shows that the assessment of vertebral bone marrow unsaturation is feasible with a short-echo time-stimulated echo acquisition mode MRS in subjects with a higher fat fraction.

6.2.2 Author contributions

I performed the postprocessing, quantification and statistical analysis of the magnetic resonance spectroscopy data using MATLAB (Mathworks, Natick, MA) and R and helped

to develop the Monte Carlo Simulation. In collaboration with the co-authors I performed the recruitment and MRI examinations of the study participants, analyzed and interpreted the data and wrote the manuscript of the publication.

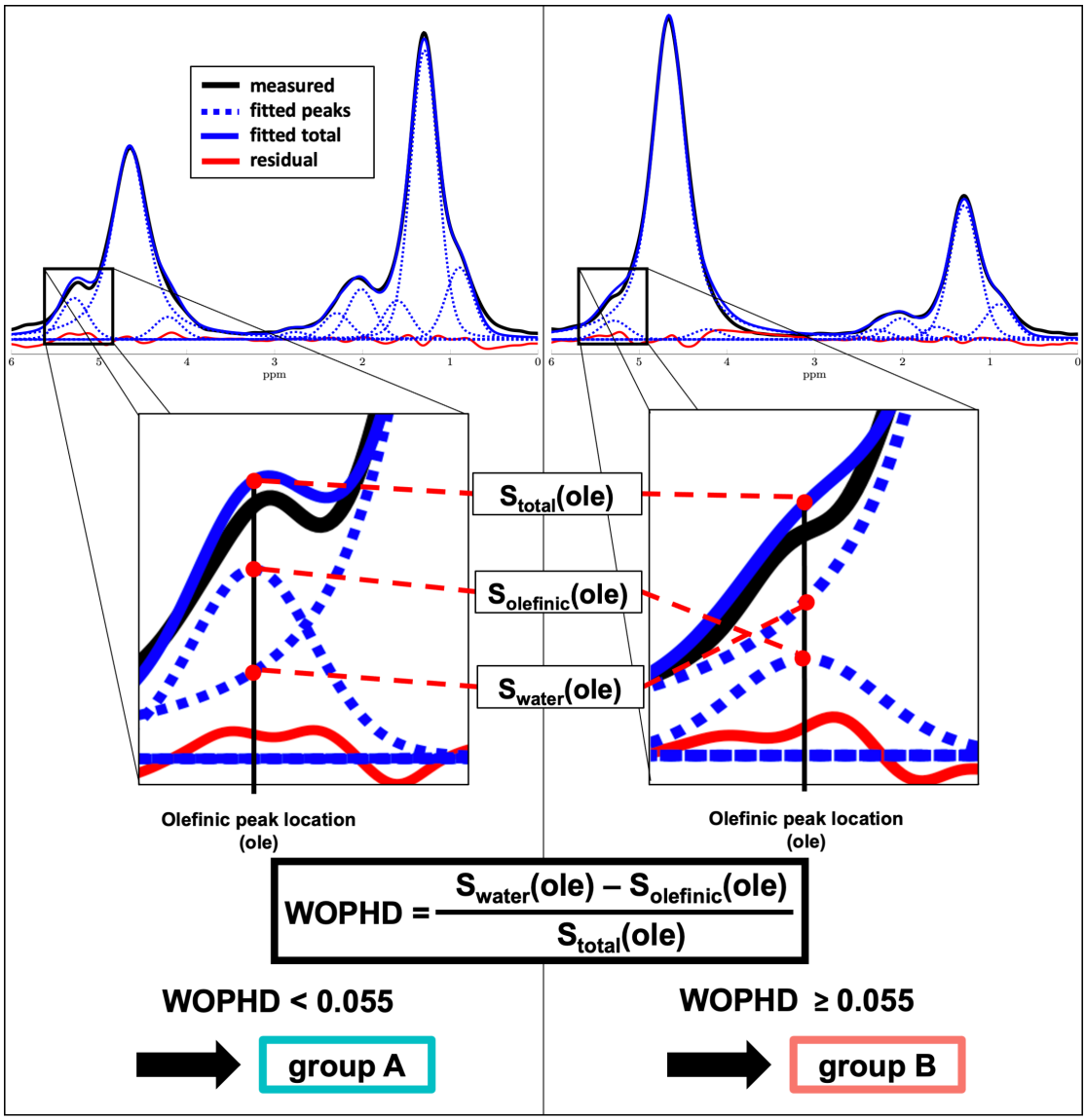

Figure 6.2: Model to define the metric WOPHD which helps the investigator to decide if the extraction of an unsaturation rate is feasible. WOPHD, water olefinic peak height difference

6.2.3 Copyright

Estimating vertebral bone marrow fat unsaturation based on short-TE STEAM MRS

Author: Dimitrios C. Karampinos, Thomas Baum, Marcus R. Makowski, et al

Publication: Magnetic Resonance in Medicine

Publisher: John Wiley and Sons

Date: Aug 11, 2020

Received: 23 March 2020 | Revised: 9 June 2020 | Accepted: 9 July 2020

DOI: 10.1002/mrm.28453

NOTE

Magnetic Resonance in Medicine

Estimating vertebral bone marrow fat unsaturation based on short-TE STEAM MRS

Jan Syväri[1] | **Stefan Ruschke**[1] | **Michael Dieckmeyer**[1] | **Hans H. Hauner**[2] | **Daniela Junker**[1] | **Marcus R. Makowski**[1] | **Thomas Baum**[3] | **Dimitrios C. Karampinos**[1]

[1]Department of Diagnostic and Interventional Radiology, School of Medicine, Technical University of Munich, Munich, Bavaria, Germany

[2]Else Kröner Fresenius Center for Nutritional Medicine, Technical University of Munich, Munich, Bavaria, Germany

[3]Department of Diagnostic and Interventional Neuroradiology, School of Medicine, Technical University of Munich, Munich, Bavaria, Germany

Correspondence
Jan Syväri, Department of Diagnostic and Interventional Radiology, Klinikum rechts der Isar, School of Medicine, Technische Universität München, Ismaninger Str. 22, Munich 81675, Germany.
Email: jan.syvaeri@tum.de

Funding information
Philips Healthcare; European Research Council, Grant/Award Number: 677661,

Purpose: To define a metric for the separability between water and olefinic fat peaks that defines a threshold beyond which the extraction of the olefinic fat peak from vertebral bone marrow short-echo time-stimulated echo acquisition mode MRS at 3T is feasible when using a constrained peak fitting based on the triglyceride fat model.
Methods: The water and olefinic peak height difference was defined as a metric for quantifying the separability of water and olefinic fat peaks. Fat unsaturation was determined using an unconstrained olefinic peak fitting and a constrained fitting of all fat peaks to the triglyceride model. The agreement between the two peak-fitting methods was used to define a threshold on water and olefinic peak height difference separating two groups (A and B), based on L5 short-echo time-stimulated echo acquisition mode (TE = 11 ms) spectra from 252 subjects measured at 3T.
Results: A threshold on water and olefinic peak height difference was defined. Group A with a good agreement of the olefinic fat peak between the two peak-fitting methods showed a mean number of double bounds = 2.95 ± 0.21, a mean number of methylene-interrupted double bounds = 0.94 ± 0.16 and also a significantly lower coefficient of variation for all fatty acid composition parameters compared to group B ($p < .001$). The water and olefinic peak height difference value showed an inverse association with fat fraction.
Conclusion: A threshold of a metric quantifying the separability of the water peak and the olefinic fat peaks was defined for the estimation of the vertebral bone marrow fat unsaturation from short-echo time-stimulated echo acquisition mode MRS. The proposed methodology shows that the assessment of vertebral bone marrow unsaturation is feasible with a short-echo time-stimulated echo acquisition mode MRS in subjects with a higher fat fraction.

KEYWORDS
bone marrow, fat unsaturation, single-voxel magnetic resonance spectroscopy, triglyceride model

1 | INTRODUCTION

The study of bone marrow adipose tissue is gaining significant attention in understanding the pathophysiology of bone matrix loss in osteoporosis.[1-3] MRI and MRS techniques have been emerging for noninvasively measuring properties of bone marrow adipose tissue.[4,5] Most of the recent MRI and MRS work has focused on measuring the bone marrow fat fraction (FF) with a wide range of applications in different diseases.[6-9] Another property of bone marrow fat, which has been shown to be relevant in relating bone marrow adipose tissue to matrix bone loss has been bone marrow fat unsaturation.[10,11] Specifically, previous studies have shown a reduction in bone marrow fat unsaturation in osteoporosis[10,12] and diabetes.[13,14]

Bone marrow fat unsaturation measurements are typically performed using single-voxel MRS experiments by resolving the olefinic fat peak in the spectral proximity of the water peak.[15] The visual appearance of MR spectra from yellow bone marrow is similar to MR spectra from subcutaneous fat,[16] with the exception that in trabecularized bone regions the spectral linewidths are significantly broader because of magnetic susceptibility effects induced by the bone matrix.[4] The measurement of bone marrow fat unsaturation in red marrow regions is, however, significantly more challenging than in yellow marrow regions.[11] In addition to the presence of broad linewidths, red marrow typically encloses a large water peak that might partially overlap with the olefinic fat peak.[17] A highly clinically relevant red marrow region is the vertebral bone marrow based on the clinical significance and prevalence of vertebral fractures in osteoporotic subjects. Vertebral bone marrow (VBM) contains a large amount of water (with a FF of the order of 50%) and is characterized by broad linewidths with both effects complicating the extraction of the olefinic fat peak.[17,18]

Many of the existing in vivo MRS studies measuring VBM fat unsaturation metrics have been based on point resolved spectroscopy (PRESS) acquisitions with longer echo times (TEs) in the range between 30 ms and 40 ms at 3T.[10,12,18] However, J-coupling effects are expected to affect the quantification of olefinic fat peak area in PRESS acquisitions with such long TEs.[19] Stimulated echo acquisition mode (STEAM) MRS acquisitions with short TEs have been shown to be less sensitive to J-coupling effects compared with PRESS MRS acquisitions.[19,20] Alternative methods to reduce the effect of J-coupling on olefinic fat peak area determination include long-TE PRESS acquisitions,[21,22] long-TE STEAM acquisitions,[23,24] and diffusion-weighted STEAM acquisitions,[20] but with all three methods being associated with reduced signal-to-noise ratio (SNR). MRS processing of short-TE STEAM MRS employing constrained peak fitting based on the triglyceride fat model has been recently applied in regions of subcutaneous and visceral adipose tissue.[25,26] However, it is not known for which measured spectra the extraction of the olefinic fat peak is feasible when using short-TE STEAM MRS combined with constrained peak fitting based on the triglyceride fat model in VBM.

The purpose of the present study was to define a metric for the separability between water and olefinic fat peaks that defines a threshold beyond which the extraction of the olefinic fat peak from vertebral bone marrow short-TE STEAM MRS at 3T is feasible when using a constrained peak fitting based on the triglyceride fat model.

2 | METHODS

2.1 | Subjects

The lumbar spine region of 252 healthy volunteers with an age range between 18 and 77 years (154 women and 98 men; mean age 43.7 ± 15.8 years) was scanned on a 3T whole-body scanner (Ingenia 3.0T, Philips Healthcare, Best, The Netherlands) using the built-in 12-channel posterior coil array. Inclusion criteria were no history of fracture and no pathological bone changes, such as bone metastases or hematological or metabolic bone disorders. The study was approved by the local institutional committee for human research. All subjects gave written informed consent before participation in the study.

2.2 | MRS acquisition

MRS was applied to the L5 vertebral body based on appropriate localizing sequences. The L5 vertebral body was selected because it usually has the largest volume of all vertebral bodies. In a small number of subjects, the L5 vertebra was subject to degenerative changes; therefore, L4 was measured. The default MRS voxel size was $15 \times 15 \times 15$ mm^3. If necessary, the MRS voxel size was reduced to fit within the vertebral body. Moreover, chemical-shift–displacement effects were considered during the positioning of the volume of interest by visualizing both the water voxel (center frequency selected at the water peak) and the fat voxel (based on the chemical shift of the main fat peak and the STEAM MRS RF pulses bandwidth). A STEAM single-voxel MRS sequence with the following parameters was used: pulse repetition time = 6 seconds (to minimize any T_1-weighting effects); Mixing Time = 16 ms (set to shortest Mixing Time to minimize J-coupling effects); TE = 11 ms (STEAM with shortest TE to minimize J-coupling effects[19]); eight repetitions with four phase cycles; 4096 sampling points; spectral acquisition bandwidth of 5 kHz; no water suppression; no regional saturation bands. The very asymmetric "spredrex" RF pulses (duration of 7 ms,

bandwidth of 2277 Hz) provided by the vendor were used to achieve a STEAM MRS voxel localization with TE = 11 ms.

2.3 | MRS processing

Frequency-based spectral fitting was performed using in-house written routines in MATLAB (Mathworks, Natick, Massachusetts). Pseudo-Voigt lineshapes[27] with a 0.8 × Gauss + 0.2 × Lorentzian lineshape for the fat peaks and a 0.2 × Gauss + 0.8 × Lorentzian lineshape for the water peak were employed. Figure 1A,C show measured VBM fat spectra with fat peaks observed at spectral locations 0.90, 1.30, 1.6, 2.02, 2.24, 2.75, 4.15, 4.30, 5.19, and 5.29 ppm. The letters A and D were assigned to peaks at 0.90 ppm [methyl: $(-CH_2)_n-CH_3$), 2.77 ppm (diallylic methylene: $-CH=CH-CH_2-CH=CH-$], respectively. The letter B was assigned to the superposition of peaks at 1.30 ppm ([methylene: $(-CH_2)_n-$] and 1.59 ppm [β-carboxyl: $-CO-CH_2-CH_2-$], the letter C to the superposition of peaks at 2.00 ppm (α-olefinic: $-CH_2-CH=CH-CH_2-$) and 2.25 ppm (α-carboxyl: $-CO-CH_2-CH_2-$), the letter E to the superposition of peaks at 4.15 ppm and 4.30 ppm (glycerol: $-CH_2-O-CO-$), and the letter F to the superposition of peaks at 5.19 ppm (glycerol: $-CH_2O-CHO-CH_2O-$) and 5.31 ppm (olefinic: $-CH=CH-$). Three different peak-fitting methods were employed. First, the method previously described by Dieckmeyer et al.[17] was used to estimate the FF. The FF determination method relied on the fitting of the olefinic and glycerol fat peaks constrained to the methylene and methyl peaks based on an a priori

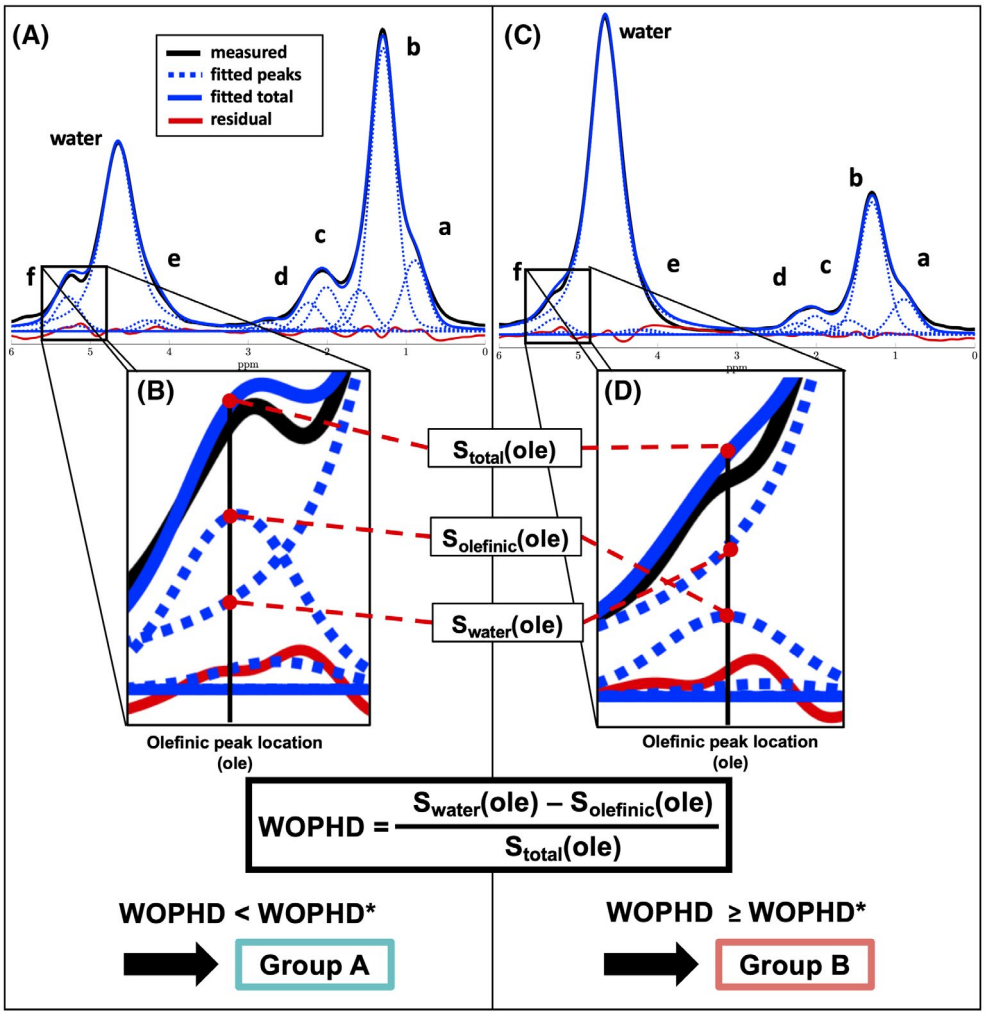

FIGURE 1 Full (A,C) and zoomed (B,D) vertebral bone marrow MR spectra with different degree of separability between the olefinic fat peak and water fat peak. A,C, MR spectrum with high fat fraction where the olefinic peak is visually separated from the water peak. B,D, MR spectrum with low fat fraction where the olefinic peak is not visually separated from the water peak. At the spectral location of the olefinic fat peak, S_{water} is the fitted signal of the water peak, $S_{olefinic}$ the fitted signal of the olefinic peak, and S_{total} is the fitted signal of all peaks combined. The height difference between the water and olefinic peak is defined based on the above signals. A cut-off value for the WOPHD* is searched to define the range of parameters for which the extraction of the olefinic fat peak is feasible (group A). Groups A and B are defined based on WOPHD* (Figure 2). WOPHD, water olefinic peak height difference

known average triglyceride model, as previously determined in Dieckmeyer et al.[17] Second, two methods were used to assess the ability to extract unsaturation parameters with different peak constraints. The unconstrained fitting method used an unconstrained fitting of the olefinic and glycerol fat peaks, independent of the main fat peak. The constrained fitting method constrained all fat peaks to a parameterized triglyceride model. The parameterized triglyceride model consisted of the three main parameters: the mean chain length, the mean number of double bonds (ndb) per triglyceride, and the mean number of methylene-interrupted double bonds (nmidb) per triglyceride.[25] In both the unconstrained fitting method and the constrained fitting method, a common fat peak linewidth and an independent water peak linewidth were constrained to be below 0.50 ppm and 1.50 ppm, respectively. The spectral locations of the fat peaks were allowed to vary by ±0.03 ppm, and the water peak location was allowed to vary by ±0.10 ppm.

Indicative SNR levels in the in vivo data were calculated in frequency domain, by dividing the highest signal by the standard deviation (SD) of the noise in a spectral region without peaks.

2.4 | Fat fraction estimation

The previous method proposed by Dieckmeyer et al.[17] was adopted. After fitting for the peaks A, B, C, and D, as well as for the water peak, the peaks E and F were calculated based on a triglyceride model,[25] with an assumed value for ndb = 3.13 and nmidb = 0.70.[17] For the two glycerol-peaks at 4.15 ppm and 4.30 ppm, the total area was calculated as 5.62% of the area of peaks A + B, respectively. Area of the glycerol peak at 5.19 ppm was calculated at 1.41% of the area of peaks A + B and the area of the olefinic peak at 8.79% of the area of peaks A + B. In total, 11 parameters were fitted (fat peak areas of six peaks at A, B, C, and D as described above; water peak area; spectral location of water peak; common spectral location of all fat peaks; linewidth of water peak; and common linewidth of all fat peaks).

2.5 | Unconstrained fitting for olefinic fat peak estimation

In the unconstrained fitting method, the spectra were fitted the same way as in the fitting for the fat fraction estimation, but the olefinic peak at 5.29 ppm was not constrained to the area of peak A + B. The glycerol peak at 5.19 ppm was constrained as 1.41% to the area of peaks A + B. The glycerol peaks at 4.15 ppm and 4.30 ppm were calculated as 5.62 % of the area of peaks A + B, respectively. In total, 12 parameters were fitted (fat peak areas of six peaks at A, B, C, and D as described above; olefinic fat peak area; water peak area; spectral location of water peak; common spectral location of all fat peaks; linewidth of water peak; and common linewidth of all fat peaks).

2.6 | Constrained fitting for olefinic fat peak estimation

The constrained fitting method was based on a constrained fitting of all peaks to the triglyceride model by Hamilton et al.[25] A fixed chain length of 17.33[28] was assumed. The peaks were fitted for free ndb and nmidb. In total, eight parameters were fitted (ndb; nmidb; triglyceride scaling factor; water peak area; spectral location of water peak; common spectral location of all fat peaks; linewidth of water peak; and common linewidth of all fat peaks).

2.7 | Metrics definition

In general, the ability to resolve the olefinic fat peak in the spectral proximity of the overlapping water peak depends on both the FF and the water/fat peaks linewidth. A metric of the water and olefinic peak height difference (WOPHD) was thus defined aiming to quantify the ability to resolve the olefinic fat peak in the spectral proximity of the overlapping water peak:

$$\mathrm{WOPHD} = \frac{S_{\mathrm{water}}(ole) - S_{\mathrm{olefinic}}(ole)}{S_{\mathrm{total}}(ole)} \quad (1)$$

where $S(ole)$ is the signal strength of the fitted signal at the spectral location of the olefinic fat peak (Figure 1). $S_{\mathrm{water}}(ole)$ is the fitted signal of the water peak at the olefinic fat peak spectral location, $S_{\mathrm{olefinic}}(ole)$ the fitted signal of the olefinic peak at the olefinic fat peak spectral location, and $S_{\mathrm{total}}(ole)$ is the fitted signal of all peaks combined at the olefinic fat peak spectral location.

To measure the WOPHD metric, the fitting method for FF estimation was used. By definition, WOPHD depends on both the FF and the water/fat peaks linewidth: High WOPHD values are associated with a strong water peak, broader linewidth, and an olefinic fat peak that cannot be separated from the overlapping water peak. Low WOPHD values are associated with a small water peak, narrow linewidth, and an olefinic fat peak that can be separated from the overlapping water peak. The results of the peak-fitting methods were then used to determine the following fat composition metrics, assuming that A_{fatpeaks} stands for the area under all fat peaks, $A_{\mathrm{waterpeak}}$ stands for the area under the water peak and $A_{\mathrm{olefinicpeak}}$ stands for the area under the olefinic peak at 5.29 ppm.

The FF was defined as:

$$FF = \frac{A_{\text{fatpeaks}}}{A_{\text{fatpeaks}} + A_{\text{waterpeak}}} \quad (2)$$

based on the peak areas determined by the method proposed by Dieckmeyer et al.[17] (fat fraction estimation method). The olefinic fraction (OF) was then defined as:

$$OF = \frac{A_{\text{olefinicpeak}}}{A_{\text{fatpeaks}}} \quad (3)$$

and determined based on the peak areas by the two fitting methods (unconstrained/constrained fitting for olefinic fat peak estimation).

A WOPHD cut-off value, labeled as WOPHD*, was defined as the WOPHD value below which the extraction of the olefinic fat peak is feasible. WOPHD* splits the experimentally measured spectra into two groups: Group A was defined as the group of spectra with WOPHD < WOPHD* that allows the separation of water from the olefinic fat peak (Figure 1). Group B was defined as the group of spectra with WOPHD ≥ WOPHD* that does not allow a reliable separation of water from the olefinic fat peak (Figure 1).

To determine WOPHD*, the agreement between the olefinic fraction results between the unconstrained olefinic fat peak-fitting method and the constrained olefinic fat peak-fitting method in the experimentally measured spectra was employed. The slope of the agreement of the OF values between the unconstrained peak-fitting method and the constrained peak-fitting method in group A was plotted as a function of WOPHD* (Figure 2). In addition, the normalized norm of residuals (normalized R^2) of the agreement for the OF values between the unconstrained peak-fitting method and the constrained peak-fitting method in group A was plotted as a function of WOPHD* (Figure 2). WOPHD* was defined as the value for which the slope of the agreement of the OF values between the unconstrained peak-fitting method and the constrained peak-fitting method in group A equals one.

2.8 | Numerical simulations

Monte Carlo simulations were performed to verify the WOPHD* extraction based on the experimentally measured spectra. Synthetic MR spectra were generated using the triglyceride model and a fixed chain length of 17.33.[28] Pseudo-Voigt lineshapes[27] with a 0.8 × Gauss + 0.2 × Lorentzian lineshape for the fat peaks and a 0.2 × Gauss + 0.8 × Lorentzian lineshape for the water peak were employed and the fat peak locations were defined as for the experimental spectra. Additional parameters were selected in a physiological range: 10% ≤ FF ≤ 100%, 0.6 ≤ ndb ≤ 4, 0 ≤ nmidb ≤ 1.6 with ndb/nmidb ≥ 2, 0.3 ppm ≤ water peak linewidth ≤ 0.8 ppm, and 0.3 ppm ≤ fat peak linewidth ≤ 0.8 ppm. Complex Gaussian noise was added in time domain and the simulations were repeated at different SNR levels: SNR = 60 (low SNR case) and SNR = 170 (average SNR case). At each SNR level and set of parameters, the simulations were repeated 50 times resulting in 841 500 number of simulated spectra per SNR level. The slope of the agreement and the normalized norm of residuals for the OF values between the unconstrained peak-fitting method and the constrained peak-fitting method in group A, now defined based on the simulated spectra, were plotted as function of WOPHD*.

2.9 | Bootstrapping and statistical analysis

To investigate the reproducibility of peak-fitting results, bootstrapping of the experimentally measured spectra was performed. Based on the acquired eight repetitions, employing four phase cycles, 16 different combinations of four repetition were subsampled for bootstrapping. The coefficient of variation (CV) was calculated for ndb, nmidb, and OF for the constrained peak-fitting method.

All statistical analyses were performed with RStudio (Version 1.1.423; RStudio, Inc., Boston, Massachusetts; http://www.rstudio.com/). Tests were performed at a significance level of $*P < .05$, $**P < .01$, and $***P < .001$. Two-sided t tests were performed to test differences in extracted parameters between subject groups A and B. The relationship between FF and WOPHD in the measured spectra was finally investigated to gain additional insights on the main parameters affecting WOPHD.

3 | RESULTS

The spectra from five subjects were excluded because of poor spectral quality. The determination of WOPHD*, which defines the separation between groups A and B, was based on the maximization of the agreement of the OF peak estimation between the unconstrained and the constrained peak-fitting methods (Figure 2A). Figure 2B plots the normalized norm of residuals and Figure 2C plots the slope of the linear agreement between the unconstrained and the constrained peak-fitting methods estimating the OF in group A. The values of WOPHD* that minimize the normalized norm of residuals (blue dot point in Figure 2C) and that result in a slope equal to one (green dot point in Figure 2D) are close and around the WOPHD* value of −0.1. Therefore, WOPHD* was set to −0.077, as for this value WOPHD* results in the slope of the linear agreement between the constrained and unconstrained peak-fitting method in group A equal to 0.997 (and closest to one). Groups A and B were thus defined by spectra with

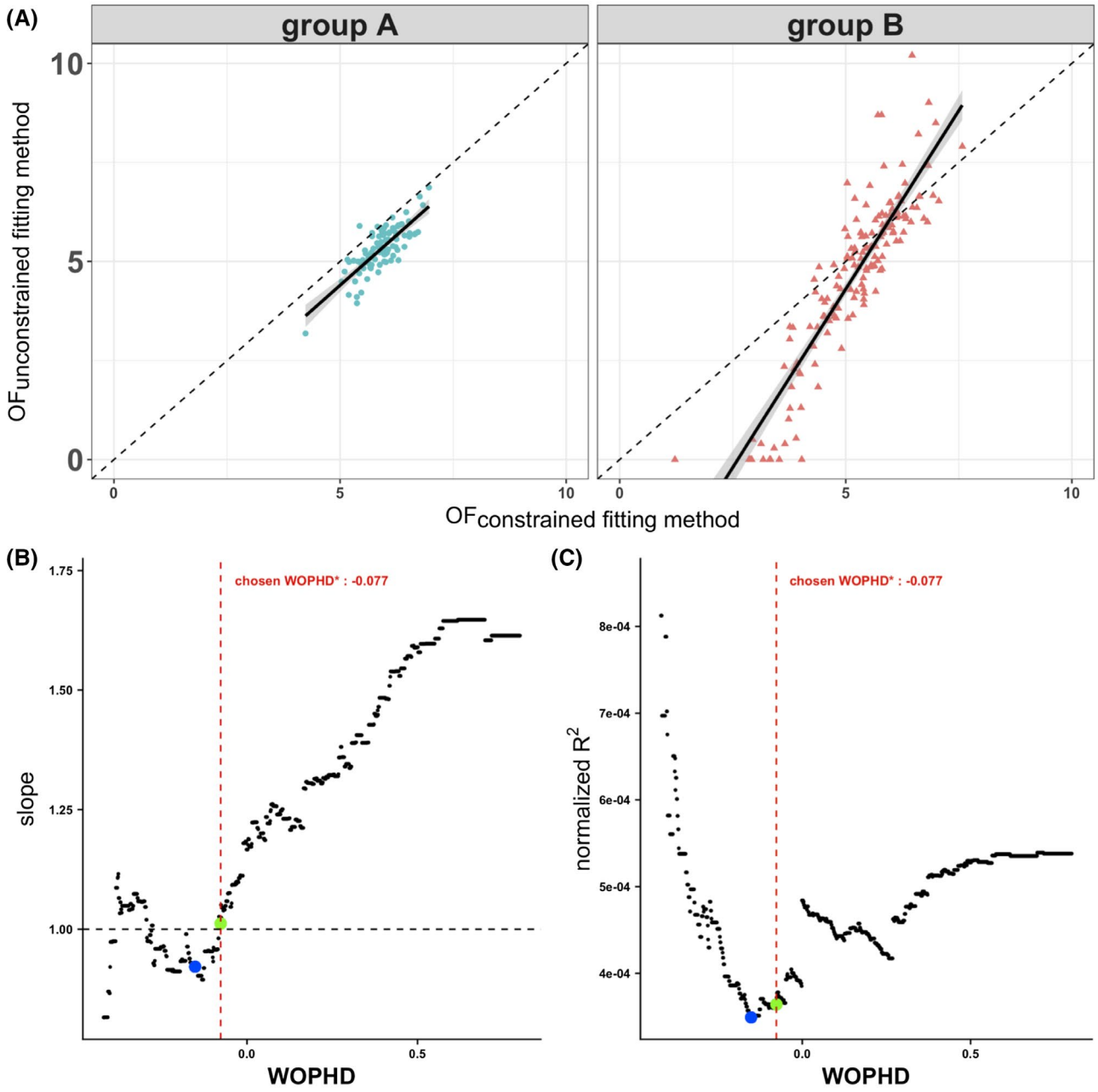

FIGURE 2 A, Agreement of the OF between unconstrained fitting method and constrained fitting method for groups A and B. B,C, The determination of WOPHD* is based on maximizing agreement of the OF between the two fitting methods. Low WOPHD* values are associated with a limited number of samples in group A. High WOPHD* values are associated with spectra where the olefinic fat peak and water peaks cannot be separated. WOPHD* was set to −0.077, resulting in (B) a slope of the correlation line of the OF between the constrained and unconstrained fitting method close to one, and (C) close to the minimum of the normalized norm of residuals in group A. WOPHD, water olefinic peak height difference; OF, olefinic fraction

WOPHD < -0.077 in group A ($n = 92$) and spectra with a WOPHD ≥ -0.077 in group B ($n = 155$).

The following values were extracted based on the constrained peak-fitting method: mean ndb was 2.95 ± 0.21 in group A and 2.62 ± 0.50 in group B. Mean nmidb was 0.94 ± 0.16 in group A and 0.60 ± 0.38 in group B. The mean linewidth of fat was 0.46 ± 0.05 ppm in group A and 0.52 ± 0.07 ppm in group B. The mean linewidth of water was 0.51 ± 0.06 ppm in group A and 0.51 ± 0.07 in group B.

Supporting Information Figures S1-S3 present the dependence of the OF results for both the constrained and unconstrained peak-fitting methods and the dependence of WOPHD on FF, linewidth, and SNR based on the numerical simulations.

Figure 3 shows the numerical simulation results at different SNR levels for the dependence of the normalized norm of residuals and the slope agreement between the two peak-fitting methods on WOPHD* (Figure 3A at SNR = 60 and Figure 3B at SNR = 170). The points of the minimum

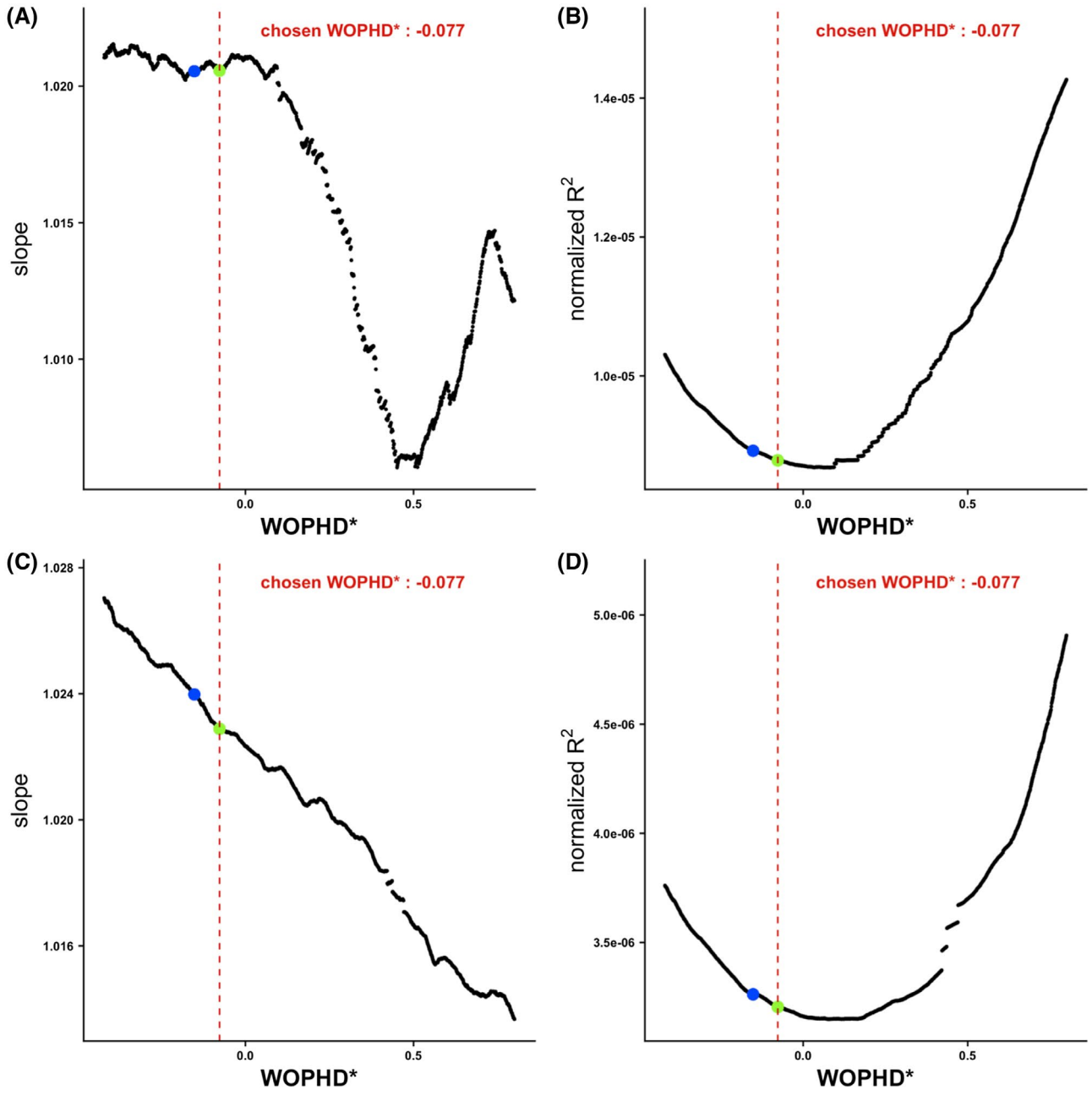

FIGURE 3 Numerical simulation results, A,B, Show the results of the numerical simulation at an SNR = 60; C,D, at an SNR = 170. Obtained slope of the correlation line of constrained and unconstrained fitting model (A,C) and the normalized norm of residuals (B,D). A WOPHD* cutoff of −0.077 yields a slope of 1.021 and a normalized norm of residuals of $8.8.0 \times 10^{-6}$ (SNR = 60) and a slope of 1.023 and a normalized norm of residuals of 3.2×10^{-6} (SNR = 170). WOPHD, water olefinic peak height difference

normalized norm of residuals and slope equal to one (blue and green points, respectively), have been determined based on the experimentally measured spectra. The slope of the OF agreement between the two peak-fitting methods in group A based on the simulated spectra was equal to 0.9925 at SNR = 60 and equal to 0.9924 at SNR = 170 (Figure 3A,C). The minimum normalized norm of residuals for the OF agreement between the two peak-fitting methods in group A based on the simulated spectra also shifted to higher WOPHD* values with increasing SNR (Figure 3B,D).

Figure 4 shows the CV resulting from the bootstrapping analysis. There was a significant difference ($P < .001$) between group A and group B in the CV results of the measured parameters (OF, ndb, and nmidb). The CV of all parameters was significantly higher in group B compared to group A ($P < .001$). The mean ± SD of the CV per parameter for each group was: OF group A: 2.47% ± 1.22%, OF group B: 5.24% ± 3.21%; ndb group A: 2.34% ± 1.15%, ndb group B: 5.00% ± 3.10%; and nmidb group A: 7.93% ± 4.39%, nmidb group B: 40.68 ± 64.58, with some values above 100%.

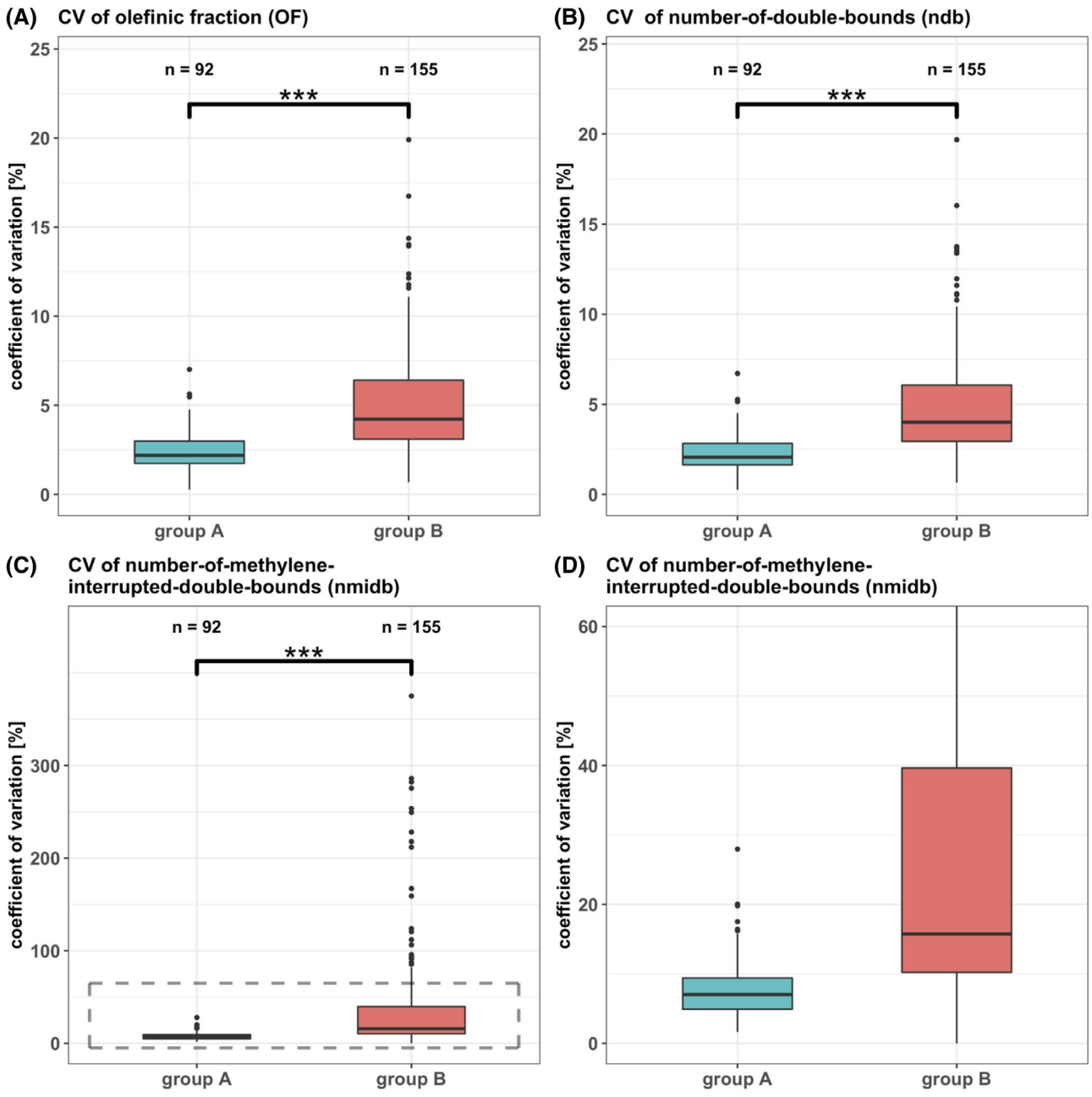

FIGURE 4 Box plot comparison between results from constrained fittings for the coefficient of variation of (A) OF, (B) ndb, and (C,D) nmidb values between group A and group B. D, A zoomed version of (C). *** indicates $p < .001$. CV, coefficient of variation; ndb, number of double bounds; nmidb, number of methylene interrupted double bounds; OF, olefinic fraction

Figure 5 shows a high correlation between the FF and WOPHD in the experimentally measured spectra, including both groups A and B ($R^2 = 0.90$, slope = −49.19, intercept = 50.4).

4 | DISCUSSION

Despite the fact that VBM fat unsaturation has been shown to be linked to bone health,[10] there is currently no consensus on which type of MRS acquisition and peak-fitting method should be employed for extracting the olefinic fat peak in the spectral proximity of the overlapping water peak. The present work employed short-TE STEAM MRS with a constrained peak fitting based on the triglyceride fat model. The short-TE STEAM MRS acquisition was selected because of its known property of reducing J-coupling effects,[19] and its already wide application in studies measuring VBM FF.[4] The constrained peak fitting based on the triglyceride fat model[25] was adopted to reduce the confounding effect of the overlapping

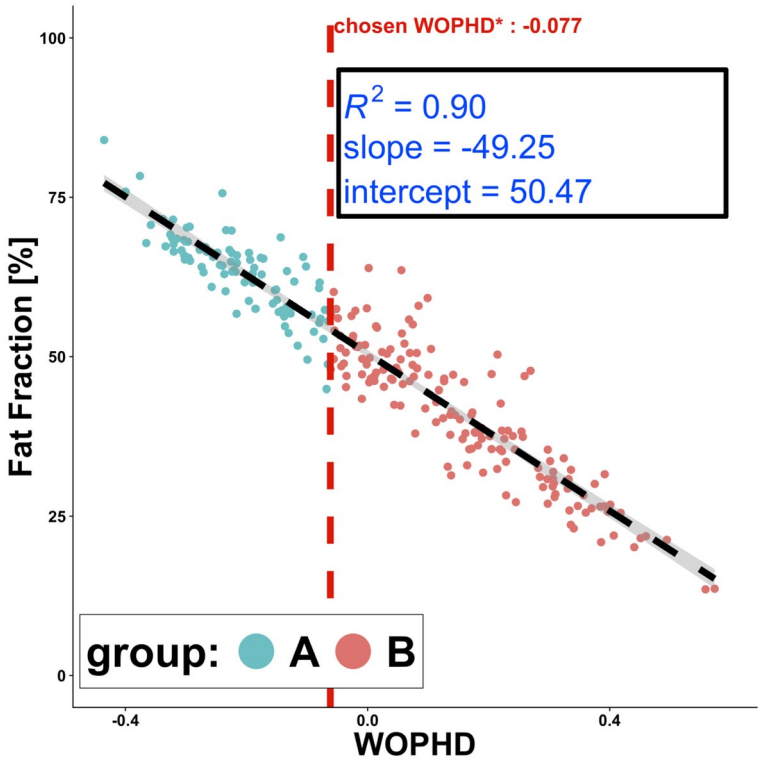

FIGURE 5 Correlation plot between fat fraction (FF) and WOPHD. Correlation between FF and WOPHD yielded $R^2 = 0.90$ and a slope = −49.25 and intercept = 50.47. Dashed line corresponds to WOPHD* and splits the measured spectra in group A (green points) and group B (red points). WOPHD, water olefinic peak height difference

water–fat peaks. A threshold on the separability of water and olefinic fat peaks was determined by comparing the self-consistency of the OF estimation using two different peak-fitting methods. Two groups were defined based on the threshold on the separability of water and olefinic fat peaks in a large pool of experimentally measured spectra. It was demonstrated that there are significant differences between the two groups concerning the mean of OF, ndb, and nmidb. Group A showed higher values for all three parameters compared to group B. The mean ndb and nmidb of group B were distinctly lower than the literature values.[17,28] Specifically, some results for nmidb with values below 0.2 in group B appeared to be out of the physiological range compared with the literature.[16,17] In group A, the mean values were close to the values mentioned in the literature,[16,17] and the within-group SD was smaller compared to group B.

In the employed numerical simulations, the OF results for both the constrained and unconstrained peak-fitting methods showed an increased precision for higher FF (Supporting Information Figure S1), narrower linewidths (Supporting Information Figure S2), and higher SNR (Supporting Information Figure S3). For higher FF and narrowed linewidths, WOPHD decreased, suggesting a better separability of the water and olefinic fat peaks (Supporting Information Figures S1 and S2). The constrained fitting method resulted overall in more precise estimation of OF compared to the unconstrained fitting method (Supporting Information Figures S1-S3).

As no gold-standard measurement for the VBM fat unsaturation was available, the simulation framework was also used to verify that a threshold on the separability of water and olefinic fat peaks can be determined by comparing the self-consistency of the OF estimation using two different peak-fitting methods. The employed simulation framework could simulate noise effects, but no signal model mismatches, in contrast to the experimentally measured data where both noise effects and model mismatches affect the measurements. Similar to the experimentally measured data, the simulation showed that the normalized norm of residuals, a function of WOPHD*, has a local minimum. For lower WOPHD*, fewer spectra are included in group A, and for higher WOPHD*, there is a big overlap of the water and the olefinic peak leading to an increase of the normalized norm of residuals. The shift of the minimum of normalized norm of residuals to higher WOPHD* for higher SNR values can be explained by the fact that at higher SNR and in the absence of model mismatches, the separation of the olefinic and water fat peak can be achieved for higher values of WOPHD. The presented SNR levels of 60 and 170 in the simulations were chosen based on the range of the indicative SNR levels from the experimental data. The simulation verified the definition of WOPHD*, as the WOPHD* value minimizing the normalized norm of residuals based on the simulated data, was close to the WOPHD* value minimizing the normalized norm of residuals based on the experimental data. In addition, the agreement slope for the

simulated data at the WOPHD* value determined from the experimental data was close to one.

By performing bootstrapping and calculating the CV for each in vivo spectrum, the reproducibility of the results was studied for groups A and B. For the parameters OF, ndb, and nmidb, group A showed significantly lower CVs than group B, suggesting that the spectra of group A can be measured with a higher reproducibility than the spectra of group B. The CV of nmdib was relatively high in both groups A and B compared with the other parameters, but the CV of nmidb in group A was still significantly lower than the CV of nmdib in group B.

In Figure 5, it is can be seen that WOPHD is mainly dependent on the FF, in accordance with the previous work by Xu et al.[18] Therefore, the proposed methodology shows that with a short-TE MRS acquisition, the VBM unsaturation is feasible for WOPHD < -0.077 (primarily spectra with high FF) using either the presently employed unconstrained or constrained peak-fitting methods for the estimation of OF. Attention should be paid when using short-TE MRS for determining VBM unsaturation in subjects with WOPHD > -0.077 (primarily spectra with low FF). However, the present work does not provide a conclusive answer to which acquisition method should be used for short-TE MRS spectra with WOPHD > -0.077.

Instead of short-TE STEAM MRS acquisitions, long-TE PRESS acquisitions,[21,22] long-TE STEAM acquisitions,[23,24] and diffusion-weighted STEAM acquisitions[20] have been previously proposed to reduce the effect of J-coupling on the olefinic fat peak area determination. Long-TE PRESS and long-TE STEAM acquisitions have been also applied for bone marrow fat applications. A major limitation of these methods is the SNR loss caused by increased T_2-weighting, which is particularly relevant when measuring VBM fat unsaturation. In addition, multi-TE STEAM MRS with short TEs has been emerging as the method of choice to measure the VBM proton density FF[4] and typically includes the shortest-TE scan included in the present study.

Here the work has been based on the agreement of the OF values between two frequency-domain–fitting methods. Both frequency-domain and time-domain peak-fitting methods have been previously employed in the analysis of vertebral bone marrow spectra. Frequency-domain methods are typically limited to fitting the real part of a well-phased spectrum. Instead, time-domain methods fit the complex time-domain data and can more easily incorporate line-shape models and phase parameters, as has been also recently shown in vertebral bone marrow applications.[18] The proposed methodology used the frequency representation of the spectra to define WOPHD* based on the agreement of two fitting methods, given that a definition of the metric for the separability of the water and olefinic fat peaks is more intuitive in the frequency domain. However, metrics for assessing the separability of the water and olefinic fat peaks could be also constructed when using time-domain fitting methods.

The present study has several limitations. First, the definition of the threshold based on WOPHD and the determination of the two groups was based on the agreement of the results between two fitting methods, and there was no gold-standard experimental measurement available. In general, it is expected that when the olefinic peak is clearly separable from the water peak, both the constrained and unconstrained peak-fitting methods would give equivalent results for the OF. The application of the above observation on a rich data set of 252 spectra was the basis of the analysis in the determination of the two groups. Despite the lack of gold-standard reference measurements assessing the accuracy of the reported fatty acid composition metrics, the proposed methodology should provide a good estimation for which the VBM unsaturation is feasible and not confounded by overlapping water–fat peaks. Second, to address the lack of a reference experimental measurement, a Monte Carlo simulation was performed, which has some limitations of its own. The simulation considered only noise effects, which could explain the decrease in the slope for the two fitting methods agreement by increasing WOPHD, whereas the experimental data show an increasing slope with increasing WOPHD. However, including parameters to also simulate a model mismatch would require too many additional degrees of freedom. Third, a measurement of reproducibility would formally require repeated measurements with patient-repositioning. The computation of the CV based on a bootstrapping analysis should in part explain why the OF CV range reported here is significantly lower from the OF CV range reported in previous studies.[11] However, the bootstrap analysis was able to characterize the difference between the two groups, given the overall low SNR of the MR spectra in VBM. Fourth, J-coupling effects were minimized, but cannot be totally excluded when using short-TE STEAM MRS acquisition. Fifth, the Voigt lineshape factors in the presently employed frequency domain-based peak-fitting routines were determined empirically and were maintained constant across spectra.

5 | CONCLUSION

A threshold on the separability of the water peak and the olefinic fat peaks was defined for the estimation of the VBM fat unsaturation from short-TE STEAM MRS using a constrained peak fitting based on the triglyceride fat model. The proposed methodology shows that the assessment of VBM unsaturation is feasible with a short-TE STEAM MRS in subjects with a higher FF.

ACKNOWLEDGMENTS

The present work was supported by European Research Council (grant agreement No 677661, ProFatMRI). The authors would also like to acknowledge research support from

Philips Healthcare. This work reflects only the authors' views. The European Union is not responsible for any use that may be made of the information this work contains. Open access funding enabled and organized by Projekt DEAL.

CONFLICT OF INTEREST

The authors declare no conflict of interest.

ORCID

Jan Syväri https://orcid.org/0000-0002-3722-6914

REFERENCES

1. Devlin MJ, Rosen CJ. The bone–fat interface: basic and clinical implications of marrow adiposity. *Lancet Diab Endocrinol*. 2015;3:141-147.
2. Scheller EL, Rosen CJ. What's the matter with MAT? Marrow adipose tissue, metabolism, and skeletal health. *Ann NY Acad Sci*. 2014;1311:14-30.
3. Scheller EL, Doucette CR, Learman BS, et al. Region-specific variation in the properties of skeletal adipocytes reveals regulated and constitutive marrow adipose tissues. *Nat Commun*. 2015;6:7808.
4. Karampinos DC, Ruschke S, Dieckmeyer M, et al. Quantitative MRI and spectroscopy of bone marrow. *J Magn Reson Imaging*. 2018;47:332-353.
5. Paccou J, Hardouin P, Cotten A, Penel G, Cortet B. The role of bone marrow fat in skeletal health: usefulness and perspectives for clinicians. *J Clin Endocrinol Metab*. 2015;100:3613-3621.
6. Griffith JF, Yeung DK, Antonio GE, et al. Vertebral bone mineral density, marrow perfusion, and fat content in healthy men and men with osteoporosis: dynamic contrast-enhanced MR imaging and MR spectroscopy. *Radiology*. 2005;236:945-951.
7. Griffith JF, Yeung DK, Antonio GE, et al. Vertebral marrow fat content and diffusion and perfusion indexes in women with varying bone density: MR evaluation. *Radiology*. 2006;241:831-838.
8. Bredella MA, Fazeli PK, Miller KK, et al. Increased bone marrow fat in anorexia nervosa. *J Clin Endocrinol Metab*. 2009;94:2129-2136.
9. Cordes C, Baum T, Dieckmeyer M, et al. MR-based assessment of bone marrow fat in osteoporosis, diabetes, and obesity. *Front Endocrinol (Lausanne)*. 2016;7:74.
10. Yeung DK, Griffith JF, Antonio GE, Lee FK, Woo J, Leung PC. Osteoporosis is associated with increased marrow fat content and decreased marrow fat unsaturation: a proton MR spectroscopy study. *J Magn Reson Imaging*. 2005;22:279-285.
11. Li X, Kuo D, Schafer AL, et al. Quantification of vertebral bone marrow fat content using 3 Tesla MR spectroscopy: reproducibility, vertebral variation, and applications in osteoporosis. *J Magn Reson Imaging*. 2011;33:974-979.
12. Li X, Shet K, Xu K, et al. Unsaturation level decreased in bone marrow fat of postmenopausal women with low bone density using high resolution magic angle spinning (HRMAS) (1)H NMR spectroscopy. *Bone*. 2017;105:87-92.
13. Baum T, Yap SP, Karampinos DC, et al. Does vertebral bone marrow fat content correlate with abdominal adipose tissue, lumbar spine bone mineral density, and blood biomarkers in women with type 2 diabetes mellitus? *J Magn Reson Imaging*. 2012;35:117-124.
14. Patsch JM, Li X, Baum T, et al. Bone marrow fat composition as a novel imaging biomarker in postmenopausal women with prevalent fragility fractures. *J Bone Miner Res*. 2013;28:1721-1728.
15. Hu HH, Kan HE. Quantitative proton MR techniques for measuring fat. *NMR Biomed*. 2013;26:1609-1629.
16. Ren J, Dimitrov I, Sherry AD, Malloy CR. Composition of adipose tissue and marrow fat in humans by 1H NMR at 7 Tesla. *J Lipid Res*. 2008;49:2055-2062.
17. Dieckmeyer M, Ruschke S, Cordes C, et al. The need for T(2) correction on MRS-based vertebral bone marrow fat quantification: implications for bone marrow fat fraction age dependence. *NMR Biomed*. 2015;28:432-439.
18. Xu K, Sigurdsson S, Gudnason V, Hue T, Schwartz A, Li X. Reliable quantification of marrow fat content and unsaturation level using in vivo MR spectroscopy. *Magn Reson Med*. 2018;79:1722-1729.
19. Hamilton G, Middleton MS, Bydder M, et al. Effect of PRESS and STEAM sequences on magnetic resonance spectroscopic liver fat quantification. *J Magn Reson Imaging*. 2009;30:145-152.
20. Ruschke S, Kienberger H, Baum T, et al. Diffusion-weighted stimulated echo acquisition mode (DW-STEAM) MR spectroscopy to measure fat unsaturation in regions with low proton-density fat fraction. *Magn Reson Med*. 2016;75:32-41.
21. Lundbom J, Hakkarainen A, Soderlund S, Westerbacka J, Lundbom N, Taskinen MR. Long-TE 1H MRS suggests that liver fat is more saturated than subcutaneous and visceral fat. *NMR Biomed*. 2011;24:238-245.
22. Troitskaia A, Fallone BG, Yahya A. Long echo time proton magnetic resonance spectroscopy for estimating relative measures of lipid unsaturation at 3T. *J Magn Reson Imaging*. 2013;37:944-949.
23. Bingolbali A, Fallone BG, Yahya A. Comparison of optimized long echo time STEAM and PRESS proton MR spectroscopy of lipid olefinic protons at 3 Tesla. *J Magn Reson Imaging*. 2015;41:481-486.
24. Fallone CJ, McKay RT, Yahya A. Long TE STEAM and PRESS for estimating fat olefinic/methyl ratios and relative omega-3 fat content at 3T. *J Magn Reson Imaging*. 2018;48:169-177.
25. Hamilton G, Yokoo T, Bydder M, et al. In vivo characterization of the liver fat (1)H MR spectrum. *NMR Biomed*. 2011;24:784-790.
26. Nemeth A, Segrestin B, Leporq B, et al. Comparison of MRI-derived vs. traditional estimations of fatty acid composition from MR spectroscopy signals. *NMR Biomed*. 2018;31:e3991.
27. Marshall I, Higinbotham J, Bruce S, Freise A. Use of voigt lineshape for quantification of in vivo 1H spectra. *Magn Reson Med*. 1997;37:651-657.
28. Bydder M, Girard O, Hamilton G. Mapping the double bonds in triglycerides. *Magn Reson Imaging*. 2011;29:1041-1046.

SUPPORTING INFORMATION

Additional Supporting Information may be found online in the Supporting Information section.

FIGURE S1 Dependence of A, OF of the constrained fitting method, B, OF of the unconstrained fitting method, C, WOPHD on the fat fraction based on simulated spectra (ndb = 3.0, nmidb = 1.0, linewidth = 0.45 ppm and SNR = 60). The red line indicates the reference OF value

FIGURE S2 Dependence of A, OF of the constrained fitting method, B, OF of the unconstrained fitting method, C, WOPHD on the linewidth based on simulated spectra

(FF = 50%, ndb = 3.0, nmidb = 1.0 and SNR = 60). The red line indicates the reference OF value

FIGURE S3 Dependence of A, OF of the constrained fitting method, B, OF of the unconstrained fitting method, C, WOPHD on SNR based on simulated spectra (FF = 50%, ndb = 3.0, nmidb = 1.0 and linewidth = 0.45 ppm). The red line indicates the reference OF value

How to cite this article: Syväri J, Ruschke S, Dieckmeyer M, et al. Estimating vertebral bone marrow fat unsaturation based on short-TE STEAM MRS. *Magn Reson Med*. 2021;85:615–626. https://doi.org/10.1002/mrm.28453

7 Discussion

7.1 Review of Existing Literature

Fat accumulation as a biomarker is a very good biomarker for characterizing and monitoring diseases. Next to the pure amount of fat, MRI also offers the possibility to look at different parameters like fat fraction or unsaturation rate. Change of fat volume and composition in most fat depots of the body depend on the nutritional state of the subject. Therefore, it can be used to monitor metabolic disorders. There is normally almost no fat in the liver of a healthy person[14]. However, with a sedentary lifestyle and an increasing prevalence of obesity, the prevalence of liver fat is also increasing. As liver fat does not occur in early stages of obesity, it is rather used for monitoring the risk of complication like liver cirrhosis[82]. Bone marrow fat content behaves differently compared to other fat depots. The content of adipose tissue in bone marrow is independent of the nutritional status of the individual. Instead, it seems to be more related to bone marrow health. Therefore, accessing adipose tissue in bone marrow with the MR could result in early detection of bone marrow diseases like osteoporosis[92, 93, 94, 23, 95, 96]. Additional to the different behaviour regarding the nutritional state, bone marrow is more difficult to access with the MR steaming from low SNR. The next sections will be a literature summary about the biomarker fat in the liver (7.1.1) and bone marrow (7.1.2) using the MR.

7.1.1 Liver Fat Fraction Biomarker

With an increasing prevalence of the metabolic syndrome the prevalence of fat deposition across organs is also increasing[1], and therefore a good biomarker tracking liver fat is needed to monitoring therapy and prevent complications to appear like liver cirrhosis, liver insufficiency or carcinoma[35, 82]. It is especially important as these complications are irreversible, in contrast to early stages of liver fat deposition[2, 3]. There are multiple ways of measuring liver fat. The gold standard is taking a biopsy. A biopsy has the disadvantage of very low spatial resolution as only on small part of the liver is covered. Additionally, a biopsy is highly invasive and therefore very uncomfortable for the patient and has a risk for complications such as infections. Especially for longitudinal setups as therapy monitoring it is not feasible. It is also possible to use ultrasound for detecting liver fat. Ultrasound is ubiquitous available in the Western world and is a very fast and cheap method. Disadvantages are that it is very depending on the examiner and it is a qualitative method and can not be quantified. However, the ultrasound is a very good method for screening for liver fat[105]. The MR offers a method to quantify liver fat non-invasively and reproducible. PDFF as a biomarker offers these advantages. MRS is

often used to quantify liver fat[106, 107, 108]. It shows very accurate results which are very reproducible. It also offers the advantage of extracting unsaturation rate. The main disadvantage is that MRS offers low spatial resolution. MRI-based PDFF-mapping offers the advantage of high spatial resolution. The results are also very robust and accurate. It is also well validated in comparison with biopsies and MRS[109, 110]. It also offers the advantage of covering the whole organ with one single sequence in one breath-hold with adequate resolution. Multiple cross-sectional studies have shown a heterogeneous distribution of fat in the liver[83, 84, 85]. The right lobe has higher fat fraction compared to the left lobe. Recently it was shown, that after bariatric weight-loss surgery the fat fraction in the right liver lobe (RLL) was reduced faster compared to left lobe (LLL)[87, 21].

7.1.2 Bone Marrow Fat Fraction and Unsaturation Rate Biomarkers

Bone marrow can be subdivided in two different kinds of bone marrow: in red and yellow bone marrow. Red bone marrow is hematopoietically active and has high amount of water next to the bone matrix. Yellow bone marrow has higher amount of lipids. With increasing age a lot of red bone marrow is converted to yellow bone marrow. This is also represented in bone marrow fat. With increasing age the fat fraction is increasing. Fat fraction in bone marrow is also sex dependent. Young male subjects have higher amounts of fat fraction in the vertebrae compared to young female subjects. With increasing age the difference is reduced and around the age of 50 the fat fraction is even between male and female subjects[23, 95]. Griffith et al even showed a higher fat fraction in female subjects in the group older than 50 years compared to the male subjects[96]. An explanation offered by the authors is a redistribution of the fat during the menopause. Baum et al showed lower fat fraction in more cranial vertebrae and higher fat fraction in the more caudal vertebrae[23]. Vertebral bone marrow can be assessed with chemical-shift encoding-based water-fat imaging or ^{1}H-MRS[100, 20, 16]. Chemical-shift encoding-based water-fat imaging has the advantage of covering the whole spine in one single sequence. ^{1}H-MRS only covers one single vertebrae, but it offers further information about the vertebrae like the unsaturation rate. Unsaturation rate becomes of higher interest for research. A decrease in unsaturation rate in vertebral bone marrow is associated with osteoporosis[15, 30, 19]. It was also shown that people suffering from DM-II also have lower unsaturation rate[16].

7.2 Present Work

The dissertation offers several contributions in the field of MR measurements for measuring fat in different fat depots across the body. The journal publications (JP) emphasize on optimizing measuring of fat properties depending on difficulties in each respective tissue. JP-I focuses on spatial distribution of fat in the liver and the differences in the changes during an intervention. JP-II describes and establishes a method to separate MR spectra in bone marrow, where the unsaturation rate of fat can be measured reliable

from spectroscopies where the unsaturation rate of fat can not be measured reliable due to broad linewidth and overlaying water peak.

7.2.1 Novelty

Both JPs contribute to the field in MR of measuring properties of fat across the body. JP-I describes a longitudinal study showing the heterogeneous liver distribution in the liver during a long-term intervention. It was shown that after bariatric surgery the fat in the RLL decreases faster compared to the LLL[87]. The novelty of the JP-I in this dissertation is that subjects with in- and decreasing liver fat were included and showing stronger changes in the RLL. This emphasizes the importance of high spatial resolution when measuring liver fat. JP-II focuses on bone marrow adipose tissue, which behaves differently than other types of adipose tissue and is more complicated to measure with the MR. Spatial resolution is less important, but therefore it is more important to focus on the fat composition. Bone marrow MRS faces technical challenges and the measurement of the unsaturation is not always reliable due to broad linewidth and an overlaying water peak. This publication proposes a new metric to quickly separate spectra in two groups, where the unsaturation rate can be measured reliably in one group compared to the other group where the measurement of unsaturation rate is not reliable.

7.2.2 Impact

This dissertation improves the noninvasive assessment of different fat depots across the body with MR.

In JP-I, PDFF was determined in all 9 Couinaud liver segments as well as in the LLL and RLL. The findings show that changes in the RLL are much stronger compared to the LLL which is very interesting for monitoring subjects with NAFLD. Even the differences between individual segments could be shown. Single-voxel ^1H-MRS and even liver biopsies which are the gold standard for measuring liver fat miss the heterogeneity of liver fat. Using these techniques with low spatial resolution could over- or underestimate the changes of liver fat. JP-I emphasis this aspect of liver fat imaging and highlights the importance of using techniques which access liver fat with high spatial resolution.

In JP-II single-voxel-^{1}H-MRS was performed in the vertebral bone marrow and a metric was developed and established for a fast estimation whether the measurement of the fat unsaturation rate is feasible. If all measured bone marrow spectra are treated equally the reproducibility of the measurement of the unsaturation in some spectra is very low. However, up to this point the investigator had no objective metric to determine the feasibility of the measurement of unsaturation rate. So far, the examiner needed to decide this based on the visibility of the olefinic peak. This leads to big differences between observers. JP-II shows big differences in the feasibility of measuring the fat unsaturation rate in bone marrow and also large differences in the reproducibility between different subjects. In the future this metric should be applied to see if the measured unsaturation rate is feasible and, therefore, improves future research regarding bone marrow fat unsaturation rate.

7.2.3 Limitations

The publications included in this dissertation are not free of limitations, which are discussed in this paragraph. JP-I was a long term lifestyle intervention study with very small control over the compliance of the included participants, leading to increasing and decreasing weight and resulting increasing and decreasing liver fat during the one year observation period. Some subjects were also included after the one-year intervention. However, further analysis showed no significant difference in weight change between these two groups. Another limitation is that not the whole liver was covered by the applied sequence. Therefore, the total liver fat could not be measured, but was calculated as the average between the ROIs of each segment[111]. Also, a larger cohort would have strengthened the conclusion of the study. Further studies should replicate the results.

In JP-II the biggest limitation is that there is no gold standard for measuring the in-vivo bone marrow fat unsaturation rate. To address this issue, a Monte Carlo simulation was performed with limitations of its own. In the simulation only noise effects were considered. Model mismatches were not considered as it would need a lot of included parameters and therefore require multiple degrees of freedom. Also, due to no gold standard measurement, the proposed metric was defined by the agreement of two different models of fitting bone marrow spectroscopy. Another limitation is the way reproducibility was measured. Usually, repeated measurements with repositioning of the subject should be performed. However, the bootstrap analysis performed in this study was able to show higher reproducibility of measuring the fat unsaturation rate in the group with better measurement of the unsaturation rate determined by the metric.

7.3 Perspective

This dissertation focuses on the improved non-invasive characterization of fat. Overall, imaging of fat and its properties with MR will increase in significance in identifying risk factors, early diagnosis of diseases and therapy monitoring. Concretely, the JPs included in this dissertation have multiple applications and also different further developments can be thought of.

JP-I included only a small number of subjects. Further studies should include more subjects and confirming the results from this study. As PDFF mapping is a very robust biomarker, a clinical application could also be a potential next step. This would improve the possibility of monitoring NASH and could also identify complications like liver cirrhosis or carcinoma earlier. The main problem could be high cost and not long scan times of the MR making it difficult to implement it in the clinical routines. Especially, as ultrasound also can detect liver fat and other changes in the liver and is much cheaper and universal available. Another direction ongoing research should continue is understanding the reason of the heterogeneous fat distribution in the liver. Some studies suggest difference in perfusion of the liver as an explanation for the heterogeneous changes in liver PDFF. However, the results of studies investigating liver perfusion are not consistent[88, 89, 90] so a clear explanation is still missing.

The new method of JP-II should find usage especially in research. So far, most studies

do not differentiate between spectra with reliable measurement of the bone marrow fat unsaturation rate from other spectra. Therefore, the measured results might differentiate from the true unsaturation rate and wrong assumption could be made. From now on, studies measuring fat unsaturation rate in bone marrow should use the metric suggested in JP-II.

7.4 Conclusion

In conclusion, this thesis focuses on the assessment of different fat parameters with MR across the body. It shows that fat in different areas of the human body must be treated differently, regarding technical approach and the interpretation of the data. The ectopic liver fat is an early indicator of an unhealthy lifestyle, while bone marrow adipose tissue is not influenced by the nutritional state but by the general bone health. In this dissertation it was shown that high spatial resolution is important when measuring liver fat as it is very heterogenous distributed. It was also shown that changes in liver fat content are very heterogeneous. Regarding bone marrow this dissertation provides a method to differentiate between olefinic peaks that can be measured reliable with Magnetic Resonance Spectroscopy and ones that are not reliably measured.

Further research must take these differences into account to develop more specific fat related biomarkers to create a clinical impact.

Acknowledgements

I am very gratful for all the support I got during my time as a medical student writing my doctoral thesis. First of all, I would like to thank Dimitrios Karampinos for his amazing support as my supervisor. He always helped me during my times in the research group independent whether the issue was explaining me the basics of MR, helping and correcting my manuscripts or discussing ideas and much, much more. I would also like to say thank you to Thomas Baum and Daniela Junker as my supervisors from the clinical side of this thesis, who always gave me constructive feedback and advice for continuing my work.

Furthermore, I want to thank Stefan Ruschke, who always helped me with technical aspects of my thesis by solving software and hardware issues whenever I needed him.

A special thanks goes to Maximilian Diefenbach who introduced me into the world of coding and being patient with me while explaining me basic principals of coding, which facilitated my work distinctly.

I also wish to thank all the members of our research group for your continuous feedback and always generating a great atmosphere. I am very glad that I was able to write my medical thesis in the Body Magnetic Resonance Research Group and had such wonderful years there.

Finally, I would like to express my deepest gratitude to my family and my friends, who always supported me on my way.

List of Symbols and Abbreviations

2D	two-dimensional
3D	three-dimensional
^{1}H	proton
B0	static main magnetic field [T]
BMD	bone mineral density
CSI	chemical shift imaging
CT	computed tomography
HCC	hepatocellular carcinoma
LLL	left liver lobe
MR	magentic resoance
MRI	magenetic resonance imaging
MRS	magnetic resonance spectroscopy
NASH	Nonalcoholic Steatohepatitis
NMD	neuromuscular disease
NMR	nuclear magnetic resonance
PDFF	proton density fat fraction
ppm	parts per million
PRESS	point-resolved spectroscopy
RF	radio frequency (pulse)
RLL	right liver lobe
ROI	region of interest
SAT	subcutaneous adipose tissue
SNR	signal-to-noise ratio

STEAM	stimulated echo aquisition mode
t	time
T_1	spin-lattice (longitudinal) relaxation time [s]
T_{2*}	effective transverse relaxation time [s]
T_{2w}	T_2 water, spin-spin (transverse) relaxation time of the water component in the tissue [s]
T_2	spin-spin (transverse) relaxation time [s]
TE	echo time
TI	inverison recovery time
TR	repetition time
TSE	turbo spin echo
VAT	visceral adipose tissue
VBM	vertebral bone marrow
VOI	volume of interest
WHO	world health organization

List of Figures

Bibliography

[1] Chris Estes, Homie Razavi, Rohit Loomba, Zobair Younossi, and Arun J Sanyal. "Modeling the epidemic of nonalcoholic fatty liver disease demonstrates an exponential increase in burden of disease". In: *Hepatology* 67.1 (2018), pp. 123–133.

[2] Lian Tock, Wagner L Prado, Danielle A Caranti, Dejaldo MJ Cristofalo, Henrique Lederman, Mauro Fisberg, Kali O Siqueira, Sergio G Stella, Hanna K Antunes, Isa P Cintra, et al. "Nonalcoholic fatty liver disease decrease in obese adolescents after multidisciplinary therapy". In: *European journal of gastroenterology & hepatology* 18.12 (2006), pp. 1241–1245.

[3] Elisabetta Bacchi, Carlo Negri, Giovanni Targher, Niccolo Faccioli, Massimo Lanza, Giacomo Zoppini, Elisabetta Zanolin, Federico Schena, Enzo Bonora, and Paolo Moghetti. "Both resistance training and aerobic training reduce hepatic fat content in type 2 diabetic subjects with nonalcoholic fatty liver disease (the RAED2 Randomized Trial)". In: *Hepatology* 58.4 (2013), pp. 1287–1295.

[4] Miriam A Bredella, Pouneh K Fazeli, Scott M Daley, Karen K Miller, Clifford J Rosen, Anne Klibanski, and Martin Torriani. "Marrow fat composition in anorexia nervosa". In: *Bone* 66 (2014), pp. 199–204.

[5] Erwin L Hahn. "Spin echoes". In: *Physical review* 80.4 (1950), p. 580.

[6] Herman Y Carr. "Free Precession Techniques in Nuclear Magnetic Resonance." In: *Ph. D. Thesis* (1953).

[7] Paul C Lauterbur. "Image formation by induced local interactions: examples employing nuclear magnetic resonance". In: *nature* 242.5394 (1973), pp. 190–191.

[8] Peter Mansfield and Peter K Grannell. "" Diffraction" and microscopy in solids and liquids by NMR". In: *Physical Review B* 12.9 (1975), p. 3618.

[9] Peter Mansfield and Andrew A Maudsley. "Medical imaging by NMR". In: *The British journal of radiology* 50.591 (1977), pp. 188–194.

[10] Daniel R Messroghli, James C Moon, Vanessa M Ferreira, Lars Grosse-Wortmann, Taigang He, Peter Kellman, Julia Mascherbauer, Reza Nezafat, Michael Salerno, Erik B Schelbert, et al. "Clinical recommendations for cardiovascular magnetic resonance mapping of T1, T2, T2* and extracellular volume: a consensus statement by the Society for Cardiovascular Magnetic Resonance (SCMR) endorsed by the European Association for Cardiovascular Imaging (EACVI)". In: *Journal of Cardiovascular Magnetic Resonance* 19.1 (2017), pp. 1–24.

[11] Vanessa M Ferreira, Stefan K Piechnik, Matthew D Robson, Stefan Neubauer, and Theodoros D Karamitsos. "Myocardial tissue characterization by magnetic resonance imaging: novel applications of T1 and T2 mapping". In: *Journal of thoracic imaging* 29.3 (2014), p. 147.

[12] Sina Meisamy, Catherine DG Hines, Gavin Hamilton, Claude B Sirlin, Charles A McKenzie, Huanzhou Yu, Jean H Brittain, and Scott B Reeder. "Quantification of hepatic steatosis with T1-independent, T2*-corrected MR imaging with spectral modeling of fat: blinded comparison with MR spectroscopy". In: *Radiology* 258.3 (2011), pp. 767–775.

[13] Gary P Liney, Adrian J Knowles, David J Manton, Lindsay W Turnbull, Stephen J Blackband, and Anthony Horsman. "Comparison of conventional single echo and multi-echo sequences with a fast spin-echo sequence for quantitative T2 mapping: application to the prostate". In: *Journal of Magnetic Resonance Imaging* 6.4 (1996), pp. 603–607.

[14] Henry R Wilman, Matt Kelly, Steve Garratt, Paul M Matthews, Matteo Milanesi, Amy Herlihy, Micheal Gyngell, Stefan Neubauer, Jimmy D Bell, Rajarshi Banerjee, et al. "Characterisation of liver fat in the UK Biobank cohort". In: *PloS one* 12.2 (2017), e0172921.

[15] David KW Yeung, James F Griffith, Gregory E Antonio, Francis KH Lee, Jean Woo, and Ping C Leung. "Osteoporosis is associated with increased marrow fat content and decreased marrow fat unsaturation: a proton MR spectroscopy study". In: *Journal of Magnetic Resonance Imaging: An Official Journal of the International Society for Magnetic Resonance in Medicine* 22.2 (2005), pp. 279–285.

[16] Janina M Patsch, Xiaojuan Li, Thomas Baum, Samuel P Yap, Dimitrios C Karampinos, Ann V Schwartz, and Thomas M Link. "Bone marrow fat composition as a novel imaging biomarker in postmenopausal women with prevalent fragility fractures". In: *Journal of bone and mineral research* 28.8 (2013), pp. 1721–1728.

[17] James F Griffith, David KW Yeung, Gregory E Antonio, Francis KH Lee, Athena WL Hong, Samuel YS Wong, Edith MC Lau, and Ping Chung Leung. "Vertebral bone mineral density, marrow perfusion, and fat content in healthy men and men with osteoporosis: dynamic contrast-enhanced MR imaging and MR spectroscopy". In: *Radiology* 236.3 (2005), pp. 945–951.

[18] Timothy JP Bray, Alan Bainbridge, Shonit Punwani, Yiannis Ioannou, and Margaret A Hall-Craggs. "Simultaneous quantification of bone edema/adiposity and structure in inflamed bone using chemical shift-encoded MRI in spondyloarthritis". In: *Magnetic resonance in medicine* 79.2 (2018), pp. 1031–1042.

[19] Thomas Baum, Samuel P Yap, Dimitrios C Karampinos, Lorenzo Nardo, Daniel Kuo, Andrew J Burghardt, Umesh B Masharani, Ann V Schwartz, Xiaojuan Li, and Thomas M Link. "Does vertebral bone marrow fat content correlate with abdominal adipose tissue, lumbar spine bone mineral density, and blood biomarkers in women with type 2 diabetes mellitus?" In: *Journal of Magnetic Resonance Imaging* 35.1 (2012), pp. 117–124.

[20] Christian Cordes, Michael Dieckmeyer, Beate Ott, Jun Shen, Stefan Ruschke, Marcus Settles, Claudia Eichhorn, Jan S Bauer, Hendrik Kooijman, Ernst J Rummeny, et al. "MR-detected changes in liver fat, abdominal fat, and vertebral bone marrow fat after a four-week calorie restriction in obese women". In: *Journal of Magnetic Resonance Imaging* 42.5 (2015), pp. 1272–1280.

[21] Jan Syväri, Daniela Junker, Lisa Patzelt, Katharina Kappo, Loubna Al Sadat, Sonia Erfanian, Marcus R Makowski, Hans Hauner, and Dimitrios C Karampinos. "Longitudinal changes on liver proton density fat fraction differ between liver segments". In: *Quantitative Imaging in Medicine and Surgery* 11.5 (2021), p. 1701.

[22] Donald G Mitchell, Jordi Bruix, Morris Sherman, and Claude B Sirlin. "LI-RADS (Liver Imaging Reporting and Data System): Summary, discussion, and consensus of the LI-RADS Management Working Group and future directions". In: *Hepatology* 61.3 (2015), pp. 1056–1065.

[23] Thomas Baum, Samuel P Yap, Michael Dieckmeyer, Stefan Ruschke, Holger Eggers, Hendrik Kooijman, Ernst J Rummeny, Jan S Bauer, and Dimitrios C Karampinos. "Assessment of whole spine vertebral bone marrow fat using chemical shift-encoding based water-fat MRI". In: *Journal of Magnetic Resonance Imaging* 42.4 (2015), pp. 1018–1023.

[24] Dimitrios C Karampinos, Gerd Melkus, Thomas Baum, Jan S Bauer, Ernst J Rummeny, and Roland Krug. "Bone marrow fat quantification in the presence of trabecular bone: initial comparison between water-fat imaging and single-voxel MRS". In: *Magnetic Resonance in Medicine* 71.3 (2014), pp. 1158–1165.

[25] Stefan Ruschke, Amber Pokorney, Thomas Baum, Holger Eggers, Jeffrey H Miller, Houchun H Hu, and Dimitrios C Karampinos. "Measurement of vertebral bone marrow proton density fat fraction in children using quantitative water–fat MRI". In: *Magnetic Resonance Materials in Physics, Biology and Medicine* 30.5 (2017), pp. 449–460.

[26] Felix W Wehrli, Jeffrey A Hopkins, Scott N Hwang, Hee Kwon Song, Peter J Snyder, and John G Haddad. "Cross-sectional study of osteopenia with quantitative MR imaging and bone densitometry". In: *Radiology* 217.2 (2000), pp. 527–538.

[27] Dimitrios C Karampinos, Stefan Ruschke, Olga Gordijenko, Eduardo Grande Garcia, Hendrik Kooijman, Rainer Burgkart, Ernst J Rummeny, Jan S Bauer, and Thomas Baum. "Association of MRS-based vertebral bone marrow fat frac-

tion with bone strength in a human in vitro model". In: *Journal of osteoporosis* 2015 (2015).

[28] GM Blake, JF Griffith, DKW Yeung, PC Leung, and I Fogelman. "Effect of increasing vertebral marrow fat content on BMD measurement, T-Score status and fracture risk prediction by DXA". In: *Bone* 44.3 (2009), pp. 495–501.

[29] James F Griffith, David KW Yeung, Gregory E Antonio, Samuel YS Wong, Timothy CY Kwok, Jean Woo, and Ping C Leung. "Vertebral marrow fat content and diffusion and perfusion indexes in women with varying bone density: MR evaluation". In: *Radiology* 241.3 (2006), pp. 831–838.

[30] Xiaojuan Li, Keerthi Shet, Kaipin Xu, Juan Pablo Rodrıguez, Ana Marıa Pino, John Kurhanewicz, Ann Schwartz, and Clifford J Rosen. "Unsaturation level decreased in bone marrow fat of postmenopausal women with low bone density using high resolution magic angle spinning (HRMAS) 1H NMR spectroscopy". In: *Bone* 105 (2017), pp. 87–92.

[31] Raghu Teja Sadineni, Ashirwad Pasumarthy, Narayan Chander Bellapa, and Sandeep Velicheti. "Imaging patterns in MRI in recent bone injuries following negative or inconclusive plain radiographs". In: *Journal of clinical and diagnostic research: JCDR* 9.10 (2015), TC10.

[32] World Health Organization. "Obesity: preventing and managing the global epidemic". In: (2000).

[33] N Holman, NG Forouhi, E Goyder, and SH Wild. "The Association of Public Health Observatories (APHO) diabetes prevalence model: estimates of total diabetes prevalence for England, 2010–2030". In: *Diabetic Medicine* 28.5 (2011), pp. 575–582.

[34] King Sun Leong and John P Wilding. "Obesity and diabetes". In: *Best Practice & Research Clinical Endocrinology & Metabolism* 13.2 (1999), pp. 221–237.

[35] Rohit Loomba and Arun J Sanyal. "The global NAFLD epidemic". In: *Nature reviews Gastroenterology & hepatology* 10.11 (2013), pp. 686–690.

[36] Gary J Cowin, Julie R Jonsson, Judith D Bauer, Susan Ash, Azmat Ali, Emma J Osland, David M Purdie, Andrew D Clouston, Elizabeth E Powell, and Graham J Galloway. "Magnetic resonance imaging and spectroscopy for monitoring liver steatosis". In: *Journal of Magnetic Resonance Imaging: An Official Journal of the International Society for Magnetic Resonance in Medicine* 28.4 (2008), pp. 937–945.

[37] Bernadette E Vitola, Sheela Deivanayagam, Richard I Stein, Balsamanirina S Mohammed, Faidon Magkos, Erik P Kirk, and Samuel Klein. "Weight loss reduces liver fat and improves hepatic and skeletal muscle insulin sensitivity in obese adolescents". In: *Obesity* 17.9 (2009), pp. 1744–1748.

[38] Victor J Stevens, Eva Obarzanek, Nancy R Cook, I-Min Lee, Lawrence J Appel, Delia Smith West, N Carole Milas, Mildred Mattfeldt-Beman, Lorna Belden, Charlotte Bragg, et al. "Long-term weight loss and changes in blood pressure: results of the Trials of Hypertension Prevention, phase II". In: *Annals of internal medicine* 134.1 (2001), pp. 1–11.

[39] Kenneth Fearon, Florian Strasser, Stefan D Anker, Ingvar Bosaeus, Eduardo Bruera, Robin L Fainsinger, Aminah Jatoi, Charles Loprinzi, Neil MacDonald, Giovanni Mantovani, et al. "Definition and classification of cancer cachexia: an international consensus". In: *The lancet oncology* 12.5 (2011), pp. 489–495.

[40] Madhusmita Misra and Anne Klibanski. "Anorexia nervosa, obesity and bone metabolism". In: *Pediatric endocrinology reviews: PER* 11.1 (2013), p. 21.

[41] Nancy A Rigotti, Samuel R Nussbaum, David B Herzog, and Robert M Neer. "Osteoporosis in women with anorexia nervosa". In: *New England Journal of Medicine* 311.25 (1984), pp. 1601–1606.

[42] Madhusmita Misra and Anne Klibanski. "Anorexia nervosa and osteoporosis". In: *Reviews in Endocrine and Metabolic Disorders* 7.1 (2006), pp. 91–99.

[43] Daniela Franz, Jan Syväri, Dominik Weidlich, Thomas Baum, Ernst J Rummeny, and Dimitrios C Karampinos. "Magnetic resonance imaging of adipose tissue in metabolic dysfunction". In: *RöFo-Fortschritte auf dem Gebiet der Röntgenstrahlen und der bildgebenden Verfahren*. Vol. 190. 12. © Georg Thieme Verlag KG. 2018, pp. 1121–1130.

[44] WA Spencer and Gr Dempster. "The lipids of mouse brown fat". In: *Canadian journal of biochemistry and physiology* 40.12 (1962), pp. 1705–1715.

[45] Charmaine S Tam, Virgile Lecoultre, and Eric Ravussin. "Brown adipose tissue: mechanisms and potential therapeutic targets". In: *Circulation* 125.22 (2012), pp. 2782–2791.

[46] Jürgen Machann, Norbert Stefan, Robert Wagner, Malte Bongers, Erwin Schleicher, Andreas Fritsche, Hans-Ulrich Häring, Konstantin Nikolaou, and Fritz Schick. "Intra-and interindividual variability of fatty acid unsaturation in six different human adipose tissue compartments assessed by 1H-MRS in vivo at 3 T". In: *NMR in Biomedicine* 30.9 (2017), e3744.

[47] Anwar Borai, Callum Livingstone, Fatima Abdelaal, Ali Bawazeer, Vuyolethu Keti, and Gordon Ferns. "The relationship between glycosylated haemoglobin (HbA1c) and measures of insulin resistance across a range of glucose tolerance". In: *Scandinavian journal of clinical and laboratory investigation* 71.2 (2011), pp. 168–172.

[48] Matthew Harms and Patrick Seale. "Brown and beige fat: development, function and therapeutic potential". In: *Nature medicine* 19.10 (2013), pp. 1252–1263.

[49] JULIET M Heaton. "The distribution of brown adipose tissue in the human." In: *Journal of anatomy* 112.Pt 1 (1972), p. 35.

[50] Carmel G Cronin, Priyanka Prakash, Gilbert H Daniels, Giles W Boland, Mannudeep K Kalra, Elkan F Halpern, Edwin L Palmer, and Michael A Blake. "Brown fat at PET/CT: correlation with patient characteristics". In: *Radiology* 263.3 (2012), pp. 836–842.

[51] Aaron M Cypess, Sanaz Lehman, Gethin Williams, Ilan Tal, Dean Rodman, Allison B Goldfine, Frank C Kuo, Edwin L Palmer, Yu-Hua Tseng, Alessandro Doria, et al. "Identification and importance of brown adipose tissue in adult humans". In: *New England journal of medicine* 360.15 (2009), pp. 1509–1517.

[52] Wouter D van Marken Lichtenbelt, Joost W Vanhommerig, Nanda M Smulders, Jamie MAFL Drossaerts, Gerrit J Kemerink, Nicole D Bouvy, Patrick Schrauwen, and GJ Jaap Teule. "Cold-activated brown adipose tissue in healthy men". In: *New England Journal of Medicine* 360.15 (2009), pp. 1500–1508.

[53] Saverio Cinti. "The role of brown adipose tissue in human obesity". In: *Nutrition, metabolism and cardiovascular diseases* 16.8 (2006), pp. 569–574.

[54] Aaron M Cypess and C Ronald Kahn. "Brown fat as a therapy for obesity and diabetes". In: *Current opinion in endocrinology, diabetes, and obesity* 17.2 (2010), p. 143.

[55] Patrick Seale and Mitchell A Lazar. "Brown fat in humans: turning up the heat on obesity". In: *Diabetes* 58.7 (2009), pp. 1482–1484.

[56] Daniela Franz, Dimitrios C Karampinos, Ernst J Rummeny, Michael Souvatzoglou, Ambros J Beer, Stephan G Nekolla, Markus Schwaiger, and Matthias Eiber. "Discrimination between brown and white adipose tissue using a 2-point Dixon water–fat separation method in simultaneous PET/MRI". In: *Journal of Nuclear Medicine* 56.11 (2015), pp. 1742–1747.

[57] Houchun H Hu, Daniel L Smith Jr, Krishna S Nayak, Michael I Goran, and Tim R Nagy. "Identification of brown adipose tissue in mice with fat–water IDEAL-MRI". In: *Journal of Magnetic Resonance Imaging: An Official Journal of the International Society for Magnetic Resonance in Medicine* 31.5 (2010), pp. 1195–1202.

[58] Vanessa Stahl, Florian Maier, Martin T Freitag, Ralf O Floca, Moritz C Berger, Reiner Umathum, Mauricio Berriel Diaz, Stephan Herzig, Marc-André Weber, Antonia Dimitrakopoulou-Strauss, et al. "In vivo assessment of cold stimulation effects on the fat fraction of brown adipose tissue using DIXON MRI". In: *Journal of Magnetic Resonance Imaging* 45.2 (2017), pp. 369–380.

[59] Jerod M Rasmussen, Sonja Entringer, Annie Nguyen, Theo GM van Erp, Ana Guijarro, Fariba Oveisi, James M Swanson, Daniele Piomelli, Pathik D Wadhwa, Claudia Buss, et al. "Brown adipose tissue quantification in human neonates using water-fat separated MRI". In: *PloS one* 8.10 (2013), e77907.

[60] Gavin Hamilton, Daniel L Smith Jr, Mark Bydder, Krishna S Nayak, and Houchun H Hu. "MR properties of brown and white adipose tissues". In: *Journal of Magnetic Resonance Imaging* 34.2 (2011), pp. 468–473.

[61] Wei Shen, ZiMian Wang, Mark Punyanita, Jianbo Lei, Ahmet Sinav, John G Kral, Celina Imielinska, Robert Ross, and Steven B Heymsfield. "Adipose tissue quantification by imaging methods: a proposed classification". In: *Obesity research* 11.1 (2003), pp. 5–16.

[62] Daniel Deschênes, Patrick Couture, Pierre Dupont, and André Tchernof. "Subdivision of the subcutaneous adipose tissue compartment and lipid-lipoprotein levels in women". In: *Obesity research* 11.3 (2003), pp. 469–476.

[63] Rachel Golan, Ilan Shelef, Assaf Rudich, Yftach Gepner, Elad Shemesh, Yoash Chassidim, Ilana Harman-Boehm, Yaakov Henkin, Dan Schwarzfuchs, Sivan Ben Avraham, et al. "Abdominal superficial subcutaneous fat: a putative distinct protective fat subdepot in type 2 diabetes". In: *Diabetes care* 35.3 (2012), pp. 640–647.

[64] Juraj Koska, Norbert Stefan, Susanne B Votruba, Steven R Smith, Jonathan Krakoff, and Joy C Bunt. "Distribution of subcutaneous fat predicts insulin action in obesity in sex-specific manner". In: *Obesity* 16.9 (2008), pp. 2003–2009.

[65] David E Kelley, F Leland Thaete, Fred Troost, Trina Huwe, and Bret H Goodpaster. "Subdivisions of subcutaneous abdominal adipose tissue and insulin resistance". In: *American Journal of Physiology-Endocrinology And Metabolism* 278.5 (2000), E941–E948.

[66] Gavin Hamilton, Alexandra N Schlein, Michael S Middleton, Catherine A Hooker, Tanya Wolfson, Anthony C Gamst, Rohit Loomba, and Claude B Sirlin. "In vivo triglyceride composition of abdominal adipose tissue measured by 1H MRS at 3T". In: *Journal of Magnetic Resonance Imaging* 45.5 (2017), pp. 1455–1463.

[67] J Lundbom, A Hakkarainen, N Lundbom, and Marja-Riitta Taskinen. "Deep subcutaneous adipose tissue is more saturated than superficial subcutaneous adipose tissue". In: *International journal of obesity* 37.4 (2013), pp. 620–622.

[68] A Onat, G Ş Avcı, MM Barlan, H Uyarel, B Uzunlar, and V Sansoy. "Measures of abdominal obesity assessed for visceral adiposity and relation to coronary risk". In: *International journal of obesity* 28.8 (2004), pp. 1018–1025.

[69] Jiankang Liu, Caroline S Fox, DeMarc A Hickson, Warren D May, Kristen G Hairston, J Jeffery Carr, and Herman A Taylor. "Impact of abdominal visceral and subcutaneous adipose tissue on cardiometabolic risk factors: the Jackson Heart Study". In: *The Journal of Clinical Endocrinology & Metabolism* 95.12 (2010), pp. 5419–5426.

[70] A Shuster, M Patlas, JH Pinthus, and M Mourtzakis. "The clinical importance of visceral adiposity: a critical review of methods for visceral adipose tissue analysis". In: *The British journal of radiology* 85.1009 (2012), pp. 1–10.

[71] Luigi Fontana, J Christopher Eagon, Maria E Trujillo, Philipp E Scherer, and Samuel Klein. "Visceral fat adipokine secretion is associated with systemic inflammation in obese humans". In: *Diabetes* 56.4 (2007), pp. 1010–1013.

[72] SA Ritchie and JMC Connell. "The link between abdominal obesity, metabolic syndrome and cardiovascular disease". In: *Nutrition, Metabolism and cardiovascular diseases* 17.4 (2007), pp. 319–326.

[73] MRI Ancillary Study Group of the Look AHEAD Research Group Gallagher Dympna dg108@ columbia. edu Kelley David E Yim Jung-Eun Spence Natasha Albu Jeanine Boxt Lawrence Pi-Sunyer F Xavier Heshka Stanley. "Adipose tissue distribution is different in type 2 diabetes". In: *The American journal of clinical nutrition* 89.3 (2009), pp. 807–814.

[74] Tae-Hoon Oh, Jeong-Sik Byeon, Seung-Jae Myung, Suk-Kyun Yang, Kwi-Sook Choi, Jun-Won Chung, Benjamin Kim, Don Lee, Jae Ho Byun, Se Jin Jang, et al. "Visceral obesity as a risk factor for colorectal neoplasm". In: *Journal of gastroenterology and hepatology* 23.3 (2008), pp. 411–417.

[75] David V Schapira, Robert A Clark, Peter A Wolff, Anne R Jarrett, Nagi B Kumar, and Noreen M Aziz. "Visceral obesity and breast cancer risk". In: *Cancer* 74.2 (1994), pp. 632–639.

[76] Pedro Von Hafe, Francisco Pina, Ana Pérez, Margarida Tavares, and Henrique Barros. "Visceral fat accumulation as a risk factor for prostate cancer". In: *Obesity research* 12.12 (2004), pp. 1930–1935.

[77] Per Björntorp. "Metabolic implications of body fat distribution". In: *Diabetes care* 14.12 (1991), pp. 1132–1143.

[78] Bernardo Leo Wajchenberg. "Subcutaneous and visceral adipose tissue: their relation to the metabolic syndrome". In: *Endocrine reviews* 21.6 (2000), pp. 697–738.

[79] Margaret M Harris, June Stevens, Neal Thomas, Pam Schreiner, and Aaron R Folsom. "Associations of fat distribution and obesity with hypertension in a bi-ethnic population: the ARIC study". In: *Obesity research* 8.7 (2000), pp. 516–524.

[80] Jesper Lundbom, Antti Hakkarainen, Sanni Söderlund, Jukka Westerbacka, Nina Lundbom, and Marja-Riitta Taskinen. "Long-TE 1H MRS suggests that liver fat is more saturated than subcutaneous and visceral fat". In: *NMR in Biomedicine* 24.3 (2011), pp. 238–245.

[81] Jürgen Machann, Norbert Stefan, Christoph Schabel, Erwin Schleicher, Andreas Fritsche, Christian Würslin, Hans-Ulrich Häring, Claus D Claussen, and Fritz Schick. "Fraction of unsaturated fatty acids in visceral adipose tissue (VAT) is lower in subjects with high total VAT volume–a combined 1H MRS and volumetric MRI study in male subjects". In: *NMR in Biomedicine* 26.2 (2013), pp. 232–236.

[82] Christopher D Byrne and Giovanni Targher. "NAFLD: a multisystem disease". In: *Journal of hepatology* 62.1 (2015), S47–S64.

[83] Susanne Bonekamp, An Tang, Arian Mashhood, Tanya Wolfson, Christopher Changchien, Michael S Middleton, Lisa Clark, Anthony Gamst, Rohit Loomba, and Claude B Sirlin. "Spatial distribution of MRI-determined hepatic proton density fat fraction in adults with nonalcoholic fatty liver disease". In: *Journal of Magnetic Resonance Imaging* 39.6 (2014), pp. 1525–1532.

[84] Keitaro Sofue, Achille Mileto, Brian M Dale, Xiaodong Zhong, and Mustafa R Bashir. "Interexamination repeatability and spatial heterogeneity of liver iron and fat quantification using MRI-based multistep adaptive fitting algorithm". In: *Journal of Magnetic Resonance Imaging* 42.5 (2015), pp. 1281–1290.

[85] Steven P Larson, Steven P Bowers, Nicole A Palekar, John A Ward, Joseph P Pulcini, and Stephen A Harrison. "Histopathologic variability between the right and left lobes of the liver in morbidly obese patients undergoing Roux-en-Y bypass". In: *Clinical Gastroenterology and Hepatology* 5.11 (2007), pp. 1329–1332.

[86] Vlad Ratziu, Frédéric Charlotte, Agnès Heurtier, Sophie Gombert, Philippe Giral, Eric Bruckert, André Grimaldi, Frédérique Capron, Thierry Poynard, LIDO Study Group, et al. "Sampling variability of liver biopsy in nonalcoholic fatty liver disease". In: *Gastroenterology* 128.7 (2005), pp. 1898–1906.

[87] Soudabeh Fazeli Dehkordy, Kathryn J Fowler, Adrija Mamidipalli, Tanya Wolfson, Cheng William Hong, Yesenia Covarrubias, Jonathan C Hooker, Ethan Z Sy, Alexandra N Schlein, Jennifer Y Cui, et al. "Hepatic steatosis and reduction in steatosis following bariatric weight loss surgery differs between segments and lobes". In: *European radiology* 29.5 (2019), pp. 2474–2480.

[88] Roberto J Groszmann, Bernardo Kotelanski, and Jay N Cohn. "Hepatic lobar distribution of splenic and mesenteric blood flow in man". In: *Gastroenterology* 60.6 (1971), pp. 1047–1052.

[89] Glover H Copher and Bruce M Dick. "Stream line phenomena in the portal vein and the selective distribution of portal blood in the liver". In: *Archives of Surgery* 17.3 (1928), pp. 408–419.

[90] Toshinobu Tsukuda, Katsuyoshi Ito, Shinji Koike, Katsumi Sasaki, Ayame Shimizu, Takeshi Fujita, Mitsue Miyazaki, Hitoshi Kanazawa, Chisaki Jo, and Naofumi Matsunaga. "Pre-and postprandial alterations of portal venous flow: evaluation with single breath-hold three-dimensional half-Fourier fast spin-echo MR imaging and a selective inversion recovery tagging pulse". In: *Journal of Magnetic Resonance Imaging: An Official Journal of the International Society for Magnetic Resonance in Medicine* 22.4 (2005), pp. 527–533.

[91] RE Ellis. "The distribution of active bone marrow in the adult". In: *Physics in Medicine & Biology* 5.3 (1961), p. 255.

[92] Maureen J Devlin and Clifford J Rosen. "The bone–fat interface: basic and clinical implications of marrow adiposity". In: *The Lancet Diabetes & Endocrinology* 3.2 (2015), pp. 141–147.

[93] Erica L Scheller and Clifford J Rosen. "What's the matter with MAT? Marrow adipose tissue, metabolism, and skeletal health". In: *Annals of the New York Academy of Sciences* 1311.1 (2014), p. 14.

[94] Erica L Scheller, Casey R Doucette, Brian S Learman, William P Cawthorn, Shaima Khandaker, Benjamin Schell, Brent Wu, Shi-Ying Ding, Miriam A Bredella, Pouneh K Fazeli, et al. "Region-specific variation in the properties of skeletal adipocytes reveals regulated and constitutive marrow adipose tissues". In: *Nature communications* 6.1 (2015), pp. 1–15.

[95] Thomas Baum, Alexander Rohrmeier, Jan Syväri, Maximilian N Diefenbach, Daniela Franz, Michael Dieckmeyer, Andreas Scharr, Hans Hauner, Stefan Ruschke, Jan S Kirschke, et al. "Anatomical variation of age-related changes in vertebral bone marrow composition using chemical shift encoding-based water–fat magnetic resonance imaging". In: *Frontiers in endocrinology* 9 (2018), p. 141.

[96] James F Griffith, David KW Yeung, Heather Ting Ma, Jason Chi Shun Leung, Timothy CY Kwok, and Ping Chung Leung. "Bone marrow fat content in the elderly: a reversal of sex difference seen in younger subjects". In: *Journal of Magnetic Resonance Imaging* 36.1 (2012), pp. 225–230.

[97] Miriam A Bredella, Pouneh K Fazeli, Karen K Miller, Madhusmita Misra, Martin Torriani, Bijoy J Thomas, Reza Hosseini Ghomi, Clifford J Rosen, and Anne Klibanski. "Increased bone marrow fat in anorexia nervosa". In: *The Journal of Clinical Endocrinology & Metabolism* 94.6 (2009), pp. 2129–2136.

[98] Pouneh K Fazeli, Miriam A Bredella, Lauren Freedman, Bijoy J Thomas, Anne Breggia, Erinne Meenaghan, Clifford J Rosen, and Anne Klibanski. "Marrow fat and preadipocyte factor-1 levels decrease with recovery in women with anorexia nervosa". In: *Journal of bone and mineral research* 27.9 (2012), pp. 1864–1871.

[99] Xiaojuan Li, Daniel Kuo, Anne L Schafer, Anne Porzig, Thomas M Link, Dennis Black, and Ann V Schwartz. "Quantification of vertebral bone marrow fat content using 3 Tesla MR spectroscopy: reproducibility, vertebral variation, and applications in osteoporosis". In: *Journal of Magnetic Resonance Imaging* 33.4 (2011), pp. 974–979.

[100] Jan Syväri, Stefan Ruschke, Michael Dieckmeyer, Hans H Hauner, Daniela Junker, Marcus R Makowski, Thomas Baum, and Dimitrios C Karampinos. "Estimating vertebral bone marrow fat unsaturation based on short-TE STEAM MRS". In: *Magnetic Resonance in Medicine* 85.2 (2021), pp. 615–626.

[101] Beatrijs H Wokke, Clemens Bos, Monique Reijnierse, Carla S van Rijswijk, Holger Eggers, Andrew Webb, Jan J Verschuuren, and Hermien E Kan. "Comparison of dixon and T1-weighted MR methods to assess the degree of fat infiltration in duchenne muscular dystrophy patients". In: *Journal of Magnetic Resonance Imaging* 38.3 (2013), pp. 619–624.

[102] Benjamin Marty, Bertrand Coppa, and Pierre G Carlier. "Monitoring skeletal muscle chronic fatty degenerations with fast T1-mapping". In: *European radiology* 28.11 (2018), pp. 4662–4668.

[103] Christopher J Hanrahan and Lubdha M Shah. "MRI of spinal bone marrow: part 2, T1-weighted imaging-based differential diagnosis". In: *American Journal of Roentgenology* 197.6 (2011), pp. 1309–1321.

[104] W Thomas Dixon. "Simple proton spectroscopic imaging." In: *Radiology* 153.1 (1984), pp. 189–194.

[105] U Rajendra Acharya, Oliver Faust, Filippo Molinari, S Vinitha Sree, Sameer P Junnarkar, and Vidya Sudarshan. "Ultrasound-based tissue characterization and classification of fatty liver disease: A screening and diagnostic paradigm". In: *Knowledge-Based Systems* 75 (2015), pp. 66–77.

[106] Frank Fischbach and Harald Bruhn. "Assessment of in vivo 1H magnetic resonance spectroscopy in the liver: a review". In: *Liver International* 28.3 (2008), pp. 297–307.

[107] Renata Longo, CLAUDIO Ricci, FLORA Masutti, ROSSELLA Vidimari, LORY S Crocé, LUISA Bercich, CLAUDIO Tiribelli, and LUDOVICO Dalla Palma. "Fatty infiltration of the liver. Quantification by 1H localized magnetic resonance spectroscopy and comparison with computed tomography." In: *Investigative radiology* 28.4 (1993), pp. 297–302.

[108] Carsten Thomsen, Ulrik Becker, Kjeld Winkler, Per Christoffersen, Mikael Jensen, and Ole Henriksen. "Quantification of liver fat using magnetic resonance spectroscopy". In: *Magnetic resonance imaging* 12.3 (1994), pp. 487–495.

[109] Benjamin Wildman-Tobriner, Michael M Middleton, Cynthia A Moylan, Stephen Rossi, Omar Flores, Zac Anchi Chang, Manal F Abdelmalek, Claude B Sirlin, and Mustafa R Bashir. "Association Between Magnetic Resonance Imaging–Proton Density Fat Fraction and Liver Histology Features in Patients with Nonalcoholic Fatty Liver Disease or Nonalcoholic Steatohepatitis". In: *Gastroenterology* 155.5 (2018), pp. 1428–1435.

[110] Michael S Middleton, Elhamy R Heba, Catherine A Hooker, Mustafa R Bashir, Kathryn J Fowler, Kumar Sandrasegaran, Elizabeth M Brunt, David E Kleiner, Edward Doo, Mark L Van Natta, et al. "Agreement between magnetic resonance imaging proton density fat fraction measurements and pathologist-assigned steatosis grades of liver biopsies from adults with nonalcoholic steatohepatitis". In: *Gastroenterology* 153.3 (2017), pp. 753–761.

[111] An Tang, Justin Tan, Mark Sun, Gavin Hamilton, Mark Bydder, Tanya Wolfson, Anthony C Gamst, Michael Middleton, Elizabeth M Brunt, Rohit Loomba, et al. "Nonalcoholic fatty liver disease: MR imaging of liver proton density fat fraction to assess hepatic steatosis". In: *Radiology* 267.2 (2013), pp. 422–431.